



THE JOINT EDUCATION MASTER PROGRAM
UNIVERSITY OF LIÈGE – BELGIUM
WATER RESOURCES UNIVERSITY – VIETNAM



DESIGN MONOPILE FOUNDATION OF OFFSHORE WIND TURBINES

A master thesis submitted in partial
fulfillment of the requirements for the
Master of Science degree in
Sustainable Hydraulic Structures
by

Mai Anh Quang

Supervisor:

Professor Philippe Rigo

Assoc. Professor Trinh Minh Thu

ACADEMIC YEAR 2011 – 2012

Lời cảm ơn

Qua luận văn này, những dòng đầu tiên tác giả muốn được bày tỏ lòng biết ơn chân thành tới những người đã nhiệt tình giúp đỡ, chỉ bảo, tạo mọi điều kiện thuận lợi suốt từ những buổi đầu của khóa học cho đến những ngày hoàn thiện luận văn.

Đầu tiên tác giả muốn được bày tỏ lòng biết ơn sâu sắc tới thầy Philippe Rigo, giáo sư hướng dẫn chính, người đã định hướng nghiên cứu, tận tình đọc và sửa lỗi cả về mặt học thuật và câu chữ trong luận văn.

Lời cảm ơn chân thành xin được gửi tới ban ANAST – khoa ARGENCO – đại học Liège (Bỉ), nơi đã hỗ trợ kinh phí và hướng dẫn khoa học để luận văn này được thực hiện tại Ulg. Tác giả xin được bày tỏ lòng biết ơn đến giáo sư Federic Colin (địa kỹ thuật) và giáo sư Vincent Denoel (động lực học) đã tận tình giúp đỡ trong các vấn đề chuyên ngành liên quan trong thời gian thực hiện luận văn.

Tác giả mong muốn được nói lời cảm ơn tới các lãnh đạo Viện Thủy Lợi và Môi Trường – trường ĐHTL vì những sự giúp đỡ về vật chất và khoa học trong quá trình học tập tại thành phố HCM. Đặc biệt là hai người thầy đáng kính, phó giáo sư, tiến sĩ Trịnh Công Ván và phó giáo sư, tiến sĩ Trịnh Minh Thụ, những người không chỉ động viên, giúp đỡ về khoa học mà còn là chỗ dựa tinh thần của tác giả trong suốt khóa học này.

Tác giả không quên công ơn của những người tâm huyết xúc tiến sự hình thành và phát triển của chương trình hợp tác đào tạo có chất lượng này. Một môi trường học tập thực sự hữu ích cho những kỹ sư đã có kinh nghiệm thực tế.

Lời cảm ơn của tác giả cũng xin được trân trọng gửi tới các thầy cô giáo đến từ WRU và Ulg đã nhiệt tình chỉ bảo và dành nhiều cảm tình cho tác giả trong suốt sáu mô đun của chương trình tại thành phố HCM.

Cuối cùng xin được dành những tình cảm chân thành gửi tới các anh chị em lớp Cao học Việt – Bỉ khóa 1, những người đã dành cho tác giả nhiều tình cảm ưu ái và sự động viên giúp đỡ trong quá trình học tập xa nhà.

Acknowledgments

I wish to thank, first and foremost, Professor Philippe Rigo – University of Liège (Belgium) – the promoter and supervisor of my master thesis, who read and corrected all technical as well as English mistakes in the thesis.

This thesis would have remained a dream had it not been for ANAST Department – ARGENCO Faculty – University of Liège (Ulg), who gave me financial support to do my research in Ulg.

It gives me great pleasure in acknowledge the support and help of Professor Frederic Collin and Professor Vincent Denoël – ARGENCO Faculty – on geotechnical and dynamic issues of the foundation pile under cyclic loading.

I owe my deepest gratitude to leaders of Institute for Water and Environment Research – Water Resources University – for all the academic helps and financial support that they gave me during the time I was taking this master course in Ho Chi Minh City.

I cannot find words to express my gratitude to Associate Professor Trinh Minh Thu and Associate Professor Trinh Cong Van for their scientific supports and wisely advices.

I would like to thank all Professors and Lecturers giving lectures in six modules of the “Sustainable Hydraulic Structures” master course for all their favors given to me.

This thesis would not have been possible unless Coordinators from both WRU and Ulg have made their greatest efforts to establish this Joint Master Course between the two Universities.

I share the credit of my work with all of my colleagues in the master class for their supporting and encouraging while I was living in Ho Chi Minh City.

I am indebted to my parents and my wife for all the loves they have given and all the difficulties they have borne during my study.

Tóm tắt nội dung luận văn

THIẾT KẾ NỀN CỌC ĐƠN CHO TUABIN GIÓ NGOÀI KHƠI

Sự tối ưu hóa thiết kế là vấn đề cấp thiết cho sự phát triển của ngành công nghiệp điện gió ngoài khơi. Vì tiến trình này mất rất nhiều thời gian nên các thông số được lựa chọn để tính toán tối ưu hóa càng giảm được nhiều càng tốt. Từ đó, một vấn đề nảy sinh là có thể loại bỏ được phần nền móng trong quá trình tối ưu hóa này hay không. Để thấy được tầm quan trọng của việc kể đến cọc nền trong ứng xử động lực học của toàn bộ công trình, trước tiên cần phải xác định các kích thước của nó dựa trên các yêu cầu về thiết kế theo trạng thái giới hạn cực hạn và trạng thái điều kiện làm việc sử dụng các tiêu chuẩn thiết kế hiện hành, sau đó so sánh ứng xử động lực học giữa mô hình ngầm tại đáy biển và mô hình có phần kết cấu nền. Việc mô hình hóa phần nền được tiến hành bằng phương pháp dầm trên nền đàn hồi phi tuyến có kể đến ứng xử của đất dính và đất rời đối với cọc nền. Với dự án tuabin gió ngoài khơi được chọn có công suất 7MW và chiều cao 115m đến đáy biển, việc tính toán cho thấy cần phải có cọc nền chiều dài 26m, đường kính 6m và chiều dày 8cm. Ứng xử động lực học của hai mô hình cho thấy rằng sẽ là không an toàn nếu bỏ qua phần kết cấu nền trong quá trình tối ưu hóa thiết kế. Ngoài ra khả năng đóng góp sự giảm chấn của đất nền chiếm tỷ trọng lớn nhất trong ứng xử động lực học của toàn bộ kết cấu. Kết quả nghiên cứu sẽ có ích trong việc xem xét các thông số cần tối ưu hóa trong thiết kế tuabin gió ngoài khơi, cũng như việc chọn lựa phương pháp giải thích hợp cho các phương trình động lực học trong tiến trình tối ưu hóa.

Abstract

DESIGN MONOPILE FOUNDATIONS OF OFFSHORE WIND TURBINES

Design optimization is crucial to the development of the offshore wind turbine industry. This time consuming process is better to be done with a number of input parameters that is as short as possible. Whether the foundation pile part can be neglected in the design optimization process of an offshore wind turbine structure is a question need to be answer. In order to see the importance of the presence of the foundation pile in dynamic behavior of the whole structure, dimensions of the foundation pile must be determined basing on requirements in ultimate limit state and serviceability limit state in current design standards. Afterward, the differences in dynamic behavior between a fixed-at-seabed tower model and a tower with foundation model must be observed. Beam nonlinear Winkler Foundation model in addition to gapping and non-gapping behavior in pile-soil interface were used to model the foundation. With the chosen offshore wind turbine project of 7MW and 115m high to seabed, a foundation pile with a penetration length of 26m, diameter of 6m and wall thickness of 8cm had been found. The dynamic behavior of the two models showed that it was not on the safe side if the foundation was neglected in design optimization process. And that the internal damping of the soil was the most important factor in behavior of the structure. These results will be useful for reconsidering parameters in design optimization process of monopile offshore wind turbines as well as choosing suitable methods to solve dynamic equations in the optimization procedure.

Table of Contents

Chapter I.	Introduction	12
1.1.	Foundation of offshore wind turbines	12
1.2.	Design Optimization Project for Offshore Wind Turbines.....	16
1.3.	Which type of foundation should be chosen?	17
1.4.	Tasks of the thesis.....	17
1.5.	Method to carry out.....	18
1.6.	Structure of the thesis	18
Chapter II.	Support structure of monopile OWTs - components, fabrication and installation	19
2.1.	Introduction.....	19
2.2.	How it works?	19
2.3.	Components of the support structure	20
2.3.1.	Definitions	20
2.3.2.	Design elevations	20
2.3.3.	Support structure components	20
2.4.	Fabrication	21
2.5.	Installation	22
Chapter III.	Design Methodology	28
3.1.	Introduction.....	28
3.2.	Design objective	28
3.3.	Design process for offshore wind turbine support structures	29
3.3.1.	Design Sequence	29
3.3.2.	Design Load Cases	30
3.3.3.	Limit State Checks.....	30
3.3.4.	Design evaluation	31
3.4.	Design criteria.....	32
3.4.1.	From requirements to criteria	32
3.4.2.	Natural frequencies	32
3.4.3.	Strength criteria	33
3.4.4.	Design criteria for monopile foundations	34
3.4.5.	Design requirements for manufacturing and installation	36
Chapter IV.	Related Theories	38
4.1.	Introduction.....	38
4.2.	The basics of dynamics	38
4.3.	Damping in offshore wind turbines structures	40
4.3.1.	Definition of damping.....	40
4.3.2.	Damping for piled offshore support structure	41
4.3.3.	Damping of soil (piled structure).....	42
4.4.	Sources of excitations	43
4.5.	Statistical methods and Deterministic approach	43
4.6.	Wind	45
4.6.1.	Mean annual wind speed and wind speed frequency distribution.....	45
4.6.2.	Increase wind speed with altitude	46
4.6.3.	Wind turbulence.....	46

4.6.4.	Wind turbine classes	47
4.6.5.	Wind Rose	48
4.6.6.	Assessment of wind loads on the support structure	48
4.7.	Wave	49
4.7.1.	General characteristics of waves	50
4.7.2.	Reference sea states	50
4.7.3.	Wave Modeling	51
4.8.	Current	53
4.9.	Combined Wind and Wave Loading	54
4.9.1.	Horizontal to Moment Load Ratio	54
4.9.2.	Combination Methods	54
4.10.	Effect of cyclic loading to foundation	54
4.10.1.	Cyclic degradation effects	54
4.10.2.	Loading rate effects	55
4.11.	Basis of Soil Mechanics	56
4.11.1.	Stress-strain behavior, stiffness and strength	56
4.11.2.	Elasticity	57
4.11.3.	Perfect Plasticity	57
4.11.4.	Combined Elasto-Plastic Behavior	58
4.12.	Types of Soil Model	59
4.12.1.	Plasticity Models	59
4.12.2.	Finite Element Models	60
4.12.3.	Other Technique	60
4.13.	Winkler model	61
4.13.1.	Beam Nonlinear Winkler Foundation	61
4.13.2.	Pile-soil interface	62
4.13.3.	Load-displacement relationship	62
4.14.	Sap2000 and methods to solve a nonlinear dynamic analysis	64
4.14.1.	Sap2000 software	64
4.14.2.	Dynamic equilibrium	65
4.14.3.	Step-by-step solution method	65
4.14.4.	Mode superposition method	66
4.14.5.	Solution in frequency domain	66
Chapter V.	Preliminary Design for Support Structure of a Chosen OWT Project	67
5.1.	Introduction	67
5.2.	Structure definitions and limitations	67
5.2.1.	The chosen turbine	67
5.2.2.	Tower and substructure design	68
5.2.3.	Corrosion	71
5.3.	Environmental conditions	72
5.3.1.	Site data	72
5.3.2.	Sea conditions	72
5.3.3.	Wind conditions	72
5.3.4.	Currents	72

5.3.5.	Further meteorological – oceanographical parameters.....	72
5.3.6.	Soil conditions	72
5.4.	Load combination for ULS	73
5.5.	Results of internal forces for foundation design	74
5.5.1.	For ULS design.....	74
5.5.2.	For SLS check	74
5.6.	Results of natural frequency analysis.....	74
Chapter VI.	Foundation pile design	76
6.1.	Introduction.....	76
6.2.	Ultimate limit state design	76
6.2.1.	Axial capacity.....	76
6.2.2.	Lateral capacity	85
6.2.3.	Structural Capacity of the steel pile	93
6.3.	Serviceability limit state check.....	101
6.3.1.	General	101
6.3.2.	Geometry model	101
6.3.3.	Loads	103
6.3.4.	Results of calculation.....	108
6.3.5.	Conclusions of SLS calculation	113
6.4.	Effect of foundation in dynamic behavior of the structure	114
6.4.1.	Reconsidering the model.....	114
6.4.2.	Spring foundation vs. fixed foundation	116
6.4.3.	Linear spring vs. nonlinear spring foundation	119
6.5.	Effect of p-y curve on the dynamic behavior of structure	120
Chapter VII.	Conclusions and Future works	121
7.1.	Conclusions	121
7.2.	Future works.....	121
	Bibliography.....	122
	Honor Statement	124
Appendix 1.	T-Z curves	125
Appendix 2.	Q-Z curves	128
Appendix 3.	P-Y curves	129
Appendix 4.	Sensitivity Analyses.....	132

List of Figures

Figure I.1: Nysted Offshore Wind Farm	12
Figure I.2: Mechanical system of an offshore wind turbine	13
Figure I.3: a) Standard Monopile Structure, b) Supported Monopile Structure	14
Figure I.4: a) Tripod Structure, b) Gravity Pile Structure	14
Figure I.5: Lattice Tower	15
Figure I.6: Gravity Base Structure	15
Figure I.7: Suction Bucket Structure	15
Figure I.8: Tension-Leg Platform	16
Figure I.9: Low-roll Floater	16
Figure I.10: First offshore wind facility Vindeby in Denmark	16
Figure I.11: The interface of the software EOL OS	17
Figure II.1: Overview of offshore wind turbine terminology	19
Figure II.2: Rolling and welding of a foundation pile	22
Figure II.3: Pile driving at Offshore Wind Farm Egmond aan Zee	23
Figure II.4: Drilling equipment at Blyth	24
Figure II.5: Schematic example of scour protection	24
Figure II.6: Transition piece installation	25
Figure II.7: Lifting of a tower section for installation	26
Figure II.8: Installation of a rotor in one piece	26
Figure II.9: Various stages in the installation of a turbine using the bunny-ear method	27
Figure III.1: Design process for an offshore wind turbine	29
Figure IV.1: Single degree of freedom mass-spring-damper system	38
Figure IV.2: a) Quasi-static b) resonant and c) inertia dominated response	39
Figure IV.3: Frequency response function	40
Figure IV.4: Measured time history of wind speed	47
Figure IV.5: An example of Wind Rose	48
Figure IV.6: Illustration of wake effect	49
Figure IV.7: Regular travelling wave properties	50
Figure IV.8: A typical	56
Figure IV.9: Tangent and secant stiffness moduli	56
Figure IV.10: Material behavior during load cycling	58
Figure IV.11: Yielding and Plastic Straining	58
Figure IV.12: Example Yield Surface for Footings on Sand	59
Figure IV.13: Comparison of a) Laboratory Test Data with b) Continuous Hyperplasticity Theory.	60
Figure IV.14: Typical soil reaction - pile deflection behavior for cohesive soils (gapping)	62
Figure IV.15: Typical soil reaction - pile deflection behavior for cohesionless soils (cave-in)	62
Figure IV.16: Coefficients as functions of friction angle	64
Figure IV.17: Initial modulus of subgrade reaction k as function of friction angle	64
Figure V.1: Schematic dimension of the design structure	68
Figure V.2: Determining the interface level	68

Figure V.3: Wall thickness of the tower	69
Figure V.4: Diameter of the tower	69
Figure V.5: Parameterization of the monopile support structure.....	70
Figure VI.1: Unit skin friction along the pile	78
Figure VI.2: Accumulated skin friction vs. pile length	79
Figure VI.3: Unit tip resistance vs. pile length	79
Figure VI.4: Axial pile resistance vs. pile length	80
Figure VI.5: Design Soil Strength vs. Pile Length	80
Figure VI.6: Illustration of the idealized model used in t-z load-transfer analyses	81
Figure VI.7: Illustration of the t-z curve according to API.....	81
Figure VI.8: t-z curve at X=0.5 m	83
Figure VI.9: Generic pile Tip load - Displacement (Q-z) curve	83
Figure VI.10: Q-z curve at depth X=21 m.....	84
Figure VI.11: Settlement vs. pile lengths.....	85
Figure VI.12: Lateral pile resistance vs. pile length (Diameter = 6m)	87
Figure VI.13: Total lateral pile resistance ($\gamma_M=1.15$) and the design lateral load (5642 kN)	87
Figure VI.14: Database for the p-y curve at the depth 6.75 m	88
Figure VI.15: p-y curve at the depth 6.75m (layer 5).....	89
Figure VI.16: Results of lateral analysis	90
Figure VI.17: Lateral pile head displacement vs. Pile length	90
Figure VI.18: Pile head rotation vs. Pile length	90
Figure VI.19: Process to calculate the static moment of a segment of hollow circular section.....	94
Figure VI.20: Normal stress and shear stress.....	94
Figure VI.21: Parameters to determine static moment in a circular section.....	94
Figure VI.22: Internal forces of the 26m long pile	95
Figure VI.23: Stress distribution of foundation pile at the depth 1.0 m	95
Figure VI.24: Stress distribution of foundation pile at the depth 12.0 m	96
Figure VI.25: Stress distribution of foundation pile at the depth 20.0 m	97
Figure VI.26: Maximum stresses and utilization ratios along the pile length	99
Figure VI.27: The utilization ratio after changing wall thickness	100
Figure VI.28: Kinematic model simulates non-gapping behavior	102
Figure VI.29: An example of the modified p-y curve for SLS analysis	102
Figure VI.30: An example of hysteretic behavior of Link 124 in the model	103
Figure VI.31: Wave height of Sea-state 0 in a 10 minute simulation	104
Figure VI.32: Wave height of Sea-state 0 in a 100 second simulation	104
Figure VI.33: Wave load of Sea-state 0 in a 10 minute simulation (at seabed level)	104
Figure VI.34: Wave load of Sea-state 0 in a 100 second simulation (at seabed level).....	105
Figure VI.35: Wave Spectrum of Sea States	105
Figure VI.36: Time domain of Wave and Current Load from Sea State 0 at MSL	106
Figure VI.37: Time domain of Wave and Current Load from Sea State 1 at MSL.....	106
Figure VI.38: Time domain of Wave and Current Load from Sea State 2 at MSL.....	106
Figure VI.39: Frequency domain of Wave Load from Sea State 0 at MSL	107

Figure VI.40: Frequency domain of Wave Load from Sea State 1 at MSL.....	107
Figure VI.41: Frequency domain of Wave Load from Sea State 2 at MSL.....	107
Figure VI.42: Rotation Displacement at tower top – Sea State 1.....	109
Figure VI.43: PDF of Rotation Displacement at tower top- Sea state 1	109
Figure VI.44: Horizontal Displacement at tower top - Sea State 1.....	109
Figure VI.45: PDF of Horizontal Displacement at tower top- Sea state 1	110
Figure VI.46: Horizontal Displacement at seabed - Sea State 1.....	110
Figure VI.47: PDF of Horizontal Displacement at seabed - Sea state 1	110
Figure VI.48: Rotation Displacement at seabed – Sea State 1.....	111
Figure VI.49: PDF of Rotation Displacement at seabed- Sea state 1	111
Figure VI.50: Behavior of one of the springs during and after the storm – Sea State 1	111
Figure VI.51: Ux of the tower top-single storm.....	112
Figure VI.52: Ux of the tower top-two successive storms	112
Figure VI.53: Comparing Ux at the tower top between Single storm and two successive storms.....	112
Figure VI.54: Probability distribution diagram of displacements	113
Figure VI.55: Response of structure in spring model – displacement at the tower top.....	114
Figure VI.56: Response of structure in fixed-at-seabed model – displacement at the tower top	114
Figure VI.57: Compare the responses of two models at tower top	115
Figure VI.58: PSD of Responses at tower top caused by sea state 0	115
Figure VI.59: PSD of Responses at tower top caused by sea state 1	116
Figure VI.60: PSD of Responses at tower top caused by sea state 2	116
Figure VI.61: Calculating models of offshore wind turbine structure.....	117
Figure VI.62: Wave load at sea water level (MSL).....	117
Figure VI.63: Wave load at seabed level	117
Figure VI.64: Horizontal displacement of the tower top in the fixed foundation model.....	118
Figure VI.65: Horizontal displacement of the tower top in the spring foundation model.....	118
Figure VI.66: Normal distribution of horizontal displacements at tower top	118
Figure VI.67: Power Spectral Density of horizontal displacements	119
Figure VI.68: Result of Ux at the tower top in time domain.....	119
Figure VI.69: Damping Coefficient vs. Horizontal Displacement	120

List of Tables

Table III.1: Material factors	35
Table IV.1: Basic parameters for wind turbine classes	47
Table IV.2: Estimations of Effective Fixity Length. (Zaaijer 2002)	61
Table V.1: Model of support structure	69
Table V.2: Natural frequency of the support structure in EOL OS	74
Table V.3: Excitation frequencies	75
Table VI.1: Design parameters for axial resistance of driven piles	77
Table VI.2: Result of pile settlement calculation	85
Table VI.3: Displacement and Rotation of pile head with the length.....	90
Table VI.4: Plastified soil zone of the chosen pile	92
Table VI.5: Values of stress distribution on the pile section at the depth 20.0 m	96
Table VI.6: Internal forces, stresses and utilization of steel strength	97
Table VI.7: Sea states for SLS check – taken from 112 states (TEMPEL, 2006).....	105
Table VI.8: Results of SLS calculations in single storm	108
Table VI.9: Parameters of the two normal distributions	112
Table VI.10: Linear stiffness of springs	114
Table VI.11: Tower top displacement in two models.....	119

List of abbreviations

1P	Rotation frequency of turbine
3P	Blade passing frequency of three-bladed turbine
BNWF	Beam nonlinear Winkler foundation
FRF	Frequency response function
HAT	Highest astronomical tide
LAT	Lowest astronomical tide
MSL	Mean sea level
OWT	Offshore wind turbine
RNA	Rotor nacelle assembly
SLS	Serviceability limit state
SSI	Soil-structure interaction
ULS	Ultimate limit state

List of terms

Blade-passing frequency	The frequency at which the blades of a wind turbine pass the tower.
Corrosion allowance	Extra wall thickness added during design to compensate for any reduction in wall thickness by corrosion (externally and internally) during design life.
Cut-in speed	Minimum wind speed that a wind turbine starts operating
Cut-out speed	The wind speed at which the turbine automatically stops the blades from turning and rotates out of the wind to avoid damage to the turbine
Fatigue	The phenomenon by which a repeated loading and unloading of a structure causes it various components to gradually weaken and eventually fail.
Nacelle	The structure at the top of the wind turbine tower just behind (or in some cases, in front of) the wind turbine blades that houses the key components of the wind turbine, including the rotor shaft, gearbox, and generator.
Splash zone	The part of a support structure which is intermittently exposed to seawater due to the action of tide or waves or both.

Chapter I. Introduction



1.1. Foundation of offshore wind turbines

“A one hundred yard high tower still has its foundation on the ground”

(Chinese Proverb)

All structures, large or small, require adequate foundations. A foundation is defined as that part of the structure that supports the weight of the structure and transmits the load to underlying soil or rock.



Figure I.1: Nysted Offshore Wind Farm

According to Design Standard of Offshore Wind Turbines (BSH, 2007), the overall mechanical system of an offshore wind turbine consists of the components of the turbine and support structure (see Figure I.2). The support structure can be further subdivided into the tower and substructure. The foundation elements form part of the substructure.

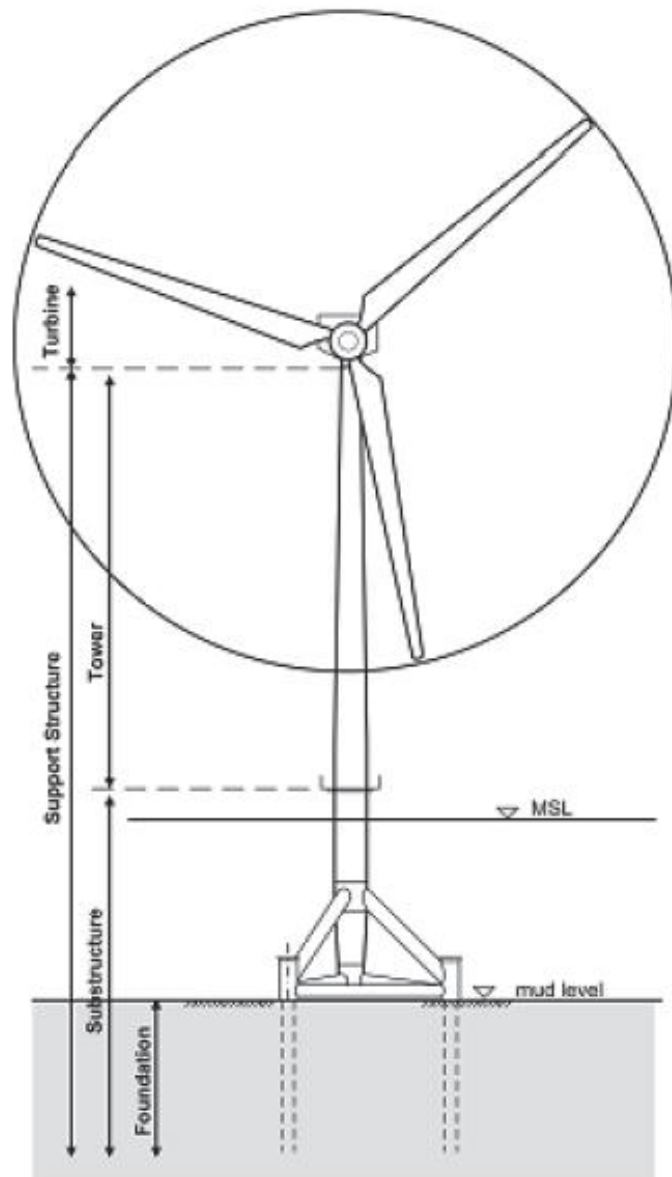


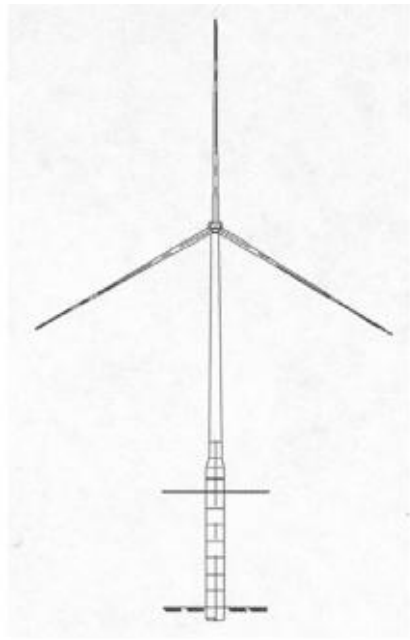
Figure I.2: Mechanical system of an offshore wind turbine

As a result of offshore wind turbines development, so far there are four main classes of offshore foundations consist of:

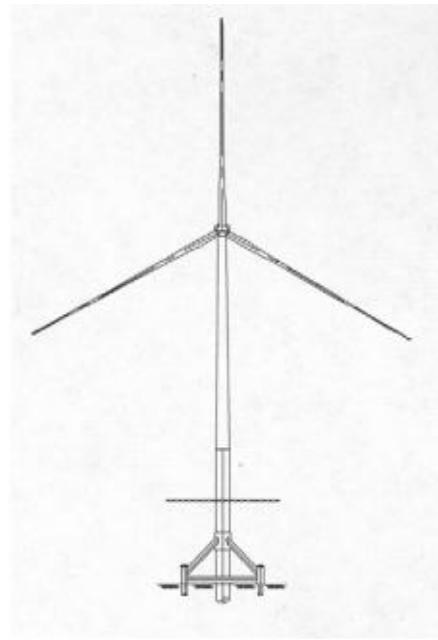
- Piled foundations (Figure I.3, Figure I.4, Figure I.5),
- Gravity base foundations (Figure I.4b, Figure I.6),
- Skirt and bucket foundations (Figure I.7),
- Floating structures with moored foundations (Figure I.8, Figure I.9).

The piled and gravity base foundations can be further classified into three structural configurations, namely:

- Monopiles, which are designed as piled foundations and exhibit simplicity in fabrication and installation,
- Tripod or quadruped configurations, which can be both piled or gravity based,
- Lattice configurations, which offer the most economical structural solution in terms of steel weight-to-capacity ratio.

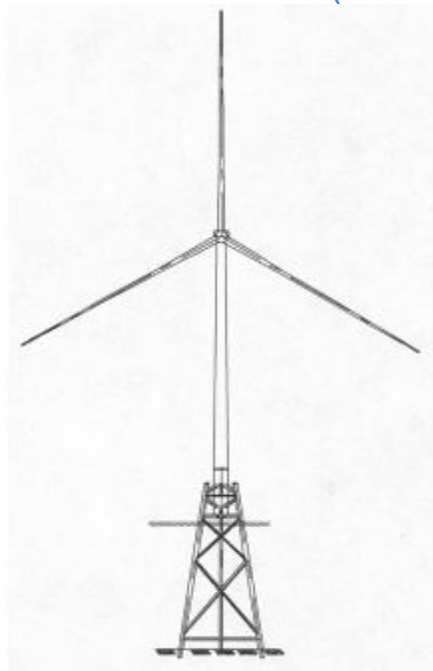


a)

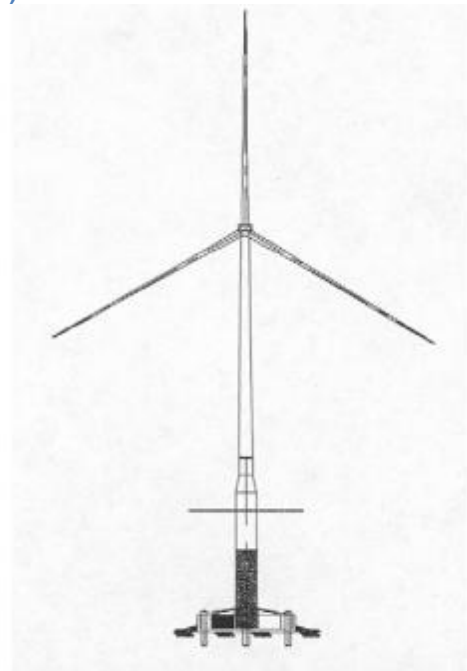


b)

Figure I.3: a) Standard Monopile Structure, b) Supported Monopile Structure.
(DNV-OS-J101 2004)



a)



b)

Figure I.4: a) Tripod Structure, b) Gravity Pile Structure.
(DNV-OS-J101 2004)

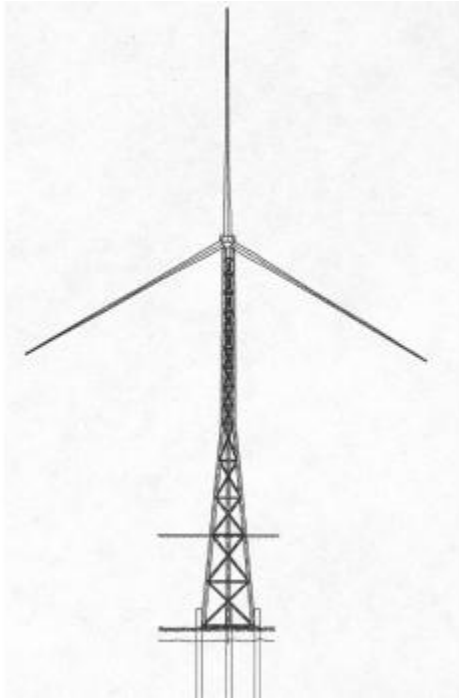


Figure I.5: Lattice Tower.
(DNV-OS-J101 2004)

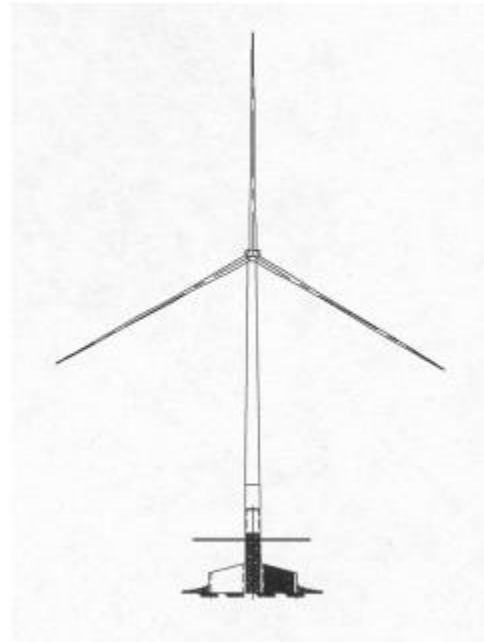
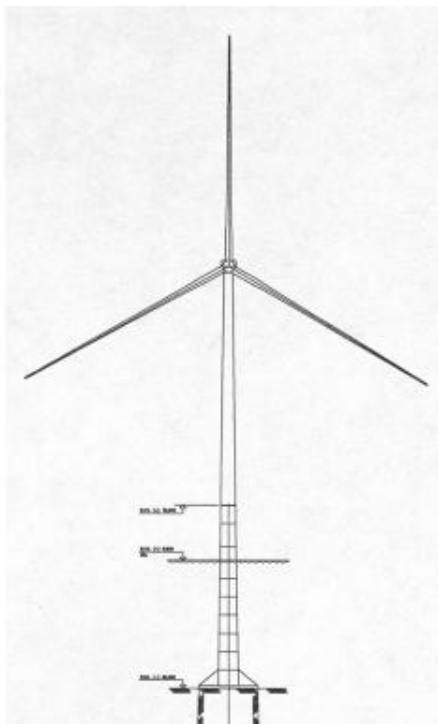
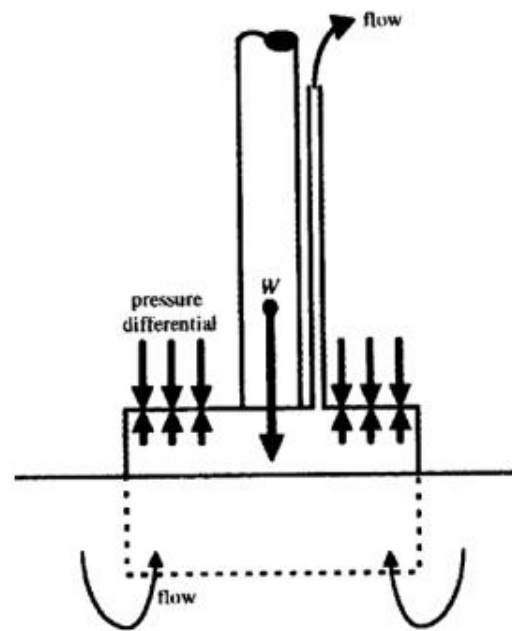


Figure I.6: Gravity Base Structure.
(DNV-OS-J101 2004)



a)



b)

Figure I.7: Suction Bucket Structure
(DNV-OS-J101 2004), and b) Installation Principle.
(Byrne and Housby 2003)

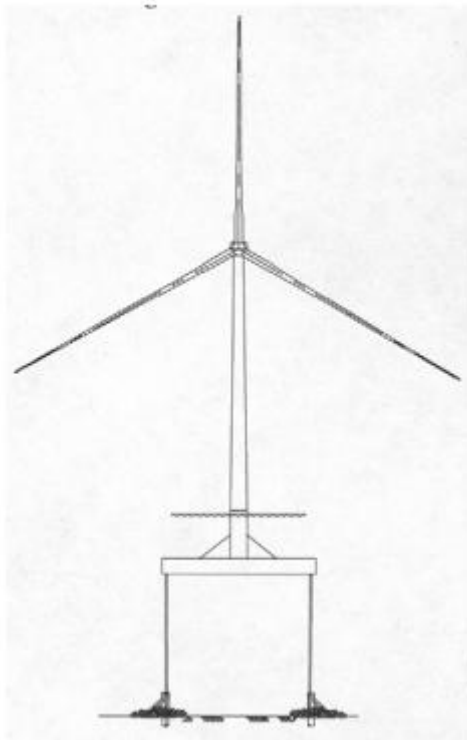


Figure I.8: Tension-Leg Platform.
(DNV-OS-J101 2004)

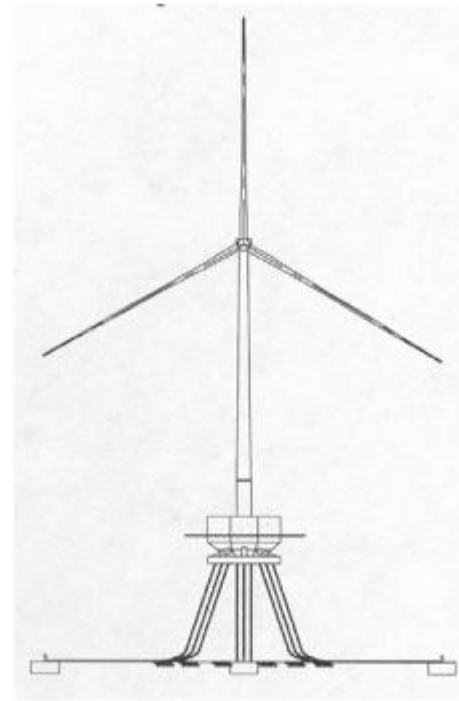


Figure I.9: Low-roll Floater.
(DNV-OS-J101 2004)

1.2. Design Optimization Project for Offshore Wind Turbines.



Figure I.10: First offshore wind facility Vindeby in Denmark

It is about two decades since installation of the first offshore wind farm in the early 1990s where there was limited land available for onshore wind energy production. The Vindeby Facility in Denmark (Figure I.10), completed in 1991, has eleven 450 kW turbines that provide a total capacity of about 5 MW. Since then, the trend has been to move wind turbines offshore to take advantage of higher wind speeds; smoother and less turbulent airflow and larger amounts of open space.

However, cost is currently a major inhibitor of offshore wind energy development. It is approximately 50-100% more costly per installed rotor area as compared to conventional onshore projects. The reasons for this are primarily the added complexity of having to install foundations and power cables offshore and secondly the increased costs of the foundation itself. For offshore wind turbines, it is proven that the foundation may account for up to 35% of the installed cost. Hence, optimization of foundation design for offshore wind turbines is crucial for the development of offshore wind farms.

“Optimization of steel monopile offshore wind turbines” project has been carrying out under the cooperation between the ANAST Department (ULg) and Arcelor Mittal Research Center (Walloon

Region) in order to develop software named EOL-OS, which is dedicated to the structural optimisation of the support structure based on minimization of production cost or weight. This master thesis is a part of the sub-project named “Design and optimization of the structural foundation of offshore wind turbines”. The general goal of this sub-project is to create an innovative module focusing on the foundation part of offshore wind turbines, which will be integrated in the existing design and optimization chain of the EOL-OS software.

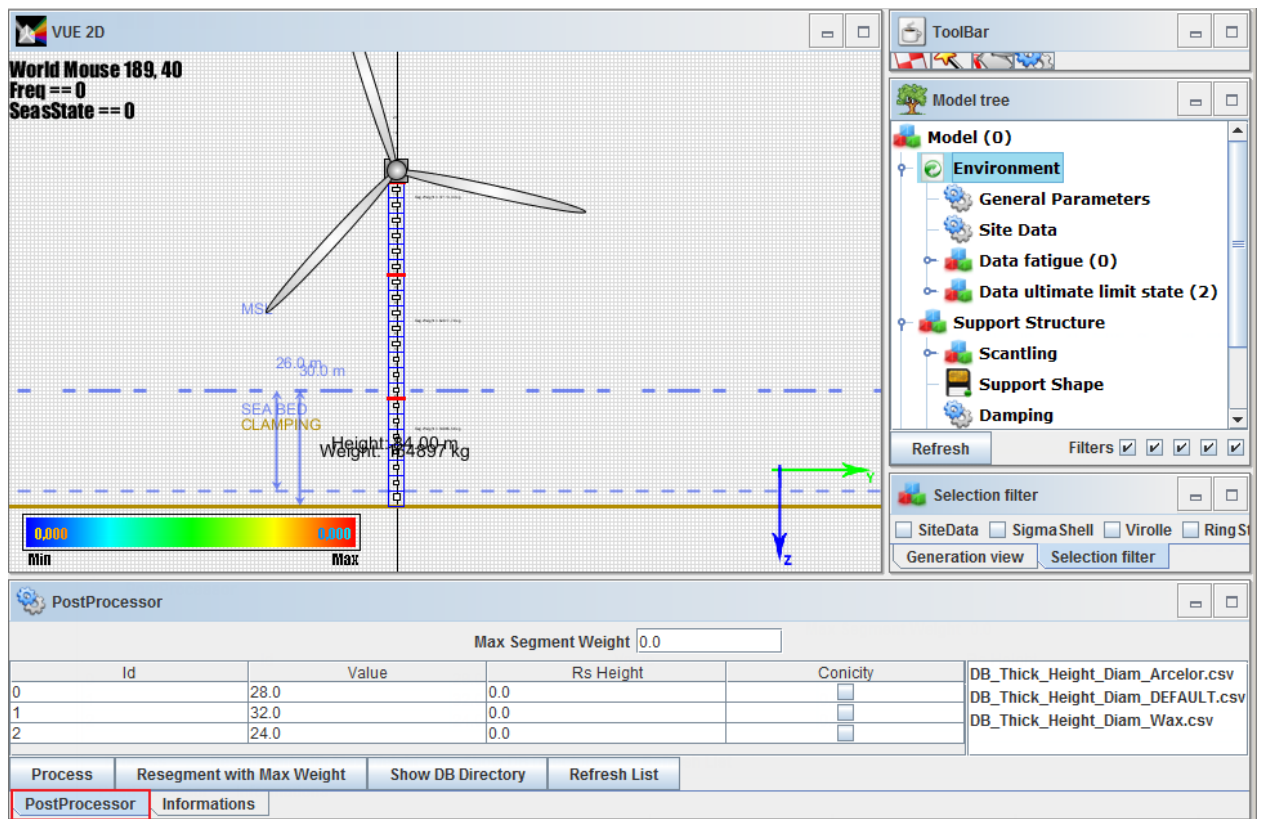


Figure I.11: The interface of the software EOL OS

1.3. Which type of foundation should be chosen?

As mentioned above, there are many types of foundations currently used, depending on geological and environmental conditions, as well as the type of wind turbine. In order to create a module for “Design and optimization of the structural foundation of offshore wind turbines”, all types of offshore foundation should be investigated and designed. However, in the framework of a master thesis, the research will mainly focus on monopile foundations.

1.4. Tasks of the thesis

Having the title: “Design monopile foundations for offshore wind turbines” this thesis will concentrate on design the structure part below water surface of offshore wind turbines, which is called foundation pile (see Figure II.1). The tasks of the thesis seem quite clear:

- To determine the dimensions of the pile basing on ULS and SLS:
 - o Penetration length,
 - o Diameter,

- Wall thickness.
- To find the optimized wall thickness of the foundation pile
- To assess the necessity of including foundation part in structure analyses of the whole OWT structure.

1.5. Method to carry out

- Dimensioning the foundation pile will be done by using DET NORSKE VERITAS STANDARD (DNV-OS-J101, 2011).
- After preliminarily having dimensions of the foundation pile, using FEM (SAP200 software) to model the whole structure with plasticity behavior of the soil (nonlinear p-y curves) and carry out time-history analyses to see the behavior of the whole structure under cyclic loading. The stiffness of the foundation will be modified to fulfill requirements of the manufacture in working ability of the turbines.

1.6. Structure of the thesis

The structure of the thesis consists of 7 chapters:

- Chapter 1: Introduce the foundations of offshore wind turbine, the context of the thesis and its tasks.
- Chapter 2: Components of a monopile offshore wind turbine structure, their fabrications and installations.
- Chapter 3: Design methodology. In this chapter design objectives, design process, and design criteria will be explained.
- Chapter 4: Related theories. In this chapter the theories of wind load, wave load, dynamic analysis, and soil model are reviewed.
- Chapter 5: Preliminary design for the chosen offshore wind turbine project. In this chapter all the input information for the chosen offshore wind turbine project will be shown. Design optimization of the tower will be done using EOL-OS software. The output of this chapter is internal forces of the tower at the seabed elevation, which will be used in ultimate limit state design of the foundation pile in the following chapter.
- Chapter 6: Foundation pile design. In this chapter the dimensions of the foundation pile will be determined using ultimate limit state. Afterwards, the suitability of its stiffness will be checked using serviceability limit state. Finally, the effect of foundation as well as the p-y curve in the dynamic behavior of the structure will be analyzed.
- Chapter 7: Conclusions and Future works

Chapter II. Support structure of monopile OWTs - components, fabrication and installation

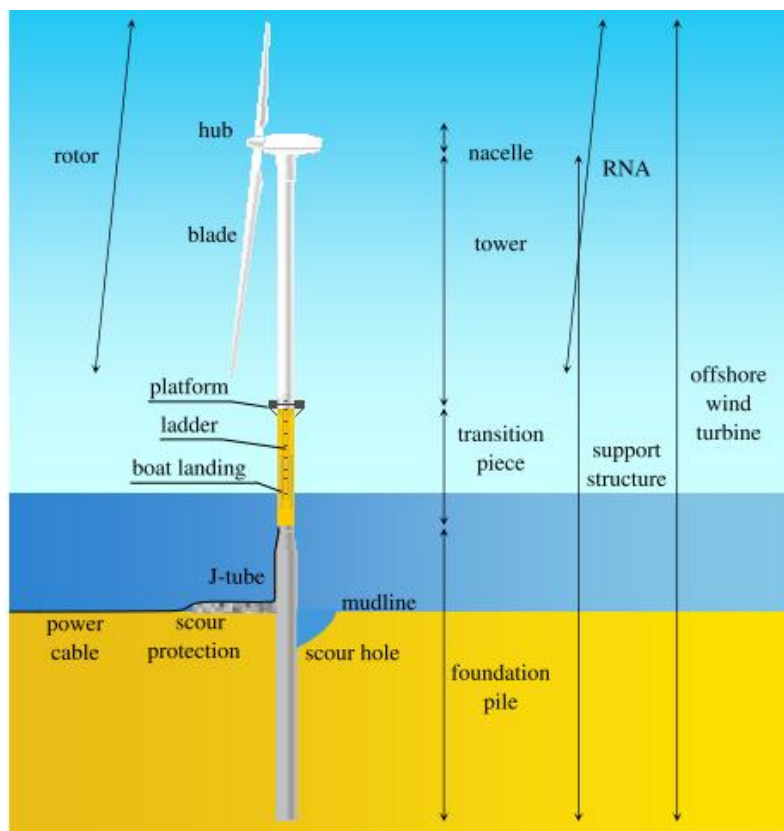


2.1. Introduction

A general knowledge of foundation piles as well as the whole OWT structure is necessary at the beginning of the pile foundation design. This chapter is devoted to survey main components of an OWT structure, how they are fabricated and their installation.

The contents are divided into four sections. Section 2.2 introduces briefly how an OWT works. As the foundation pile is a part of support structure, all the components of support structure will be surveyed to see their relationships with it in Section 2.3. The next section describes fabrication of foundation pile. Section 2.5 surveys the installation processes of all the components. It is very important when considering stabilities of foundation pile during construction phase.

2.2. How it works?



Once a suitable place for the wind facility is located, piles are driven into the seabed. For each turbine, a tower is installed on the pile foundation for supporting the turbine assembly, for housing the remaining plant components and for providing sheltered access for personnel. A matrix of fiber glass mats impregnated with polyester or epoxy is used for making the rotor blades. The turbine usually consists of a rotor with three blades, connected through the drive train to the generator. After the turbine is assembled, the wind

direction sensors turn the nacelle to face into the wind and maximize the amount of energy collected (see Figure II.1). The nacelle is the part that encloses gearbox, generator, and blade hub. The wind moving over the blades makes them

rotate around a horizontal hub connected to a shaft inside the nacelle. This shaft, through a gear box, powers a generator to convert the energy into electricity.

2.3. Components of the support structure

2.3.1. Definitions

The support structure is made up of three main components: the tower, the substructure and the foundation.

Tower	The tubular elements(s) supplied by the turbine manufacturer on top of which the turbine is installed
Substructure	The part of the structure extending from the bottom of the tower down to the seabed
Foundation	The part of the structure in direct contact with the soil, transferring the loads from the structure to the soil

Refer to Figure II.1, for the monopile support structure, its substructure consists of a transition piece and the above ground part of the foundation pile.

2.3.2. Design elevations

To facilitate communication between different parties involved in the design of an offshore wind turbine, two key elevations must be defined:

- First the interface level is set. The interface level represents the interface between the turbine manufacturer's responsibility and that of the support structure designer in both a physical and an organizational sense. The interface level is located at the connection between the tower and the substructure. The elevation is chosen such that the main platform, which is generally situated at the level of the flange connection with the tower, cannot be hit by waves under extreme conditions.
- The other elevation that must also be defined is the hub height. The hub height is the elevation at which the hub of the turbine is located.

2.3.3. Support structure components

a. Foundation pile

Foundation piles of a monopile offshore wind turbine are open-ended hollow tubular elements that are installed vertically. Lateral loads are transferred to the soil by activating the horizontal active soil pressure, whereas axial loads are taken by shaft friction and end bearing.

b. Secondary steel items

The substructure usually comprises several secondary items to enable access, export of electricity and for protection of the structure itself. For a monopile support structure, following items will be present:

- Boat landings
- Ladders
- Platforms

- J-tubes
- Anodes

Boat-landing:	The boat-landing is the structure to which a vessel can moor to transfer personnel and equipment to the substructure. The boat-landing consists of two mainly vertical fenders connected by stubs to the main structure. Depending on the environmental conditions and on the maintenance strategy of the operator, there may be one or more boat-landings connected to a support structure.
Ladders:	Ladders are required to allow personnel to access the main platform. If the distance to cover is larger than a certain limit, the ladder should be covered by a cage and have facilities for attaching fall arresters. Ladders for access to the main platform are usually combined with the boat-landing to provide protection for transferring personnel and to avoid difficult and dangerous steps to access the ladder from the vessel.
Platforms:	Platforms are intended as safe working areas for personnel that need to work on the structure. Different functions can be identified; there are access platforms, resting platforms, and depending on the type of structures service platforms and airtight platforms. Platforms on offshore wind turbines are usually equipped with grating, to prevent excessive (air) pressure build up below the platform due to passing waves and to avoid accumulation of water that would render the floor slippery.
J-tubes:	To protect and guide the export cable into the support structure, a J-tube is installed on the structure. The name derives from the shape that the tube makes as it curves to a horizontal orientation near the seabed. J-tubes can be either internal, only to protrude from the substructure at the seabed level, or external.
Anodes:	To provide cathodic protection against corrosion, blocks of aluminum may be installed as sacrificial anodes.

2.4. Fabrication

For a monopile support structure the production process for support structures starts with creating the primary elements for the foundation pile and for the transition piece. Sheets of steel produced at a steel mill are delivered at the fabrication yard. Each sheet has been produced to the required dimensions for a particular tubular section.

The edges of plate are beveled in preparation for welding. Subsequently the sheets are rolled into tubular sections. Several tack welds hold the ends of sheet together while the section is further prepared for welding. This includes welding on endplates at both ends of the longitudinal weld to ensure that no impurities end up in the welded joint.

The tubular section is welded at the seam from two sides. Whenever possible the welding is done in an automated process. The welds are ground if required to reduce stress concentrations. Tolerances with respect to out-of-roundness and eccentricities are checked and the quality of the weld is ascertained by nondestructive testing, after which the section is ready for assembly.



Figure II.2: Rolling and welding of a foundation pile

The sections are aligned into the predetermined order. Before welding can commence the edges of two adjoining sections are cut into the required weld shape. After preheating the steel surrounding the joint the two sections are welded together. This can be done automatically by rotating the pile while the welding machine remains stationary. Again, welds must be ground and tested.

When all sections are assembled, the primary structure is ready. For the foundation pile it may be required to attach lifting trunnions at the pile top to facilitate upending in the installation phase. Furthermore, when internal J-tubes are applied, holes must be cut in the pile near the seabed level for the tubes to exit. Also, to ensure proper bonding at the grout to steel interface after installation, shear keys may have to be welded at the location of the grout overlap.

Several items are still to be attached to the transition piece. The flange at the transition piece top to which the tower will be bolted is welded on top of the transition piece. Care must be taken to ensure that the transition piece is perfectly round when the flange is attached, as current large diameter structures have a tendency to ovalise under their own weight. Stubs with flanges to which the boat-landings and platforms can be connected at a later stage are welded to the primary structure. Brackets for the attachment of ladders and anodes are also welded onto the structure. The grout skirt at the bottom of the transition piece is attached and supports for the main platform are welded onto the structure. Before the coating can be applied, the surface of the structure is prepared by shot blasting. The structure is subsequently coated in a partly automated process.

Subsequently internal platforms are installed. If the J-tubes are internal, they are installed at this time as well. The J-tubes are not yet extended downwards to their full extent, as the transition pieces are transported upright. The final actions to be performed are the mounting of the main platform, the attachment of the boat-landing, resting platform and ladders and the attachment of a rubber grout seal at the base of the transition piece.

2.5. Installation

The installation process varies significantly for the different support structure concepts. Monopile foundations may be transported to site by feeder barge, on the installation vessel itself or by floating the piles out to the site. Subsequently the pile must be upended, lifted into position, aligned and driven or drilled into the seabed. The next step is to install the transition piece onto the foundation pile. It is subsequently leveled and fixed by means of grouting the annulus between the pile and transition piece.

The turbine tower is installed, generally in two pieces and bolted. Finally the rotor-nacelle assembly is installed, sometimes with two blades pre-attached and lifting the final blade in place separately or by installing the nacelle first and the pre-assembled rotor later.

In general, the installation procedure of a monopile offshore wind turbine follows the steps as listed below. However, it should be noted that in some cases a slightly different approach may be adopted. For instance, it may be decided that scour protection may not be required. It is also possible to install the nacelle with (some) blades attached.

- Foundation pile
- Scour protection
- Transition piece
- Turbine tower
- Nacelle
- Rotor/blades

a. Foundation pile

Installation of a foundation pile can be done by driving or by drilling.

- Driving

The most common way is to install the pile by driving. The foundation piles are delivered to the offshore site on a barge, usually several at a time. The pile is lifted off the barge using a crane fitted with a lifting tool. The pile is lowered onto the seabed. The weight of the pile will usually cause the pile to penetrate the soil for a few meters. The pile is gripped with an alignment tool at a certain distance above the sea surface to ensure verticality of the pile during driving.



Figure II.3: Pile driving at Offshore Wind Farm Egmond aan Zee

The hammer is lifted onto the pile, after which the pile driving can proceed. If required, driving can continue when the hammer is under water. Usually depth markings are applied to the pile before driving so that the penetration depth can be monitored visually. Driving can be done from a jack-up barge or from a stable floating system, although it should be noted that a floating system is very much dependent on favorable sea conditions.

- Drilling:

When hard soils are encountered, drilling may be the preferred option. A hole is drilled at the desired location using a drilling tool operated from a jack-up barge. The pile can subsequently be inserted in the thus created hole. Alternatively, the pile is placed on the seabed and the drilling tool is



Figure II.4: Drilling equipment at Blyth

inserted in the pile. The hole is drilled through the pile, while the pile is slowly lowered into the newly excavated space. The pile is aligned vertically using an alignment tool. Subsequently the pile is fixed in place by injecting grout into the space between the pile and the soil. During hardening of the grout the pile must be held in place to maintain the vertical alignment. When a foundation pile is installed by means of drilling the appurtenances can be pre-attached directly to the pile.

Also the flange to which the turbine can be connected can be attached. In that case there is no need for a transition piece, reducing the number of offshore operations.

b. Scour protection

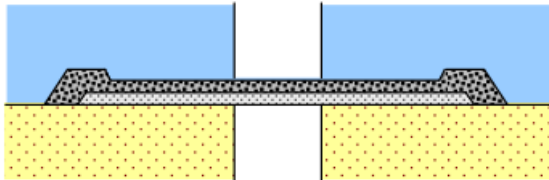


Figure II.5: Schematic example of scour protection

If a pile is situated in a current, the current is locally increased due to the disturbance in the flow caused by the presence of the pile. In combination with wave action this can cause sand particles to be picked up from the seabed and deposited further downstream. Eventually this can lead to a significant scour hole around the pile.

To prevent this scour protection can be applied.

An example of a scour protection design is given in Figure II.5. This is generally in the form of a filter layer of relatively small stones to keep the sand in place on top of which an armor layer is dumped consisting of larger rocks to keep the filter layer in place. The scour protection is installed with the use of dedicated rock-dumping vessels.

With respect to installation two different approaches can be envisaged: static scour protection and dynamic scour protection.

- Static scour protection:

In the case of static scour protection, the filter layer is put in place prior to installation of the foundation pile. The pile is subsequently installed through the filter layer. Once the pile is in place the armor layer is applied. This approach is aimed at preventing the occurrence of a scour hole during the installation process.

- Dynamic scour protection:

When using dynamic scour protection the foundation pile is installed first. Only after the foundation installation is complete the scour protection is installed. Usually the scour protection is installed in one procedure for the entire wind farm. This implies that the installation of the scour protection is commenced once (almost) all of the piles have been installed. In this case it is likely that

a scour hole will develop before the protective rock layers are installed. The scour protection then partially fills the scour hole.

- **No scour protection:**

Alternatively, it is possible to install an offshore wind farm without any scour protection. In this case the development of a large scour hole is taken into account in the design.

c. Transition piece



Figure II.6: Transition piece installation

The transition piece sits on top of the foundation pile. Its main functions are to provide a flange for the connection of the turbine tower to the foundation, to correct any misalignment of the foundation and to hold the appurtenances, such as the boat-landing, J-tube, ladder and anodes. A platform is located on top of the transition piece. The transition piece can be connected to the foundation in the following three ways: using grout, a flange or slip joint. Transition pieces can be transported to the offshore location by barge along with the foundation piles. Alternatively, they can be carried by the installation vessel.

- **Grout connection**

This is the most common way to make the connection between the foundation and the superstructure. The transition piece is lifted from the barge and is slid over the top of the foundation pile. Spacers ensure that the required space remains between the pile and the transition piece. Hydraulic jacks are used to align the transition piece vertically. Grout seals close off the bottom of the annulus between pile and transition piece, after which the annulus is filled with grout. After the grout has hardened sufficiently the seals and jacks are removed.

- **Flange**

The transition piece can also be connected to the foundation pile by means of flanges. The transition piece is lifted into place. Once the flanges are correctly aligned, bolts are used to connect the flanges. This procedure has the advantage that it can be performed quickly. However, great care must be taken to ensure that the flange is not damaged during pile driving.

- **Slip joint**

A novel way of connecting two tubulars is by means of a slip joint. Both the top of the foundation pile and the bottom of the transition piece have a conical section of which the sides make a small angle with the vertical. The transition piece is lifted onto the foundation pile. Before the transition piece is slid into place, it must be ensured that it is exactly vertical. Once this is achieved the connection can be made by simply lowering the transition piece onto the foundation pile. The friction between the conical sections of the foundation pile and the transition piece due to the weight of the transition piece

is sufficient to form a reliable connection. The advantage of this connection type is that it is simple to fabricate and allows for rapid installation. However, so far it has not been put to use for offshore wind turbines.

d. Turbine tower



Figure II.7: Lifting of a tower section for installation

The turbine tower is usually installed in two or three sections which are bolted together. Figure II.7 shows such a tower section being lifted for installation. The connection between the transition piece and the turbine tower is also made by bolting two flanges together.

e. Rotor-nacelle assembly

The rotor-nacelle assembly can be installed either separately or using the Bunny-Ear method. It should be noted that each turbine installation contractor has its preferred method.

- Separate



Figure II.8: Installation of a rotor in one piece

The nacelle is lifted onto the top of the turbine tower. The flange beneath the yaw bearing of the turbine is bolted to the flange at the tower top when the nacelle is in place, the hub and the blades can be installed. These can be installed in one piece – the rotor assembly as shown in Figure II.8, or separately. The blades are lifted in a frame that allows for easy manoeuvring. With

the blade in a vertical position and with the blade root pointing upwards, the blade is carefully positioned in line with its connection point on the hub. The connection is achieved by bolting the blade to a flange in the hub. This procedure is repeated until all blades are connected.

- Bunny-Ear method

In case of a triple bladed turbine two blades can already be attached onshore. These blades protrude upwards at an angle giving the rotor-nacelle assembly an appearance which has led to the method's distinct name. The advantage is that the rotor-nacelle assembly can be lifted into place with two blades already attached. Only one blade needs to be installed offshore, saving a lot of valuable offshore installation time.



Figure II.9: Various stages in the installation of a turbine using the bunny-ear method

Chapter III. Design Methodology



3.1. Introduction

In this chapter, the contents are divided into three sections. Section 3.2 emphasizes the design objective of the foundation pile in relation with the support structure. The next section is about the design process for offshore wind turbine support structures. Finally, in Section 3.4, design criteria are defined based on requirements to keep OWTs stable and work efficient.

3.2. Design objective

Before formulating a design objective the context of a support structure should be considered. The support structure can be seen as a part in the larger offshore wind farm development. For the offshore wind farm development the objective is to produce electricity at the lowest possible cost per produced kWh. To achieve this objective the energy yield should be as high as possible, while the costs of the overall development should be as low as possible.

For the individual components, such as the support structure this implies that the costs of the component should be as low as possible, without jeopardizing up-time.

The purpose of a support structure is to hold the wind turbine in place allowing it to produce electricity in a safe and reliable manner, such that the highest possible energy yield can be achieved. Therefore the offshore wind turbine should be able to:

- Withstand all loads during envisaged lifetime
- Remain operable in all intended operational conditions

Furthermore the structure should be able to fulfill all secondary functional requirements, such as accessibility and electricity export, while at the same time posing no threat to the environment and other users of the marine environment.

The objective of the design is therefore to define the geometric and material properties of the support structure, subject to requirements regarding the operability of the wind turbine, load resistance and economics.

3.3. Design process for offshore wind turbine support structures

3.3.1. Design Sequence

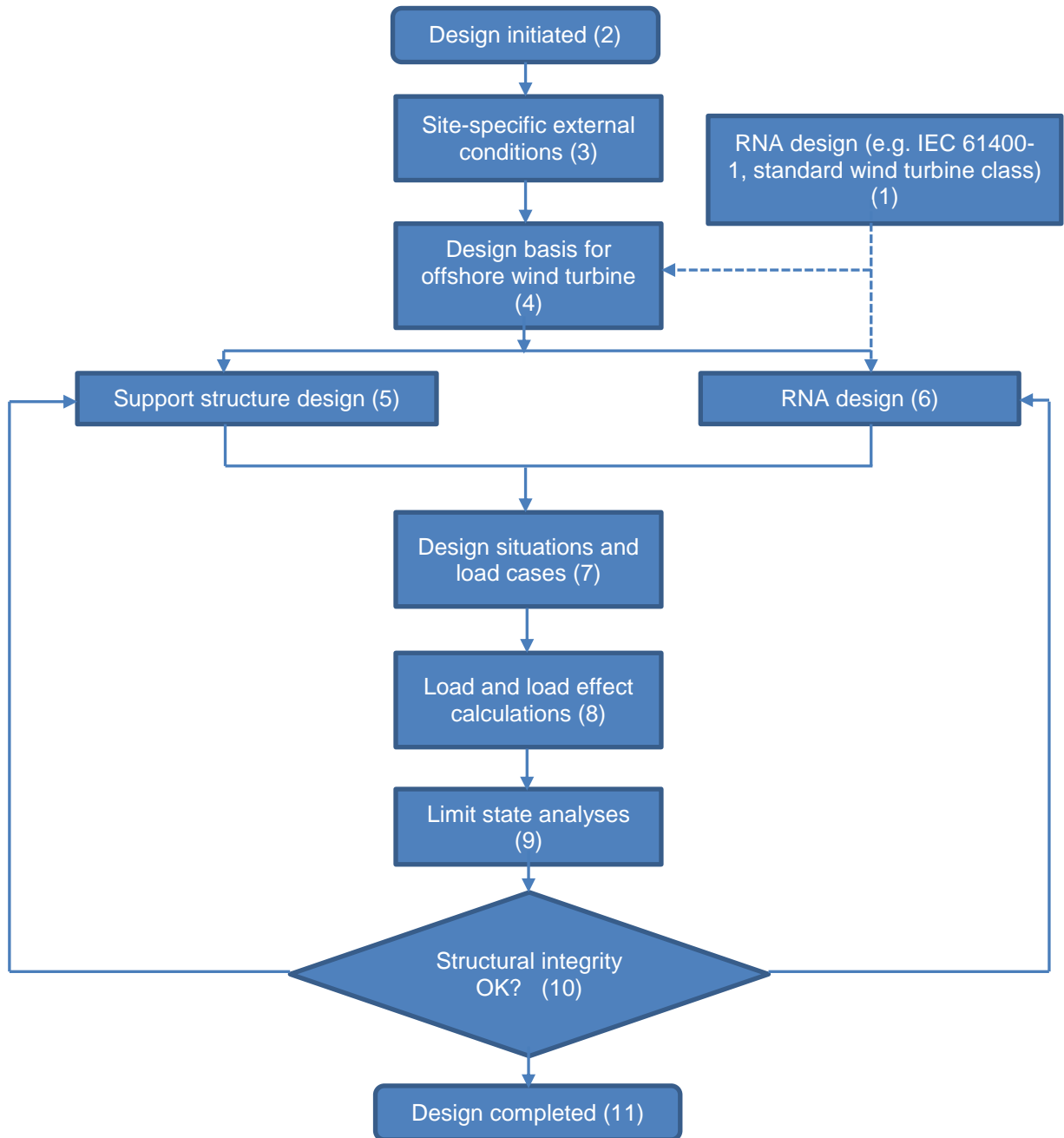


Figure III.1: Design process for an offshore wind turbine

According to (IEC, 2009) the design process for an offshore wind turbine is as depicted in Figure III.1. This process is defined for a complete offshore wind turbine system, including Rotor Nacelle Assembly (RNA). It assumes that the RNA is designed according to a standard wind turbine class (1) and as such has been type certified by a certification body. Once the design has been initiated (2) for a specific project, the external conditions for the project site must be defined (3). These include site-specific environmental data, local bathymetry, geotechnical information and other relevant oceanographic data. To allow different parties in the project to work with the same data, the

environmental conditions together with the design criteria for the RNA are recorded in a design basis (4). The design basis itself has to be certified by a certification body.

To be able to apply a type certified turbine at a specific offshore site it must be demonstrated that the RNA still meets the design criteria for the site-specific loads. In the current industry practice the verification of the RNA design (6) will be the responsibility of the wind turbine manufacturer, whereas the support structure design (5) is the responsibility of the support structure designer.

The design process as illustrated in Figure III.1 assumes that the support structure design and verification of the RNA are performed in parallel. Both structures are modeled in structural analysis packages that can account for dynamic response of the structure to external loading. Preferably this entails a fully integrated analysis, but current industry practice also makes use of parallel models in which the interaction between RNA dynamics and the support structure dynamics as well as interactions between aero- and hydrodynamics and the structural response are taken into account.

3.3.2. Design Load Cases

When an initial support structure has been established, a series of Design Load Cases must be defined (7). Different design situations can be identified covering all expected operational situations as well as fault situations. These design situations are defined as follows in the standards for the design of offshore wind turbines (DNV-OS-J101, 2011), (IEC, 2009):

1. Power production
2. Power production plus occurrence of fault
3. Start-up
4. Normal shut-down
5. Emergency shutdown
6. Parked (standing still/idling)
7. Parked and fault conditions
8. Transport, assembly, maintenance and repair

For each of the defined load cases, loads and load effects are calculated (8). This usually entails time domain simulation of the wind and wave loads on a dynamic structural model, including the aero-hydro-servo-elastic behavior of the turbine. The load effects are given by the response of the turbine to these loads in terms of displacements, velocities, accelerations and section forces at the nodes in the structural model.

3.3.3. Limit State Checks

Once the load effects for each of the simulated design load cases have been determined the limit state analyses are performed (9). For different limit states are distinguished:

- Ultimate limit state (ULS)
- Serviceability Limit State (SLS)
- Accidental Limit State (ALS)
- Fatigue Limit State (FLS)

The ALS and FLS are sometimes considered part of the ULS analysis.

In the ULS analysis, the structural strength of members and joints as well as the stability of members are checked. Also the strength of the foundation must be verified.

The SLS is related to maximum acceptable deformations of the structure, the foundation and the RNA during operational conditions.

For the ALS the effects of unintended impact loads such as ship impact and impacts due to dropped objects are evaluated.

Finally, the ability of the structure to withstand the combined environmental loading over its intended design life must be verified in the FLS analysis.

The results from these limit state analyses are usually expressed as a utilization ratio, defined as the design load divided by the characteristic resistance. A utilization ratio larger than 1.0 implies that the structure has insufficient resistance to withstand the design load. If the utilizations for all load cases are less than 1.0 the structural integrity is guaranteed (10) and, according to Figure III.1 the design is completed (11). If for some load cases the utilization is larger than 1.0 the structural integrity of the system is not assured and changes to the support structure or the RNA must be made resulting in lower utilizations for the critical load cases. To this end either the loads may be reduced or the resistance of the structure may be increased.

To achieve either load reduction or increased resistance, the support structure design and the RNA design are revised. In some cases the design load cases will have to be redefined, for instance when a more detailed description of the Design Load Cases may lead to less conservative loads and hence lower loads on the structure or RNA. Subsequently the load simulations are performed once again and the limit state checks are executed. This process is repeated until both the support structure and the RNA design meet the design criteria for all considered load cases and for all limit states.

3.3.4. Design evaluation

Figure III.1 considers the design process to be complete when the structural integrity is shown to be satisfied. If this is the only requirement very robust designs may result. Economic considerations should also be taken into account, such that the contribution of the support structure and RNA to the total cost per produced kWh is minimal. Besides checking whether the structural integrity of the structure is guaranteed, it should also be ascertained if further reduction of the overall cost is possible. Primarily this will be achieved by reducing the mass of the structure, thereby reducing the overall material costs. However, it should also be verified that reducing the mass of the support structure does not introduce unforeseen costs in other parts of the structure or for fabrication installation and maintenance issues. To reflect the economic considerations the process shown in Figure III.1 should be updated to include a check for the minimum structure mass and costs. If the structural mass can be further reduced the dimensions should be changed and the structural integrity should be checked again. Only when the mass of the structure can be reduced no further without compromising the structural integrity the design may be considered completed.

3.4. Design criteria

3.4.1. From requirements to criteria

In Section 3.2 the design objective is formulated as defining the geometric and material properties of the support structure subject to requirements regarding the operability of the wind turbine, load resistance and economics, thereby allowing safe, reliable and economical operation of the wind farm. To assess the suitability of the support structure design, it should fulfill certain design criteria. These criteria are related to the requirements for the wind turbine and for the support structure itself. For the wind turbine the following requirements are considered:

- The turbine should be situated at a certain elevation above the sea surface, for effective electricity production and to ensure sufficient safety
- The electricity produced by the generator must be fed into the electricity grid. For this purpose provisions for the exporting of the electricity must be incorporated.
- To allow reliable operation the turbine must regularly undergo maintenance and repair. Therefore provisions must be present for accessing the turbine.
- Sufficient clearance between the blades and the support structure must be maintained to reduce loads on the turbine and to avoid collision of the blades with the structure.
- To avoid damage to components in the wind turbine the tower head motions should be within predefined limits.

The support structure should ensure that all aforementioned requirements are fulfilled. Furthermore the structural integrity of the support structure must be guaranteed. Therefore the support structure must be able to withstand all loads from the wind turbine and from the environment onto itself and to transfer these loads to the soil.

To satisfy these requirements criteria can be formulated regarding natural frequencies, strength and deformations. In the following sections these criteria are discussed for the main components making up the overall support structure: tubular members, joints and foundation elements. Also requirements and criteria with regard to fabrication and installation are put forward.

3.4.2. Natural frequencies

Natural frequencies of the support structure are very important as they determine the dynamic behavior of the offshore wind turbine. If the frequency of excitation is near a natural frequency, resonance occurs and the resulting response will be larger than in the quasi-static case. This leads to higher stresses in the support structure and, more importantly to higher stress ranges, an unfavorable situation with respect to the fatigue life of the offshore wind turbine. Therefore it is important to ensure that the excitation frequencies with high energy levels do not coincide with a natural frequency of the support structure.

In the case of an offshore wind turbine excitation is due to both wind and waves. For fatigue considerations sea states with a high frequency of occurrence have the largest effect. These are

generally relatively short waves with a significant wave height H_s of around 1 m to 1.5 m and a zero-crossing period T_z of around 4 s to 5 s.

The wind excitation frequencies that should be avoided are those that coincide with the range of rotational frequencies of the rotor. This will be illustrated for the chosen 7MW turbine which will be used during subsequent stages of this project. With a minimum rotational speed at the cut-in wind speed of 4(1/min) and a maximum rotational speed of 14.2(1/min), the rotational frequency interval ranges from 0.067 Hz to 0.237 Hz. This interval is indicated with 1P. Furthermore, the blade-passing frequency interval should also be avoided. This interval, indicated with 3P for a triple bladed turbine is equal to the rotational frequency interval times the number of blades, this value ranges from 0.2 Hz to 0.71 Hz.

3.4.3. Strength criteria

Yielding

Stresses in elements must remain below the yield stress for metallic materials. Wind loads, wave loads, gravity and inertia loads and pressure differences between inside and outside of element (hoop stresses) all contribute to the acting stress in the element.

Buckling may occur before the full yield capacity of a cross section is reached. For foundation piles, buckling is generally not considered a critical failure mode as the pile is normally supported by the soil on both the inside and outside. Pile strength should be checked under extreme compression loads.

Buckling

For monopiles the wall thickness can vary along the length of the pile as the bending moment increases from the top of the tower toward the seabed due to hydrodynamic and aerodynamic loading and then decreases as load is gradually transferred to the soil.

The wall thickness should be sufficient to prevent buckling. Two forms of buckling can be identified: global or beam buckling and local or sheet buckling. In the case of global buckling the structure collapses in its entirety, whereas in the case of local buckling the buckling occurs only locally. However, the occurrence of local buckling may initiate global buckling. The most important parameters in the buckling analysis are:

- The buckling length, which is different for local and global buckling,
- The normal force in the structure or element under consideration,
- The bending moment in the structure or element under consideration,
- A slenderness parameter

The outcome of the buckling check is a usage factor, which indicates to what extent the cross section is utilized with respect to the buckling capacity. This value can be used to optimize the wall thickness. Furthermore, the top of the pile usually requires a large wall thickness to cope with the high

stresses due to pile driving. The pile toe is usually also dimensioned with a larger wall thickness to prevent buckling during pile driving.

Fatigue

As the support structure is subjected to continuous load variations, the fatigue of the structure needs to be checked. Preferably all load combinations of wind and waves with their directions are incorporated in this check. But as the number of load cases is usually very large, it is desirable to use a reduced number of load cases. This can be achieved by two methods, preferably simultaneously. The first is by assuming that all loads act in the same direction. This approach is conservative as it leads to an accumulation of fatigue damage in a single location on the circumference of the pile. This is only valid in the power production state. For idling states (non-power producing states with unlocked rotor) wind-wave misalignment may result in higher loads than when wind and waves are aligned. The main reason for this is the lack of aerodynamic damping. Idling situations occur below cut-in and above cut-out but may also occur within the range of power production, due to non-availability of the wind turbine due to turbine errors. Therefore, the portion of idling state simulations must consider wind-wave misalignment for the fatigue analysis of the support structure, especially for monopiles.

In reality, the fatigue damage is lower than estimated by the first method, as the damage is spread over multiple locations on the circumference. In the second method, all the environmental states in a wind speed bin are grouped. The corresponding H_s and T_z are associated with the state within the wind speed bin with the largest probability of occurrence.

The probability of occurrence of the grouped state is the summed probability of all contributing states. Sometimes it may be more realistic to group the environmental states in a wind speed bin into two or more grouped states. Either way, the resulting number of environmental states that serve as input for the fatigue analysis is significantly reduced.

For each of these environmental states a time domain simulation is performed and the bending stresses in the support structure are recorded. Near the welds, where there are discontinuities in the structure, the local stress should be multiplied by an appropriate stress concentration factor. Using a stress cycle counting method, the number of cycles in each stress range bin is counted. With this information and using an S-N curve corresponding to the weld detail under consideration the fatigue damage due to environmental loads can be determined. Furthermore, fatigue damage due to transient events such as start-up and shutdown procedures and fatigue damage due to pile driving should be included in assessing the total fatigue damage.

3.4.4. Design criteria for monopile foundations

For geotechnical design of monopile foundations, both the ultimate limit state and the serviceability limit state shall be considered.

a. Design for the ultimate limit state

For the design of the ultimate limit state, design soil strength values are to be used for the soil strength (R_D), defined as the characteristic soil strength values (R_k) divided by the specified material factor (γ_M):

$$R_D = \frac{R_k}{\gamma_M} \quad (3.1)$$

According to (DNV-OS-J101, 2011), the material factors (γ_M) is given as following table:

Table III.1: Material factors

Type of geotechnical analysis	Limit states	
	ULS	SLS
	γ_M	γ_M
Effective stress analysis	1.15	1.0
Total stress analysis	1.25	1.0

Each design load (S_D) is defined as the characteristic load multiplied by the relevant specified load factor. The loads are to be representative of the extreme load conditions (see (DNV-OS-J101, 2011)).

The safety level of the foundation in ULS is considered to be satisfactory when the design load does not exceed the design soil strength:

$$S_D \leq R_D \quad (3.2)$$

Two cases are to be considered:

- Axial loading
- Combined lateral loading and moment loading

Axial loading

For axial loading in the ULS, sufficient axial pile capacity shall be ensured by checking that the design axial load on the pile head does not exceed the design axial resistance, obtained as the design unit skin friction, integrated over the pile surface area, plus a possible pile tip resistance.

The effects of cyclic loading on the axial pile resistance should be considered in design. The main objective is to determine the shear strength degradation, i.e. the degradation of the unit skin friction, along the pile shaft for the appropriate prevailing loading intensities.

Combined lateral loading and moment loading

For combined lateral loading and moment loading in the ULS, sufficient pile capacity against this loading shall be ensured. The pile capacity is formed by lateral pile resistance. Verification of sufficient pile capacity implies that the following two requirements shall be fulfilled:

- (1) The theoretical design total lateral pile resistance, which is found by vectorial integration of the design lateral resistance over the length of the pile, shall not be less than the design lateral load applied at the pile head.
- (2) The lateral displacement at the pile head shall not exceed some specified limit. The lateral displacement shall be calculated for the design lateral load and moment in conjunction with characteristic values of the soil resistance and soil stiffness.

b. Design for the serviceability limit state

For design for the serviceability limit state, characteristic soil strength values are to be used for the soil strength. Characteristic loads are to be used for the loads. The loading shall be representative of loads that will cause permanent deformations of the soil in the long term, and which in turn will lead to permanent deformations of the pile foundation, e.g. a permanent accumulated tilt of the pile head. For this purpose, the behavior of the soil under cyclic loading needs to be represented in such a manner that the permanent cumulative deformations in the soil are appropriately calculated as a function of the number of cycles at each load amplitude in the applied history of SLS loads.

For design in the serviceability limit state, it shall be ensured that deformation tolerances are not exceeded. The deformation tolerances refer to permanent deformations.

3.4.5. Design requirements for manufacturing and installation

Beside the design requirements listed so far there are also numerous practical limitations to what can be produced and installed. From the review of the manufacturing and installation processes in Chapter 2 it could be seen that many handling and lifting procedures must be performed and that accessibility during the fabrication and installation phases is important. Also during the operational phase requirements can be set for accessibility for inspection.

Manufacturing

The first limitation encountered in the manufacturing process is the size of the plates that can be handled. This is usually linked to a maximum mass, defined by the capacities of the steel mills producing the plates. This means that the height of a section with a certain diameter and wall thickness is limited. Usually segments of up to 4m are used in monopile fabrication. This affects the number of welds that have to be made.

Furthermore the maximum thickness of plates that can be rolled may limit the design. Large diameter sections with high D/t ratios are susceptible to elastic deformation or ovalisation under their own weight. This may present additional costs during manufacturing. Therefore limits should be set for the maximum D/t ratios (see Section 6.2.3)

For the manufacturing of tubular joints, the angle between two connecting elements should not be less than 30° , to ensure that the joint is suitably accessible for welding.

Installation

Structural elements are designed for their in-place situation. However, during transport and installation loads act on the structure, for instance dynamic wave loads leading to deformations and accelerations during transport and bending moments in piles during upending. Structural elements should therefore also be checked for transport and installation load situations.

Although strictly speaking not a technical limitation, but more related to the economics and the availability of vessels is the lifting capacity of the installation vessel. The weight of components to be installed in one piece should not exceed the operational lifting capacity of a vessel that can be secured for the installation at an economically acceptable rate.

Pile driving equipment is currently limited to a maximum pile diameter that can be driven due to the limited size of anvils. The largest pile top diameter is currently 5.2 m (Vries, 2011).

The footprint of substructures and of piles on barges determines the number of structures that can be transported at one time, thereby influencing the logistics of the installation process.

It should be noted that the limitations mentioned in this section represent the current state of the industry. If the market requires the development of larger and more powerful equipment or facilities to increase cost effectiveness the industry will likely respond to meet this demand.

Chapter IV. Related Theories



4.1. Introduction

Although the main tasks of this thesis concerns the design of the foundation pile for offshore wind turbines, understanding of the dynamic behavior as well as excitation forces of the offshore wind turbines is essential beside the behavior of soil under cyclic loading.

The content of this chapter is divided into fourteen small sections, listed as following:

- Section 4.2: The basics of dynamics
- Section 4.3: Damping in offshore wind turbines structures
- Section 4.4: Sources of excitations
- Section 4.5: Statistical methods and Deterministic approach
- Section 4.6: Wind
- Section 4.7: Wave
- Section 4.8: Current
- Section 4.9: Combined Wind and Wave Loading
- Section 4.10: Effect of cyclic loading to foundation
- Section 4.11: Basis of Soil Mechanics
- Section 4.12: Types of Soil Model
- Section 4.13: Winkler model
- Section 4.14: Sap2000 and methods to solve a nonlinear dynamic analysis

4.2. The basics of dynamics

The importance of detailed modeling of the structural dynamics can be illustrated most conveniently by considering a single degree of freedom mass-spring-damper system, as shown in Figure IV.1. Note that a complete (offshore) wind turbine system can be thought of as being constructed of a number of coupled mass-spring-damper systems (Jan van der Tempel and David-Pieter Molenaar, 2004).

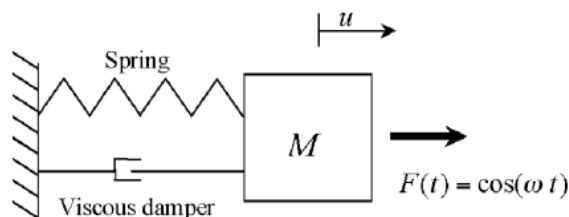


Figure IV.1: Single degree of freedom mass-spring-damper system

When a harmonic excitation force $F(t)$, i.e. a sinusoid, is applied to the mass, the magnitude and phase of the resulting displacement u strongly depends on the frequency of excitation ω . Three response regions can be distinguished:

- a) Quasi-static
- b) Resonance
- c) Inertia dominated

For frequencies of excitation well below the natural frequency of the system, the response will be quasi-static as illustrated in Figure IV.2 a: the displacement of the mass will follow the time varying force almost instantaneously, i.e. with a small phase lag, as if it were excited by a static force.

Figure IV.2 b shows a typical response for frequencies of excitation within a narrow region around the system's natural frequency. In this region, the spring force and inertia force almost cancel, producing a response that is a number of times larger than it would be statically. The resulting amplitude is governed by the damping present in the system.

For frequencies of excitation well above the natural frequency, the mass cannot "follow" the movement any longer. Consequently, the response level is low and almost in counter-phase, as illustrated in Figure IV.2 c. In this case the inertia of the system dominates the response.

It should be stressed, that in all three figures the magnitude of the excitation force $F(t)$ is identical, but applied at different excitation frequencies.

The normalized ratio of the amplitudes in Figure IV.3, illustrate the general fact that, in steady state, sinusoidal inputs applied to a linear system generate sinusoidal outputs of the same frequency, but differ in magnitude and phase (i.e. shift between the sinusoidal input and output).

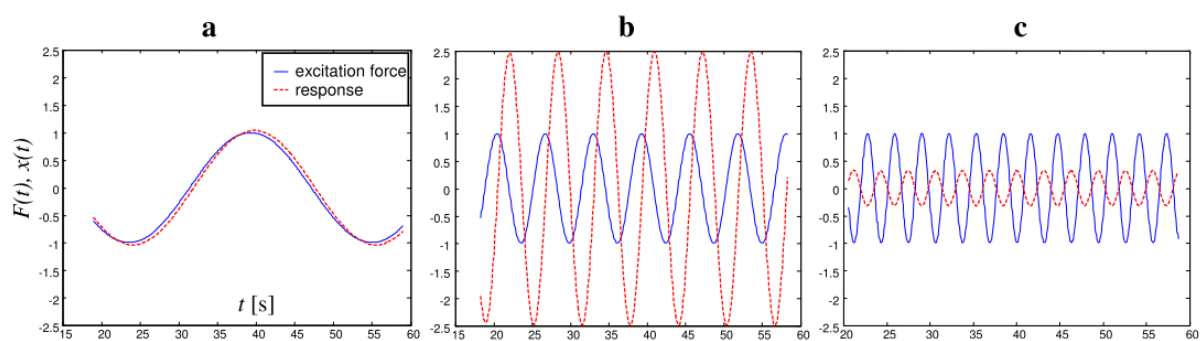


Figure IV.2: a) Quasi-static b) resonant and c) inertia dominated response
Solid line: excitation, dashed line: displacement

The magnitude and phase modifying property of linear systems can be conveniently summarized in one plot: the frequency response function. The frequency response function (FRF) depicts the amplitude ratio of the sinusoidal output to input, as well as the corresponding phase shift,

as a function of the frequency of excitation. Figure IV.3 shows the FRF of the single degree of freedom system depicted in Figure IV.1.

The peak in Figure IV.3 corresponds to the system's natural frequency. The height of the peak is determined by damping. Therefore any resonant problem can be counteracted with adequate damping controls, should the budget allow for it. In dynamics, the frequency of the force is at least as important as its magnitude. Resonant behavior can cause severe load cases, even failure, but it is most feared for fatigue difficulties. For structure where dynamics are expected to be a problem, detailed knowledge of the expected frequencies of the excitation forces and the natural frequencies of the structure, or parts of the substructure, is vital.

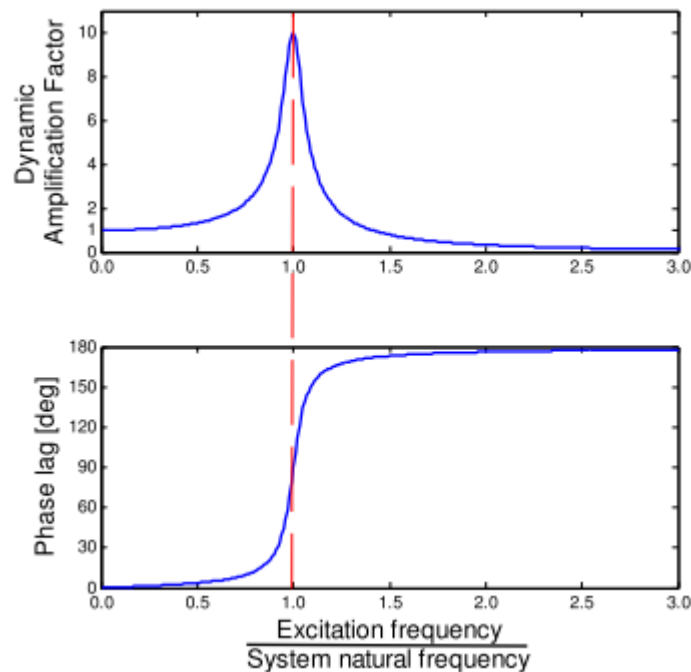


Figure IV.3: Frequency response function

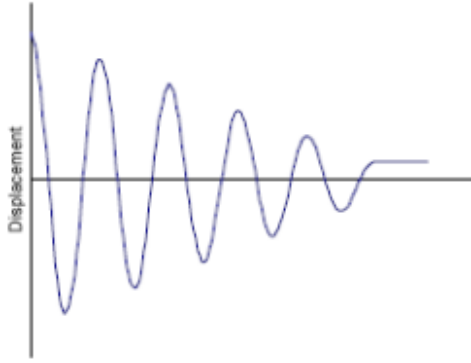
Upper figure: magnitude versus frequency, and lower figure: phase lag versus frequency

The “normalized amplitude ratio” is also known as the “Dynamic Amplification Factor” (DAF). The DAF is commonly used in calculations by the wind energy and the offshore technology communities, in the preliminary design phase, to account for the effect of dynamic loads from static response (thereby neglecting the phase information). In general, the required DAF’s are derived from time-domain simulations similar to the ones shown in Figure IV.3.

In rules given by classification societies (for example (GL, 2005)), extreme loads are generally multiplied by a dynamic amplification factor in order to take into account the modification of loads due to the motions of the structure. This factor depends on the hub height, the average tower diameter, the natural frequency of the structure and the average wind speed.

4.3. Damping in offshore wind turbines structures

4.3.1. Definition of damping



Damping is a phenomenon by which mechanical energy is dissipated (usually converted as thermal energy) in dynamic systems.

Representation of Damping in vibration analysis

For an n-DOF mechanical system, its motion is represented by vector x of n generalized coordinates x_i . Equations of motion expressed in vector-matrix form:

$$M\ddot{x} + d + Kx = f(t) \quad (4.1)$$

- M is mass (inertia) matrix
- K is Stiffness matrix
- $f(t)$ is forcing function vector
- d is damping force vector (nonlinear function of x and \dot{x})

Or this equation can be rewritten as:

$$M\ddot{x} + C\dot{x} + Kx = f(t) \quad (4.2)$$

where:

$$C = c_m M + c_k K \text{ - is damping coefficient.}$$

c_m - inertial damping matrix

c_k - stiffness damping matrix.

Usually, a parameter named damping ratio (ζ) is used to provide a mathematical means of expressing the level of damping in a system relative to critical damping:

$$\zeta = \frac{C}{C_c} \quad (4.3)$$

And the corresponding critical damping coefficient is: $C_c = 2\sqrt{K.M}$

There are three primary mechanisms of damping:

- Internal damping – of material
- Structural damping – at joints and interface
- Fluid damping – through fluid-structure interactions.

4.3.2. Damping for piled offshore support structure

The damping of offshore wind turbines significantly influences the turbine reaction and the dynamic loading. The overall damping of the first bending eigenvector frequency of wind turbine support structures consists of the aerodynamic damping, damping due to vortex shedding and due to constructive devices and additional damping, e.g. structural damping. Compared to onshore support structures, the additional damping is influenced by further effects, e.g. soft soil and hydrodynamic damping. As a result, the additional damping for offshore support structures is higher than for onshore support structures.

This additional offshore damping $\zeta_{add, offsh}$ (as fraction of critical damping) consists of:

$$\zeta_{add, offsh} = \zeta_{radiation} + \zeta_{vis, hydro} + \zeta_{steel} + \zeta_{soil} \quad (4.4)$$

With:	$\zeta_{radiation}$	Damping from wave creation due to structure vibration
	$\zeta_{vis, hydro}$	Viscous damping due to hydrodynamic drag
	ζ_{steel}	Material damping of steel
	ζ_{soil}	Soil damping due to inner soil friction

- **Damping from wave creation**

Radial propagation of waves from the oscillation of the structure results in highly frequency dependent damping that is proportional to the relative velocity between water and structure. $\zeta_{radiation}$ is considered in the Morison equation by accounting for the relative velocities. For cylindrical structures with slowly changing diameters in deep water, the linear potential theory may be applied according to (Micheal F.Cook and J. Kim Vandiver, 1982). For a structure of several meters in diameter as well as for a minimum diameter of $D=1.2$ m the result according to (Micheal F.Cook and J. Kim Vandiver, 1982) then is: $\zeta_{radiation} = 0.11\%$

- **Viscous damping**

The viscous damping of the fluid results from the relative velocity of the structure. As a drag force it is proportional to the square of the relative velocity, increasing non-linearly with that. $\zeta_{vis, hydro}$ is considered in the Morison by accounting for the relative velocities. The upper limit of the viscous damping for uni-directional sea states is according to (Micheal F.Cook and J. Kim Vandiver, 1982): $\zeta_{vis, hydro} = 0.15\%$

- **Steel damping**

The material damping of steel from internal friction is, as common in the literature, stated in (Micheal F.Cook and J. Kim Vandiver, 1982) as:

$$0.2\% \leq \zeta_{steel} \leq 0.3\%$$

Additional damping of the grouted connection is not considered.

4.3.3. Damping of soil (piled structure)

Soil damping consists of internal and geometric soil damping. Compared to all other damping contributions discussed, the internal soil damping is the most complex parameter having the highest damping contribution. The internal frictional soil damping depends on the material hysteresis, thus on the type of soil material. The geometric damping from wave creation of the structure in the soil (comparable to the wave creation of the structure in water) is of much less importance. In (Micheal F.Cook and J. Kim Vandiver, 1982) a value ζ_{soil} of 0.53% is experimentally determined whereas the

important to identify the exciting forces, and the resultant responses of the structure, completely with respect to their natural frequencies and the frequency of occurrence within the life of the structure. For this reason, statistical methods are particularly well suited to this task. This is, of course, also true because of the stochastic nature of wind turbulence. The two most important mathematical methods are known as the time-history method and the spectral method.

Time history method

If the time history of the active force is known, for example the variation of wind speed with time, the resultant response of the structure versus time can be calculated. This requires an aerodynamic model of the rotor, so that the variation of the aerodynamic force can be determined from that of the wind speed. Using the elastic structure model, the response of the structure over time is obtained.

The advantage of this method is that all parameters are time-dependent, a form of presentation which is advantageous for several purposes. Moreover, functional algorithms, for example for the influence of the control system, can be taken into consideration. The influence of periodic forces, for example from the shear wind gradient or tower interference, can also be determined well by means of the time history approach. The serious disadvantage of this method is the more or less random “segment” of wind turbulence used as a basis. This does not lead to a comprehensive picture. If this were attempted, the calculation effort would become extremely high. Hence, this method is more suitable for a selective “check”, rather than for comprehensive structural dimensioning with respect to fatigue life.

Spectral method

In the so-called spectral method, frequency-dependent representations (spectra) of forces and responses are processed instead of their progression over time. This method uses a statistical turbulence spectrum of the wind as the load input.

It must be possible to represent the structure in the form of linear or linearized equations (linear systems theory). The excitation spectrum causes excessive dynamic peaks of response in the regions of the natural frequencies of the structure. The extreme values of the required parameters (deformations, forces, etc.) which are decisive for the dimensioning of the structure can be represented as follows:

$$x_{max} = \bar{x} + K\sigma_x$$

Where: \bar{x} is the quasi-statically calculated mean value, σ_x the standard deviation of the dynamic excursions about the mean value and K the so-called peak factor based on statistical reliability calculations.

The link between the excitation spectrum and the spectra of the response reaction is established via so-called transfer functions. “Aerodynamic admittance” leads from the wind spectrum to the aerodynamic force parameters, “mechanical admittance” represents the link between the active forces and the deformations or stresses of the structure.

The decisive advantage of the spectral method is the reliable acquisition of the entire, real load spectrum caused by the wind turbulence. This method is thus predestined for calculating structural

fatigue. The fact that the required deformation and stress parameters are only available as frequency-dependent spectral, and not as plots against time is, admittedly, a disadvantage in view of some of the technical problems at hand. For example, it is difficult to process the functional characteristics of a wind turbine methodically, with respect to the influence of the control system on the loads (functional model).

Deterministic approach

In contrast to the statistical methods described above, it is also possible to follow a deterministic approach for calculating the dynamic structure responses. As in the example of the time history method, one single event, for example a discrete gust, can be used as load input, rather than the continuous progression of wind speed. The structural response derived from this provides information on the dynamic load magnifications to be expected. From the results, all-inclusive “dynamic magnification factors” for the quasi-statically calculated stress can be derived.

The continuous nature of wind turbulence and of the response of the structure is, of course, lost in the process. It is also not possible to cover all of the load inputs with respect to the overall load spectrum by this method. Up to a certain point, one can get by with assuming a certain frequency of the various discrete events (gusts), but the validity of the results with respect to the structure’s fatigue nevertheless remains questionable.

4.6. Wind

Knowledge of certain parameters and physical laws is of particular importance if the energy of the wind is to be exploited. While the short-term behavior of the wind, the turbulence, is of significance with regard to the structural strength and the control function of a wind turbine, the long-term characteristics of the wind have relevance with regard to the energy yield. The long-term characteristics of the wind can only be determined by means of statistical surveys over many years.

4.6.1. Mean annual wind speed and wind speed frequency distribution

The mean annual wind speed (v_{ave}), understood to be the “invariable” long-term mean value of the wind speed at one location can only be determined on the basis of measurements taken over decades. Since there are not many reliable measurements available for periods longer than 30 years, the measurements are limited to this period.

In practice, the problem is frequently that insufficient data about the frequency distribution of the wind speeds at a particular location are available. In such a case, there is no alternative but to use a mathematical approximation for the distribution curve. In normal wind regimes, a Weibull function will provide a good approximation. The Weibull function is defined as:

$$\Phi = 1 - e^{-\left(\frac{v_W}{A}\right)^k} \quad (4.5)$$

Where:

Φ = distribution function

e = logarithmic base (normally the natural log, $e=2.781$)

A = scaling factor

k = form parameter

If nothing besides the mean wind velocity is known and an “usual” frequency distribution can be assumed, this is characterized by a form factor of $k = 2$. In this special case, the Weibull distribution is called Rayleigh distribution. The relative frequency is obtained mathematically from the cumulative frequency by differentiating with respect to the wind speed v_w .

4.6.2. Increase wind speed with altitude

The increase in wind speed with height can be described as the statistical mean of an assumed steady-state speed distribution. This simplification is adequate with respect to problems based on the long-term statistical mean of the wind speed, that is to say the calculation of the energy delivery of a wind turbine. A conventional approach for describing the increase in wind speed with height is the logarithmic height formula:

$$\bar{v}_H = \bar{v}_{ref} \cdot \frac{\ln \frac{H}{z_0}}{\ln \frac{H_{ref}}{z_0}} \quad (4.6)$$

Where

\bar{v}_H = mean wind velocity at elevation H (m/s)

\bar{v}_{ref} = mean wind speed at reference elevation H_{ref} (m/s)

H = height (m)

H_{ref} = reference elevation (measuring elevation)

\ln = natural logarithm (base $e=2.7183$)

z_0 = roughness length (see (DNV-OS-J101, 2011) for more information).

4.6.3. Wind turbulence

The study of a wind speed time history measured with sufficiently high resolution enables its most important parameters to be defined. Ignoring short-term fluctuations, the level of the prevailing wind speed determines the mean wind speed \bar{v}_w . It is generally averaged over a period of 10 minutes. Using this steady mean wind speed, the instantaneous wind speed at a point in time t can be specified as follows:

$$v_w(t) = \bar{v}_w + v_T(t) \quad (4.7)$$

The superimposed fluctuating part of the wind speed $v_T(t)$ is caused by the turbulence of the wind. Thus, turbulence is the instantaneous, random deviation from the mean wind speed. The extent and characteristics of the turbulence are dependent on a variety of meteorological and geographic factors.

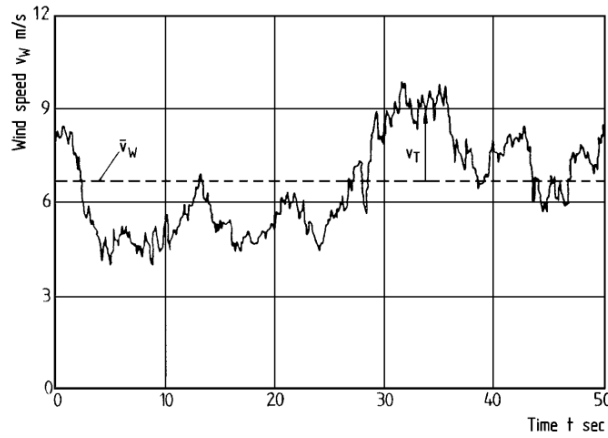


Figure IV.4: Measured time history of wind speed

To characterize the turbulence, the term of turbulence intensity is used which is occasionally also called the degree of turbulence. The turbulence intensity σ_o is defined as the ratio of the standard deviation σ_v of the wind speed to the mean wind speed \bar{v}_W in a certain averaging time and is specified in percent:

$$\sigma_o = \frac{\sigma_v}{\bar{v}_W} \quad (\%) \quad (4.8)$$

4.6.4. Wind turbine classes

Offshore wind turbines shall be designed to withstand safely the wind conditions defined for the site or the selected wind turbine class.

For an offshore wind turbine the definition of wind turbine classes in terms of wind speed and turbulence parameters remains appropriate as the basis for design of the topsides structure (turbine machinery). The values of wind speed and turbulence intensity parameters are intended to represent the characteristic values of many different sites and do not give a precise representation of any specific site. The goal is to achieve wind turbine classification with clearly varying degrees of robustness governed by the wind speed and turbulence intensity parameters. Table VI.1 specifies the basic parameters which define wind turbine classes.

Table IV.1: Basic parameters for wind turbine classes

Wind turbine class	I	II	III	S
- V_{ref} [m/s]	50	42.5	37.5	Site specific
- V_{ave} [m/s]	10	8.5	7.5	
- $A I_{15}$ [-]	0.18			
- a [-]	2			
- $B I_{15}$ [-]	0.16			
- a [-]	3			
- $C I_{15}$ [-]	0.145			
- a [-]	3			

where:

V_{ref} = reference wind speed

V_{ave} = annual average wind speed over many years at hub height

A = category for higher turbulence intensity values

B = category for medium turbulence intensity values

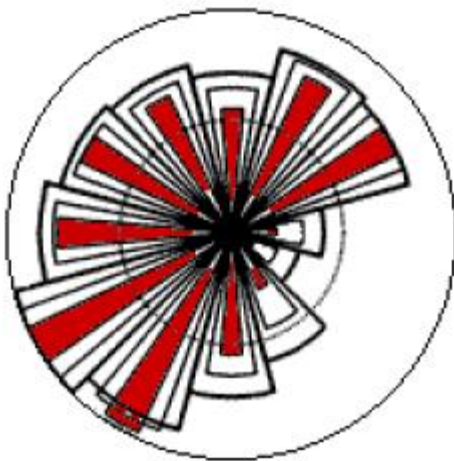
C = category for lower turbulence intensity values

I_{15} = characteristic value of the turbulence intensity at 15 m/s

a = slope parameter for turbulence characteristics.

A turbine designed according to the wind turbine class with a reference wind speed V_{ref} is designed so that it can withstand the environmental conditions in which the 10-min mean of the extreme wind speed with a recurrence period of 50 years at hub height is equal to or less than V_{ref} .

4.6.5. Wind Rose



To show the information about the distribution of wind speeds, and the frequency of the varying wind directions, one may draw a so-called wind rose on the basis of meteorological observations of wind speeds and wind directions. The compass is usually divided into 12 sectors, one for each 30 degrees of horizon.

The radius of the 12 outermost, wide wedges gives the relative frequency of each of the 12 wind directions, i.e. how many percent of the time is the wind blowing from that direction.

The second wedge gives the same information, but multiplied by the average wind speed in each particular direction. The result is then normalized to add up to 100 percent. This shows how much each sector contributes to the average wind speed at a particular location. The innermost (red) wedge gives the same information as the first, but multiplied by the cube of the wind speed in each particular location. The result is then normalized to add up to 100 percent. This shows how much each sector contributes to the energy content of the wind at a particular location.

Figure IV.5: An example of Wind Rose

4.6.6. Assessment of wind loads on the support structure

a. Loads at tower top

When the wind flow passes through the rotor of the turbine, the blades rotate with a rotational speed that depends on the torque imposed by the generator for the electricity production. The limitation of rotational speed induced by this torque slows down the air flow passing through the actuator disk, generating an axial load on the rotor. The rotor is also submitted to bending moments due to the distribution of pressures along the blades.

Loads at tower top are often assessed thanks to the statistical analysis of time simulation performed by dedicated software.

b. Distribution of wind pressure on the tower

The wind turbine tower is in an air flow and is consequently submitted to a distribution of wind pressure due to its drag. The wind pressure at a certain height depends on the air density ρ_{air} , the cross section A, the wind speed V and the drag coefficient C_{aero} :

$$F_{aero} = \frac{1}{2} C_{aero} \rho_{air} A V^2 \quad (4.9)$$

The drag coefficient is mainly related to the roughness of the surface, the shape of the structure and the wind speed.

c. Loads induced by the wake effect

The spatial distribution and the value of wind speeds in the offshore location are modified because of the wake generated by each of the structures. An illustration of this phenomenon is presented in Figure IV.6. The general consequences of the wake effect are:

- An increase of the turbulence intensity compared to the turbulence intensity in absence of wind turbines;
- A reduction of the average wind speed in the wake;
- An increase of the site roughness, which increases the wind shear phenomenon.



Figure IV.6: Illustration of wake effect

Depending on the position of the structure in the wind farm, the value of the wake induced loads are related to the wake of one single wind turbine or to the superposition of several wakes. In the absence of detailed analysis (fluid dynamic analysis, for example), the design of the wind turbine will be based on a higher turbulence intensity.

The wake effect will be more important if wind turbines are close to each other. According to the rules given by Germanischer Lloyd (GL, 2005), the mutual influence of the wake effects should be taken into account if the distance between wind turbines is smaller than 10 times the rotor diameter.

4.7. Wave

The wave loads acting on an offshore wind turbine structure affect both the sub-structure and the foundation. The wave loads can be represented by two main parameters, the significant wave height, H_s , and the spectral peak wave period, T_p .

The significant wave height is a measure of the intensity of the wave climate accounting for wave height variability. It is traditionally defined as the mean height of the 1/3 highest wave, $H_{1/3}$, but can also be defined as four times the standard deviation of the sea elevation process (i.e. four times the area under the wave spectrum, H_{m0}) (DNV-OS-J101, 2011).

The wave spectrum describes the frequency content of a sea state, typically based on a Pierson-Moskowitz spectrum for a well-developed sea state or a JONSWAP spectrum for a limited fetch and duration sea state. The spectral peak wave period, T_p , is related to the mean zero-crossing period, T_z , of the sea elevation process and is assumed to be constant (approximately 10-sec) over a short-term 3 to 6-hour sea state. The short-term 3 to 6-hour sea state is presented by a wave spectrum, or the power spectral density function of the sea elevation process, $S(\omega)$, which is a function of H_s and T_p and describes how the energy of the sea elevation is distributed between frequencies.

4.7.1. General characteristics of waves

A regular travelling wave is propagating with permanent form. It has a distinct wave length, wave period, wave height.

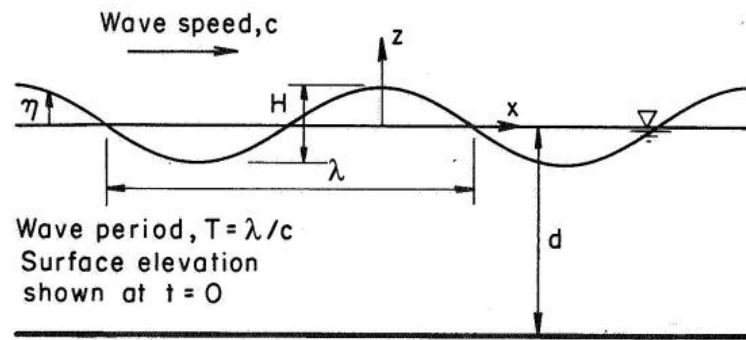


Figure IV.7: Regular travelling wave properties

- Wave length: The wave length λ is the distance between successive crests.
- Wave period: The wave period T is the time interval between successive crests passing a particular point.
- Phase velocity: The propagation velocity of the wave form is called phase velocity, wave speed or wave celerity and is denoted by $c = \lambda / T$.
- Wave frequency is the inverse of wave period: $f = 1 / T$.
- Wave angular frequency: $\omega = 2\pi / T$.
- Wave number: $k = 2\pi / \lambda$.
- Wave crest height A_c is the distance from the still water level to the crest.
- Wave trough depth A_t is the distance from the still water level to the trough.
- Wave height: The wave height H is the vertical distance from trough to crest.

$$H = A_c + A_t$$

4.7.2. Reference sea states

For use in load combinations for design, a number of reference sea states and reference wave heights are defined.

- The **Normal Sea State (NSS)**: is characterized by a significant wave height, a peak period and a wave direction. It is associated with a concurrent mean wind speed. The significant wave height $H_{S,NSS}$ of the normal sea state is defined as the expected value of the significant wave height conditioned on the concurrent 10-minute mean wind speed. The normal sea state is used for calculation of ultimate loads and fatigue loads.
- The **Severe Sea State (SSS)**: is characterized by a significant wave height, a peak period and a wave direction. It is associated with a concurrent mean wind speed. The significant wave height of the severe sea state $H_{S,SSS}$ is defined by extrapolation of appropriate site-specific metocean data such that the load effect from the combination of the significant wave height $H_{S,SSS}$ and the 10-minute mean wind speed U_{10} has a return period of 50 years. The SSS model is used in combination with normal wind conditions for calculation of the ultimate loading of an offshore wind turbine during power production.
- The **Extreme Sea State (ESS)**: is characterized by a significant wave height, a peak period and a wave direction. The significant wave height $H_{E,ESS}$ is the unconditional significant wave height with a specified return period, determined from the distribution of the annual maximum significant wave height. The Extreme Sea State is used for return periods of 50 years and 1 year, and the corresponding significant wave heights are denoted $H_{S,50-yr}$ and $H_{S,1-yr}$ respectively.

4.7.3. Wave Modeling

Wave load predictions should account for the size, shape, and type of the proposed structure. For piled foundations, Morison's equation can be used to calculate the wave loads, consisting of a drag force component and an inertial force component. The drag force is proportional to the overall combined water particle velocity, V , according to the following:

$$dF_d = \frac{1}{2} C_d \cdot \rho \cdot D \cdot V^2 \cdot dL \quad (4.10)$$

Where:

dF_d = drag force component

ρ = water mass density

D = tower diameter

dL = elemental length of tower

C_d = drag coefficient

The inertial force is proportional to the acceleration of the water particles due to Froude-Krylov forces and added mass forces according to the following:

$$dF_i = \rho.A.dL(a + C_a a_r) \quad (4.11)$$

Where:

- dF_i = inertial force component
- A = cross-sectional area of tower
- a = water particle acceleration
- C_a = added mass coefficient
- a_r = relative acceleration of water particles/tower

Diffraction effects may alter the wave pattern and loading for support towers that are large compared to the wavelength, typically significant when the tower diameter is greater than 20% of the wavelength (Watson, 2000). At this point Morison's equation is no longer valid, and the inertial force will dominate.

Where steep wave crests are prevalent, the support tower and sub-structure may be subjected to highly localized impact loads, or slap forces, which are related to the rate of change of added mass. For monopile foundations, this can be important for structural design as the slap forces are not distributed as well as would be in a multiple-leg foundation. If wave steepness is assumed to be constant and the wave height is scaled to the water depth, then the drag and slap forces are proportional to the product of the squared water depth times the diameter, and the inertial forces are proportional to the water depth times the squared diameter (Watson, 2000).

Viscous and potential flow effects should also be considered. Waves that break against the structure are more prevalent in shallower waters where wind turbines will be located than typical water depths for larger offshore platforms, and therefore should be considered separately from non-breaking wave loads. There are three classifications to consider: surging, plunging, and spilling waves. These waves can result in large amplification factors depending on the wave frequency relative to the natural frequency of the structure.

A generic distribution, or scatter diagram, can represent the long-term probability distributions of the significant wave height, H_s , and the spectral peak wave period, T_p , consisting of a Weibull distribution for H_s and a log-normal distribution of T_p .

In deeper water, the short-term probability distribution function of an arbitrary wave height H is assumed to follow a Rayleigh distribution in term of H_s . The maximum wave height in a 3-hour sea state can be estimated to be equal to $1.89(H_s)$. In shallow water, the wave height is limited by depth, and the maximum height can be assumed to be equal to 78% of the water depth (DNV-OS-J101, 2011).

The long-term probability distribution of an arbitrary wave height H is found by integration over all significant wave heights, which is used to calculate the distribution of the annual maximum wave height H_{\max} . The wavelength, λ , is given by the following equation:

$$\lambda = \frac{g}{2\pi} T^2 \frac{2\pi d}{\lambda} \quad (4.12)$$

Where:

$$\begin{aligned} T &= \text{period} \\ g &= \text{acceleration of gravity} \\ d &= \text{water depth} \end{aligned}$$

Analytical and numerical wave theories can represent the wave kinematics according to their ranges of validity. The linear wave theory that represents waves with a sine function is valid for $d/\lambda \geq 0.3$. Stokes's wave theory for high waves and the stream function theory are valid for $0.1 \leq d/\lambda \leq 0.3$, and the solitary wave theory for very shallow water is valid for $d/\lambda \leq 0.1$. The Airy theory is valid for all ratio of water depth to wavelength (DNV-OS-J101, 2011).

4.8. Current

The current load consists of two to four components, depending on water depth and geographical location: wind-generated current, tide-generated current, breaking waves (for shallow water), and ocean circulation. The waves and currents are assumed to be statistically independent (Watson, 2000). The wind and tide-generated currents can be represented by current velocities, which vary with water depth (DNV-OS-J101, 2011).

The current velocity can be estimated based on water depth according to the following:

$$v(z) = v_{\text{tide}}(z) + v_{\text{wind}}(z) \quad (4.13)$$

$$v_{\text{tide}}(z) = v_{\text{tide}0} \left(\frac{h+z}{h} \right)^{\frac{1}{7}} \quad (4.14)$$

$$v_{\text{wind}}(z) = v_{\text{wind}0} \left(\frac{h_0+z}{h_0} \right) \quad (4.15)$$

Where:

$$\begin{aligned} v(z) &= \text{total current velocity at level } z \\ v_{\text{tide}}(z) &= \text{tidal current velocity at level } z \\ v_{\text{wind}}(z) &= \text{wind-generated current velocity at level } z \\ z &= \text{distance from still water level, positive upwards} \\ v_{\text{tide}0} &= \text{tidal current at still water level} \\ v_{\text{wind}0} &= \text{wind-generated current at still water level} \\ h &= \text{water depth from still water level (positive value)} \end{aligned}$$

h_0 = reference depth for wind-generated current

4.9. Combined Wind and Wave Loading

4.9.1. Horizontal to Moment Load Ratio

Load effects can combine to result in assumed intensities of multiple parameters acting during an environmental state (i.e. when an intensity parameters acts at an assumed constant value over a 10-minute to 1-hour period of time). Combine horizontal loads are generally equal to 1 to 5% of the resultant moment created from wind, wave, and current loading due to the typical height of the rotor-nacelle assembly. However, the ratio of moment to horizontal load fluctuates rapidly with time, dependent on water depth, sea state, and wind conditions. This loading scenario is atypical to that of other offshore structures due to their larger size, where the load ratios remain relatively constant regardless of environmental conditions. Because the wind and wave loading may not be coincident, the horizontal and moment loads may also not be coincident. However, the most unfavorable structural response is when wind and wave loads do act coincidently.

4.9.2. Combination Methods

Two methods to combine wind and wave loads are the linear combination method and the combination by simulation. The linear method simply combines the calculated wind load effect and the calculated wave load effect by linear superposition. It works well as a preliminary combined load evaluation or when dynamic effects are demonstrated to be negligible (e.g. in shallow water) (DNV-OS-J101, 2011). The simulation method is based on structural analysis in the time domain for the simultaneously-applied simulated time series of the wind and wave loads.

4.10. Effect of cyclic loading to foundation

4.10.1. Cyclic degradation effects

Laboratory and field data show that cyclic loading may cause a reduction in load capacity and an increase in displacement of piles.

a. For piles in clay:

In order to express degradation effects conveniently, the concept of degradation factors has been introduced, the degradation factor being defined as:

$$D = \frac{\text{property after cyclic loading}}{\text{property for static loading}} \quad (4.16)$$

Cyclic effects cause the degradation for skin friction, ultimate base resistance and soil modulus.

The degradation factor depends on the number of cycles, but the majority of degradation occurs in the first 10 or 20 cycles.

Degradation for skin friction has been introduced in DNV standard (DNV-OS-J101, 2011) and will be used to calculate T-Z curves in Section 6.2.1 (page 76) of this thesis.

Data on modulus degradation from cyclic triaxial tests by Idriss et al (1978) indicated that the modulus degradation factor D_E could be approximated as follows:

$$D_E = N^{-t} \quad (4.17)$$

where N : number of cycles

t : a degradation parameter which is a function of cyclic strain

Unfortunately, no direct data is yet available on the cyclic degradation of ultimate base resistance of a pile in clay, as most tests to date have concentrated on cyclic effects on skin friction (H.G.Poulos).

The p-y curves used in the following part of this thesis, which is based on DNV standard, includes a coefficient of 0.9 to account the degradation effects.

b. For piles in sand:

The limited information available on the effects of cyclic loading on piles in sand indicates that remarkable reductions in load capacity and pile stiffness can occur. Permanent settlement of the pile may continue to increase, even after a very large number of cycles. It was deduced that degradation of base resistance was more severe than degradation of skin friction, and close examination of the sand near the tip showed appreciable crushing of the grains.

Detailed data on the degradation of soil modulus has not yet been obtained for piles in sand. The cyclic stiffness of a pile tends to decrease with increasing numbers of cycles, but it is not yet clear whether the expression in Equation (4.17) can be applied in this case. Moreover, no data on the degradation of ultimate base resistance is available, although the tests of Van Weele suggest that this degradation may be important.

Consequently, it must be concluded that, at this time, there is a dearth of experimental data on the effects of cyclic loading on piles in sand, although indications are that they can be more critical than for piles in clay.

4.10.2. Loading rate effects

For piles in clay, the rate application has a significant effect on pile load capacity. The more rapid the loading rate, the greater the pile capacity in clay. Typically, the load capacity increases by between 10 and 20% per decade increase in loading rate (H.G.Poulos). In situations where relatively rapid cyclic loading is being applied to a pile, (such as with offshore piles subjected to wave loading) the beneficial effects of high loading rate may be offset by the degradation of load capacity due to the cycling of the load, and the ultimate load capacity may be less than or more than the ultimate static capacity. For example, in the tests conducted by Kraft et al. (1981), the combined effects of one-way cycling and rapid loading rate resulted in a load capacity which exceeded the static value by up to

20%. Thus it is necessary to consider both cyclic and rate effects simultaneously in order to assess the ultimate load capacity of offshore piles (H.G.Poulos).

There is no published evidence on the effects of loading rate on piles in sand. Laboratory static triaxial tests show that the shear strength of sand is largely unaffected by loading rate (in contrast to clays which are influenced in a similar manner to piles in clay). Thus it would seem that no rate effects could be relied upon for piles in sand, so that cyclic loading would serve only to cause degradation of pile load capacity and stiffness; if this is so, the significance of cyclic loading effects on piles in sand may indeed be much greater than for piles in clay.

4.11. Basis of Soil Mechanics

4.11.1. Stress-strain behavior, stiffness and strength

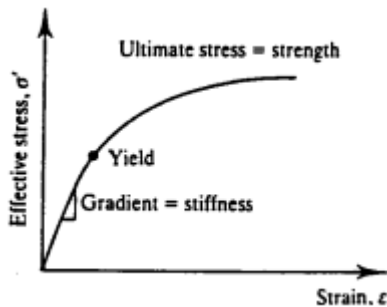


Figure IV.8: A typical stress-strain curve for soil

Figure IV.8 shows an idealized relationship between stress and strain and it is similar to the stress-strain curves for common engineering materials like metals, plastics, ceramics and engineering roils.

For soils and other granular materials, it is necessary to deal with something called effective stress to take account of pore pressures in the fluid in the voids between the grains behavior including stiffness and strength, is governed by an effective stress which is denoted by a prime (as in σ')

Stiffness is the gradient of the stress-strain line. If this is linear the gradient is easy to determine but, if it is curved, the stiffness at a point such as A may be quoted as a tangent or as a secant, as shown in Figure IV.9 and given by:

$$\text{Tangent stiffness} = \frac{d\sigma'}{d\varepsilon}$$

$$\text{Secant stiffness} = \frac{\Delta\sigma'}{\Delta\varepsilon}$$

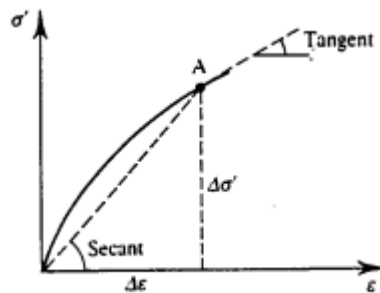


Figure IV.9: Tangent and secant stiffness moduli

In simple terms the strength of a material is the largest stress that the material can sustain and it is this which governs the stability or collapse of structures.

Stiffness and strength are quite different things: one governs displacements at working load and the other governs the maximum loads that a structure can sustain.

4.11.2. Elasticity

Materials that are elastic are conservative so that all of the work done by the external stresses during an increment of deformation is stored and is recovered on unloading; this means that all of the strains that occur during an increment of loading are recovered if the increment is removed.

The usual elastic parameters are Young's modulus E' and Poisson's ratio ν' . These are obtained directly from the results of uniaxial compression (or extension) tests with the radial stress held constant (or zero), and are given by:

$$E' = \frac{d\sigma_a'}{d\varepsilon_a^e} \quad (4.18)$$

$$\nu' = -\frac{d\varepsilon_r^e}{d\varepsilon_a^e} \quad (4.19)$$

Most texts on the strength of materials give the basic relationships among the various elastic parameters and, for isotropic materials, there are:

$$G' = \frac{E'}{2(1+\nu')} \quad (4.20)$$

$$K' = \frac{E'}{3(1-2\nu')} \quad (4.21)$$

In soil mechanics the shear and bulk moduli, G' and K' are preferable to Young's modulus E' and Poisson's ratio ν' because it is important to consider shearing or change of shape separately, or decoupled, from compression or change of size.

4.11.3. Perfect Plasticity

When the loading has passed the yield point in Figure IV.8 simultaneous elastic and plastic strains occur and the stiffness decreases. During an increment of plastic deformation the work done is dissipated and so plastic strains are not recovered on unloading.

At the ultimate state there are no further changes of stress (because the stress-strain curve is horizontal) and so all the strains at failure are irrecoverable. The plastic strains at failure in Figure IV.8 are indeterminate; they can go on more or less forever and so we can talk about plastic flow.

4.11.4. Combined Elasto-Plastic Behavior

With reference to Figure IV.8, the stress-strain behavior is elastic up to the yield point and is perfectly plastic at the ultimate state. Between the first yield and failure there are simultaneous elastic and plastic components of strain.

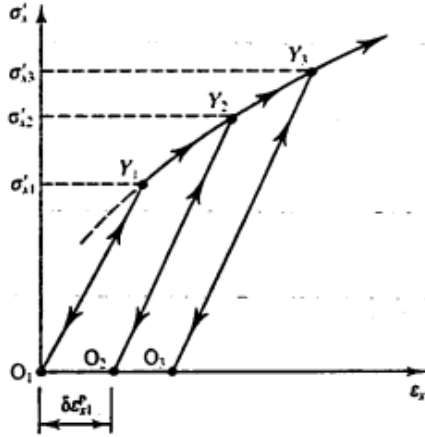
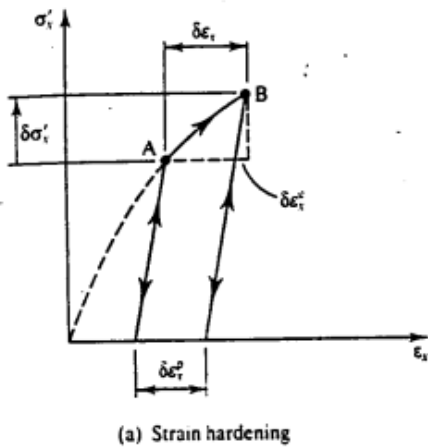
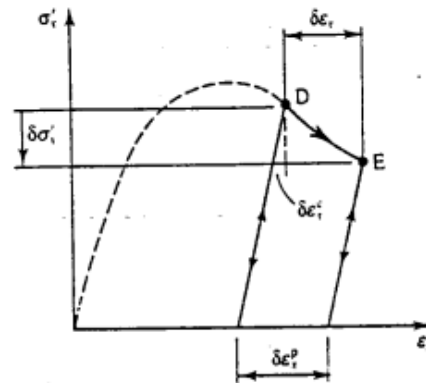


Figure IV.10: Material behavior during load cycling

In Figure IV.10 material is loaded from O_1 and is elastic until yielding occurs at Y_1 , where the yield stress is σ'_{x1} . It is then strained further and unloaded to O_2 where there are irrecoverable plastic strains $\delta\epsilon_{x1}^p$. When the material is reloaded from O_2 it is elastic until yielding occurs at Y_2 , where the yield stress is σ'_{x2} . If the material is then strained further and unloaded to O_3 on reloading, it will have a new yield stress σ'_{x3} and so on. Thus the principal consequences of straining from Y_1 to Y_2 (or from Y_2 to Y_3) are to cause irrecoverable plastic strains and to raise the yield point from σ'_{x1} to σ'_{x2} (or from σ'_{x2} to σ'_{x3}). This increase of the yield point due to plastic straining is called hardening and the relationship between the increase in the yield stress $\delta\sigma'_x$ and the plastic straining $\delta\epsilon_x^p$ is known as a hardening law.



(a) Strain hardening



(b) Strain softening

Figure IV.11: Yielding and Plastic Straining

Yielding and plastic straining may cause hardening (i.e. an increase in the yield stress), as shown in Figure IV.11(a), or softening (i.e. a decrease in the yield stress), as shown in Figure IV.11(b). In the latter case the state has reached, and passed, a peak in the stress-strain curve, and this is a feature commonly found in the behavior of soil. In each case the total strains are the sum of elastic and plastic components and the plastic strains are related to the change of the yield stress by a hardening law.

4.12. Types of Soil Model

Various modeling techniques have been used to model offshore foundations. Some of these models have been proven through industry implementation, while others are still in the research and development stage.

4.12.1. Plasticity Models

The foundation response can be expressed in terms of force resultants on the footing and the corresponding displacements, consistent with the time-domain approach used for structures which enables simultaneous modeling between soil behavior and structure analysis.

Plasticity models include four components consisting of the yield surface which defines allowable load combinations, a strain-hardening expression that defines how the yield surface expands or contracts, a flow rule that defines the plastic displacements at yield, and a model for the elastic response within the yield surface (see Figure IV.12).

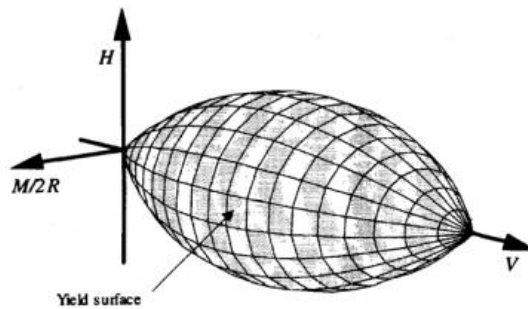


**Figure IV.12: Example Yield Surface for Footings on Sand
(Byrne and Housby 2002)**

The rule of behavior in the model is such that if a load combination is within the yield surface, an elastic response results, otherwise plastic response results as defined by the flow rule.

A disadvantage to using this model is that the specific parameters, sometimes difficult to assess, must be specified for each surface. However, the concept of continuous hyperplasticity, based on thermodynamic principles, replaces plastic strain in conventional plasticity theory with a continuous field of an infinite number of yield surface-specific plastic strain components. As indicated in Figure IV.13, this theory closely matches laboratory behavior, and may prove to be a useful method of implementing plasticity models.

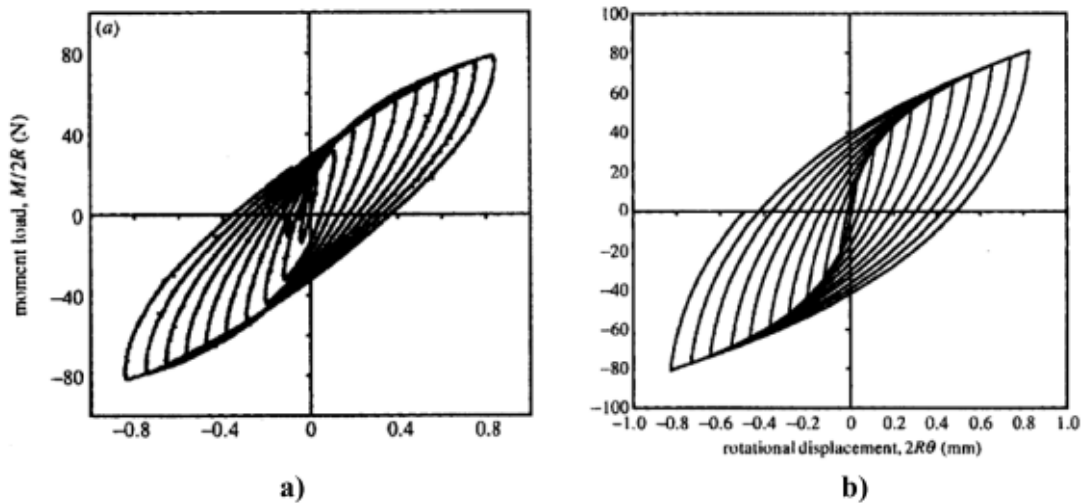


Figure IV.13: Comparison of a) Laboratory Test Data with b) Continuous Hyperplasticity Theory. (Byrne & Houlsby 2003)

4.12.2. Finite Element Models

Finite element models (FEM) that evaluate foundation behavior are composed of structural elements for the foundation and soil elements for the surrounding seafloor. FEM analysis accounts for initial conditions, nonlinear soil-structure interaction, and nonlinear soil behavior.

Boundary conditions determine the constraints for coupling of the structural and soil elements. They are described using differential and integral operators of time and space developed through local schemes that are independent of the frequency of excitations, making them applicable for a time domain transient analysis. For static analysis, boundary elements are assumed to connect to a rigid surrounding, whereas in dynamic analysis, radiation damping at the soil interface needs consideration through multiple degree-of-freedom models. Under typical conditions, a Winkler assumption is preferred.

Many computer programs using FEM have been developed for the offshore industry. Examples include ABAQUS, which uses different models such as the Mohr-Coulomb theory with soil hardening/softening effects or a Drucker-Prager material model with a non-associated flow rule, or Ramboll's multiple FEM programs (e.g. ROSAP, RONJA, ROSOIL) for wind industry, which combine linear structures with nonlinear foundations. Most of these programs automatically generate the range of environmental and structural loads, in which any standard wave theory can be applied that comprise load situations in all limit states, incorporating both elastic and plastic behavior of the soil in the design.

4.12.3. Other Technique

The effective fixity length technique, which is based on the clamping effect of the soil surrounding piles, can be modeled using a rigid restraint located at an effective depth below the seafloor (Zaaijer, 2002). Using this approximate value of the effective fixity length (Table IV.2), preliminary dynamic analyses can be conducted for offshore structures. Due to the lack of bracing through a support frame as seen in typical offshore structures, monopile foundations exhibit different mode shapes of the effective fixity model.

Table IV.2: Estimations of Effective Fixity Length. (Zaaijer 2002)

Effective fixity length	
Stiff clay	3.5 D – 4.5 D
Very soft silt	7 D – 8 D
General calculations	6 D
From measurement of an offshore turbine (500 kW)	3.3 D – 3.7 D

A stiffness matrix can be also used to represent the pile-soil stiffness at the seafloor, comprised of forces, moments, displacements, and rotations of the pile head (Zaaijer, 2002). The advantages of a stiffness matrix include the consolidation of foundation properties helping facilitate information exchange between the geotechnical and structural engineers for frequency calculations. There are two methods for obtaining the stiffness matrix: a load-displacement analysis with p-y curves, or Randolph elastic continuum model (Zaaijer, 2002), which is based on the inverse of a matrix expression for pile head flexibility derived from dimensional and finite element analyses of piles in an elastic continuum. The Randolph model is parameterized in terms of both constant and linearly-increasing soil shear modulus, and therefore works well for sandy soils.

4.13. Winkler model

4.13.1. Beam Nonlinear Winkler Foundation

The most common method for analysis of laterally loaded piles is based on the use of so-called p-y curves. The p-y curves give the relation between the integral value p of the mobilized resistance from the surrounding soil when the pile deflects a distance y laterally. The pile is modeled as a number of consecutive beam-column elements, supported by nonlinear springs applied at the nodal points between the elements. The nonlinear support springs are characterized by one p-y curve at each nodal point.

The solution of pile displacements and pile stresses in any point along the pile for any applied load at the pile head results as the solution to the differential equation of the pile:

$$EI \frac{d^4 y}{dx^4} + Q_A \frac{d^2 y}{dx^2} - p(y) + q = 0 \quad (4.22)$$

With

$$EI \frac{d^3 y}{dx^3} + Q_A \frac{dy}{dx} = Q_L \quad \text{and} \quad EI \frac{d^2 y}{dx^2} \quad (4.23)$$

Where x denotes the position along the pile axis, y is the lateral displacement of the pile, EI is the flexural rigidity of the pile, Q_A is the axial force in the pile, Q_L is the lateral force in the pile, $p(y)$ is the lateral soil reaction, q is a distributed load along the pile, and M is the bending moment in the pile, all at the position x .

4.13.2. Pile-soil interface

The pile-soil interface is modeled separately on each side of the pile, thus allowing gapping and slippage to occur on each side independently. The soil and pile nodes in each layer are connected using a no-tension spring, that is, the pile and soil will remain connected and will have equal displacement for compressive stresses. The spring is disconnected if tensile stress is detected in the soil spring to allow a gap to develop. This separation or gapping results in permanent displacement of the soil node dependent on the magnitude of the load. The development of such gaps is often observed in experiments, during offshore loading, and after earthquake excitation in clays. These gaps eventually fill in again over time until the next episode of lateral dynamic loading. The pile-soil interface for sands does not allow for gap formation, but instead the sand caves in, resulting in the virtual backfilling of sand particles around the pile during repeated dynamic loading. When the pile is unloaded, the sand on the tension side of the pile follows the pile with zero stiffness instead of remaining permanently displaced as in the clay model (M. Hesham El Naggar and Kevin J. Bentley, 2000).

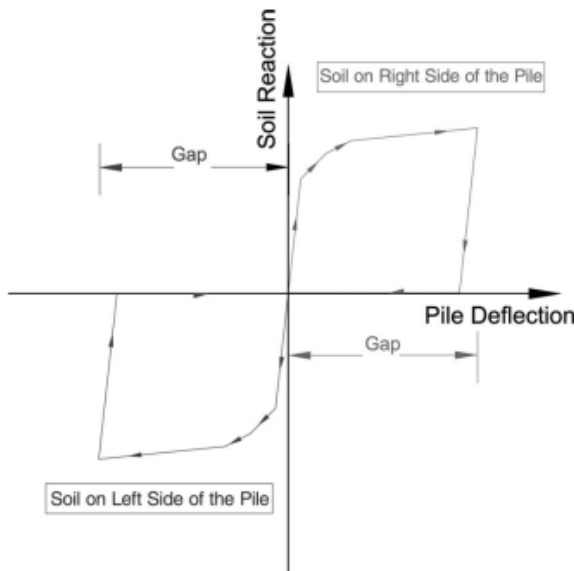


Figure IV.14: Typical soil reaction - pile deflection behavior for cohesive soils (gapping)

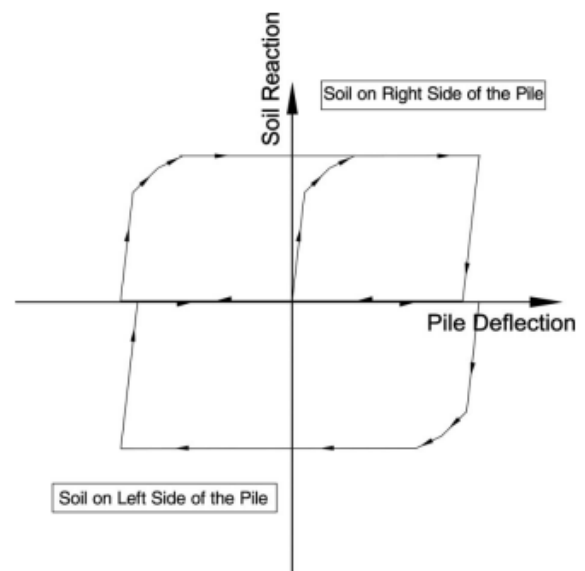


Figure IV.15: Typical soil reaction - pile deflection behavior for cohesionless soils (cave-in)

4.13.3. Load-displacement relationship

The design procedure for offshore wind energy plants in Germany is given in the Germanische Lloyd rules and regulations (GL, 2005). In this regulation, concerning the behavior of piles under horizontal loading reference is made to the regulation code of the American Petroleum Institute (API, 2000). The Norwegian guidelines (DNV-OS-J101, 2011) also refer to API code. In the API code the p-y method is recommended for the design of horizontally loaded piles.

In principle, the p-y method is a subgrade modulus method with non-linear and depth-dependent load-deformation (p-y) characteristics of the soil springs.

API (API, 2000) describes the construction of p-y curves for soft and stiff clay as well as for sandy soils. Due to API, p-y curves for clay and sandy soils can be derived as follows:

a. Clay

For piles in cohesive soils, the static ultimate lateral resistance is recommended to be calculated as:

$$p_u = \begin{cases} (3.s_u + \gamma'.X)D + J.s_u.X & \text{for } 0 < X \leq X_R \\ 9.s_u.D & \text{for } X > X_R \end{cases} \quad (4.24)$$

Where X is the depth below soil surface and X_R is a transition depth, below which the value of $(3.s_u + \gamma'.D)D + J.s_u.X$ exceeds $9.s_u.D$. Further, D is the pile diameter, s_u is the undrained shear strength of the soil, γ' is the effective unit weight of soil, and J is a dimensionless empirical constant whose value is in the range 0.25 to 0.50 with 0.50 recommended for soft normally consolidated clay.

For static loading, the p-y curve can be generated according to:

$$p = \begin{cases} \frac{p_u}{2} \left(\frac{y}{y_c} \right)^{1/3} & \text{for } y \leq 8y_c \\ p_u & \text{for } y > 8y_c \end{cases} \quad (4.25)$$

For cyclic loading and $X > X_R$, the p-y curve can be generated according to:

$$p = \begin{cases} \frac{p_u}{2} \left(\frac{y}{y_c} \right)^{1/3} & \text{for } y \leq 3y_c \\ 0.72p_u & \text{for } y > 3y_c \end{cases} \quad (4.26)$$

For cyclic loading and $X \leq X_R$, the p-y curve can be generated according to:

$$p = \begin{cases} \frac{p_u}{2} \left(\frac{y}{y_c} \right)^{1/3} & \text{for } y \leq 3y_c \\ 0.72p_u \left(1 - \left(1 - \frac{X}{X_R} \right) \frac{y - 3y_c}{12y_c} \right) & \text{for } 3y_c < y \leq 15y_c \\ 0.72p_u \frac{X}{X_R} & \text{for } y > 15y_c \end{cases} \quad (4.27)$$

Here, $y_c = 2.5\varepsilon_c D$, in which D is the pile diameter and ε_c is the strain which occurs at one-half the maximum stress in laboratory undrained compression tests of undisturbed soil samples.

b. Sand

The maximum mobilized soil reaction force per unit length of the pile (or the static ultimate lateral resistance) p_u depends on the regarded depth under seabed X , the submerged unit weight of the soil γ' , the pile diameter D and on the angle of internal friction ϕ' of the sand:

$$p_u = \begin{cases} (C_1X + C_2X)\gamma'X & \text{for } 0 < X \leq X_R \\ C_3D\gamma'X & \text{for } X > X_R \end{cases} \quad (4.28)$$

Where the coefficients C_1 , C_2 and C_3 depend on the friction angle ϕ as shown in

Figure IV.16:

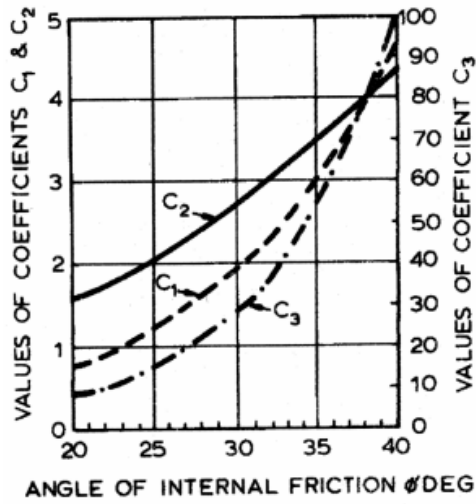


Figure IV.16: Coefficients as functions of friction angle

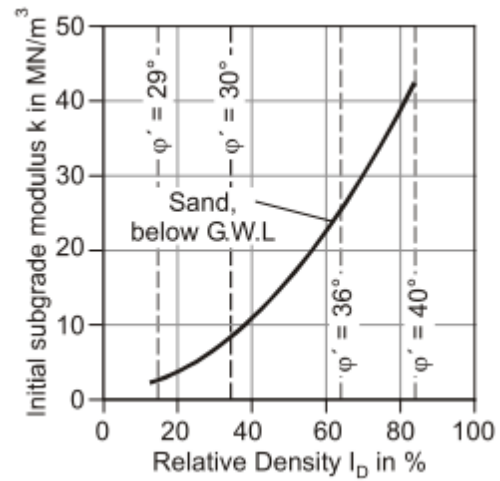


Figure IV.17: Initial modulus of subgrade reaction k as function of friction angle

The p-y curve is described by the following equation:

$$p = A.p_u \tanh\left(\frac{k.X}{A.p_u} y\right) \quad (4.29)$$

In which p is the soil resistance per unit length of the pile and y is the actual horizontal deflection; k is the initial modulus of subgrade reaction and depends on the friction angle ϕ as given in Figure IV.17, and A is a factor to account for static or cyclic loading conditions as follows:

$$A = \begin{cases} 0.9 & \text{for cyclic loading} \\ \left(3 - 0.8 \frac{X}{D}\right) \geq 0.9 & \text{for static loading} \end{cases} \quad (4.30)$$

The equations (4.28) and (4.29) are based on investigations of Reese and Cox (Reese, L. C.; Cox, W. R.; Koop, F.D., 1974). They tested a 21 m long steel tube pile having a diameter of 61 cm under different loading and then evaluated their results. For cyclic tests, a maximum number of 100 load cycles was realized. The correction factor A according to equation (4.30) was adjusted based on the measurements done.

4.14. Sap2000 and methods to solve a nonlinear dynamic analysis

4.14.1. Sap2000 software

SAP2000, a product of Computer and Structures, Inc. (CSI), is intended for use on civil structures such as dams, communication towers, stadiums, industrial plants and buildings. The software has many features necessary for offshore structures (CSI, 2011):

- Static and dynamic analysis
- Linear and nonlinear analysis
- Geometric nonlinearity, including P-delta and large-displacement effects
- Staged (incremental) construction
- Buckling analysis

- Steady-state and power-spectral-density analysis
- Frame and shell structural elements, including beam-column, truss, membrane, and plate behavior
- Nonlinear link and support elements
- Frequency-dependent link and support properties
- ...etc.

4.14.2. Dynamic equilibrium

The force equilibrium of a multi-degree-of-freedom lumped mass system as a function of time can be expressed by the following relationship:

$$F(t)_I + F(t)_D + F(t)_S = F(t) \quad (4.31)$$

in which the force vectors at time t are:

$F(t)_I$ is a vector of inertia forces acting on the node masses

$F(t)_D$ is a vector of viscous damping, or energy dissipation, forces

$F(t)_S$ is a vector of internal forces carried by the structure

$F(t)$ is a vector of externally applied loads

Equation (4.31) is based on physical laws and is valid for both linear and nonlinear systems if equilibrium is formulated with respect to the deformed geometry of the structure.

For many structural systems, the approximation of linear structural behavior is made to convert the physical equilibrium statement, Equation (4.31), to the following set of second-order, linear, differential equations:

$$M\ddot{u}(t)_a + C\dot{u}(t)_a + Ku(t)_a = F(t) \quad (4.32)$$

in which M is the mass matrix (lumped or consistent), C is a viscous damping matrix (which is normally selected to approximate energy dissipation in the real structure) and K is the static stiffness matrix for the system of structural elements. The time-dependent vectors $u(t)_a$, $\dot{u}(t)_a$ and $\ddot{u}(t)_a$ are the absolute node displacements, velocities and accelerations, respectively.

There are several different methods that can be used for the solution of Equation (4.32). Each method has advantages and disadvantages that depend on the type of structure and loading.

4.14.3. Step-by-step solution method

The most general solution method for dynamic analysis is an incremental method in which the equilibrium equations are solved at times Δt , $2\Delta t$, $3\Delta t$, etc. There are a large number of different incremental solution methods. In general, they involve a solution of the complete set of equilibrium equations at each time increment. In the case of nonlinear analysis, it may be necessary to reform the stiffness matrix for the complete structural system for each time step. Also, iteration may be required within each time increment to satisfy equilibrium. As a result of the large computational requirements, it can take a significant amount of time to solve structural systems with just a few hundred degrees-of-freedom.

The advantages of this method are:

- It is easy to use because one does not have to worry about choosing master degree-of-freedom or mode shapes.
- It allows all type of nonlinearities.
- It uses full matrices, so no mass matrix approximation is involved.
- All displacements and stresses are calculated in a single pass.

The main disadvantage of the step-by-step method (or called Full method – Ansys Documentation) is that it is more expensive than either of the other methods.

4.14.4. Mode superposition method

Another common approach is the mode superposition method. After a set of orthogonal vectors have been evaluated, this method reduces the large set of global equilibrium equations to a relatively small number of uncoupled second order differential equations. The numerical solution of those equations involves greatly reduced computational time.

The advantages of this method are:

- It is faster and less expensive than the Full method for many problems
- It accepts modal damping (damping ratio as a function of mode number)

The disadvantages of the method are:

- The only nonlinearity allowed is simple node-to-node contact (gap condition)
- It does not accept imposed (nonzero displacements)

Because the behavior of the foundation will be modeled using nonlinear p-y curves, the mode superposition method will not suitable to use in this thesis.

4.14.5. Solution in frequency domain

The basic approach used to solve the dynamic equilibrium equations in the frequency domain is to expand the external loads $F(t)$ in terms of Fourier series or Fourier integrals. The solution is in terms of complex numbers that cover the time span from $-\infty$ to ∞ . Therefore, it is very effective for periodic types of loads such as mechanical vibrations, acoustics, sea-waves and wind. However, the use of the frequency domain solution method for solving offshore wind turbine structure in this thesis has some disadvantages:

- The method is restricted to the solution of linear structural systems
- The method does not have a sufficient theoretical justification, for the approximate nonlinear solution of soil/structure interaction problems. Typically, it is used in an iterative manner to create linear equations. The linear damping terms are changed after each iteration to approximate the energy dissipation in the soil. Hence, dynamic equilibrium within the soil is not satisfied.

Chapter V. Preliminary Design

for Support Structure of a Chosen OWT Project



5.1. Introduction

The aim of this chapter is to get roughly internal forces at the seabed for determining dimensions of the foundation pile in the next chapter.

For that purpose, an optimization process taking into account the material strength and fatigue criteria had been done using EOL-OS software. It should be pointed out here that the model in EOL-OS software is a seabed-fixed one.

The structure of this chapter is as following:

- Section 5.2: Structure definitions and limitations. All parameters of the chosen turbine as well as the tower (after optimization) will be shown.
- Section 5.3: Environmental conditions. It consists all the information such as site data, sea conditions, wind conditions, etc... that will be the input for the software. Besides, the soil conditions for the next chapter also included.
- Section 5.4: Load combinations for ULS. In fact, due to the limitation of the time for a master thesis, there is only one load combination being used. For the load combinations for SLS of the foundation, only wave load coming from some sea states will be considered.
- Section 5.5 and 5.6 are the relevant result getting from EOL-OS software.

5.2. Structure definitions and limitations

5.2.1. The chosen turbine

Parameter	Value	Unit
Rated power	7	MW
Hub height	115.0	m
Rotor diameter	118.0	m
Number of blades	3.0	-
Tower top mass (nacelle + rotor + wind turbine and equipment)	390.0	t
Minimum rotor speed	4.0	1/min
Maximum rotor speed	14.2	1/min
Rated rotor speed	12.2	1/min
Technical design life time	20.0	year

5.2.2. Tower and substructure design

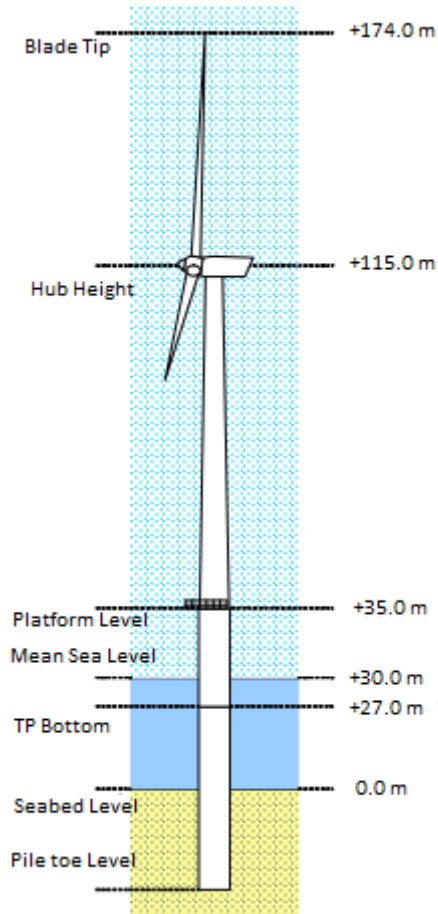


Figure V.1: Schematic dimension of the design structure

a. Platform

The platform is placed at the base of the tower. The determination of the height is based on the GL standard (GL, 2005) with the expression:

$$z_{platform} = LAT + \Delta z_{tide} + \Delta z_{surge} + \Delta z_{air} + \xi^* \quad \text{and} \quad \xi^* = \delta \cdot H_{S,50\max}$$

Parameters in this formula are expressed in the following figure:

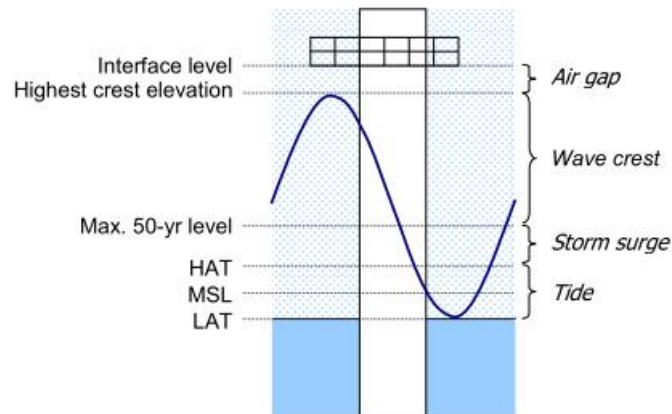


Figure V.2: Determining the interface level

In this thesis, the interface level is +35 m Seabed.

b. Support structure

In EOL OS software, the support structure is modeled from tower top to seabed in order to get the internal forces at the seabed for foundation design. In Table V.1, $Z_{top_0} = 5$ m is the seabed level.

Table V.1: Model of support structure

ID	Z Bottom	Z Top	Height	Thickness	Diameter Inf.	Diameter Sup.	Material
0	0.000	5.000	5.000	0.08000	6.000	6.000	S235
1	5.000	10.00	5.000	0.08000	6.000	6.000	S235
2	10.00	15.00	5.000	0.08000	6.000	6.000	S235
3	15.00	20.00	5.000	0.08000	6.000	6.000	S235
4	20.00	25.00	5.000	0.07600	6.000	6.000	S235
5	25.00	30.00	5.000	0.07000	6.000	6.000	S235
6	30.00	35.00	5.000	0.06400	6.000	6.000	S235
7	35.00	40.00	5.000	0.05600	6.000	6.000	S235
8	40.00	45.00	5.000	0.04800	6.000	5.700	S235
9	45.00	50.00	5.000	0.04800	5.700	5.700	S235
10	50.00	55.00	5.000	0.04400	5.700	5.700	S235
11	55.00	60.00	5.000	0.04200	5.700	5.700	S235
12	60.00	65.00	5.000	0.04000	5.700	5.700	S235
13	65.00	70.00	5.000	0.03800	5.700	5.700	S235
14	70.00	75.00	5.000	0.03600	5.700	5.500	S235
15	75.00	80.00	5.000	0.03400	5.500	5.300	S235
16	80.00	85.00	5.000	0.03400	5.300	5.100	S235
17	85.00	90.00	5.000	0.03200	5.100	5.100	S235
18	90.00	95.00	5.000	0.03000	5.100	5.000	S235
19	95.00	100.0	5.000	0.03000	5.000	4.000	S235
20	100.0	105.0	5.000	0.03000	4.000	3.500	S235
21	105.0	110.0	5.000	0.02800	3.500	3.500	S235
22	110.0	112.0	2.000	0.02400	3.500	3.500	S235

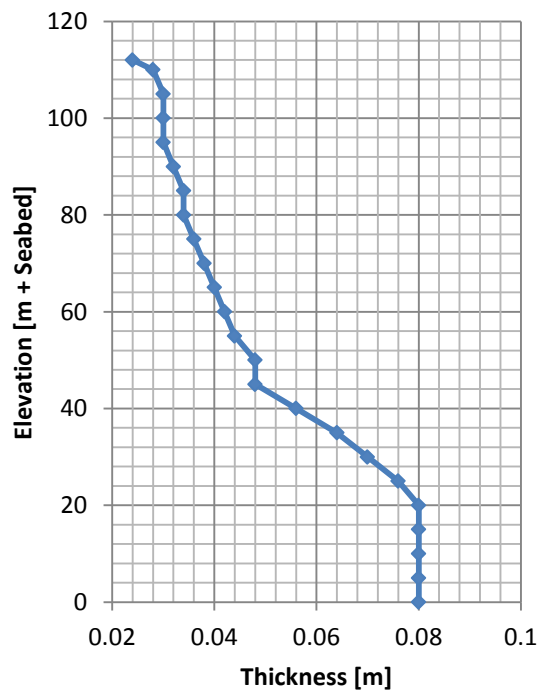


Figure V.3: Wall thickness of the tower

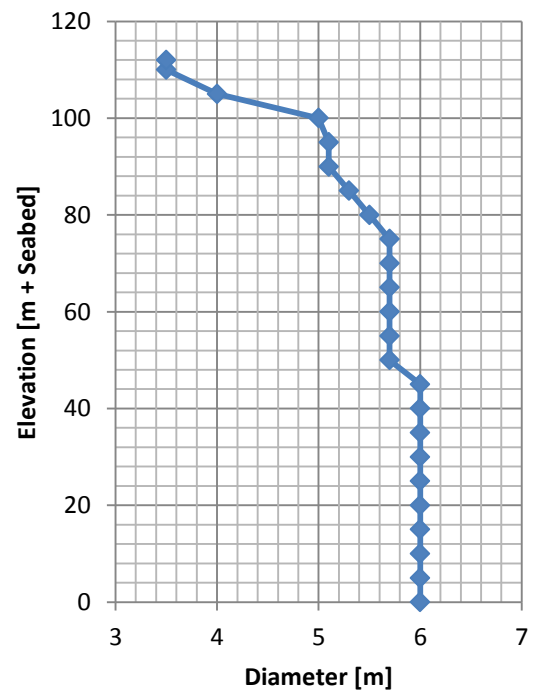


Figure V.4: Diameter of the tower

Foundation pile:

The pile top elevation should be above MSL so that it is above the splash zone at all times in order to facilitate installation. The diameter at the top of the foundation pile is fixed at 5.5 m as larger diameter piles cannot be driven due to the limited size of anvils currently in the market. A conical section tapers outward to a larger diameter. This allows the stiffness of the foundation to be controlled while respecting installation limitations. A schematic representation of the foundation pile can be seen in Figure V.5 page 70.

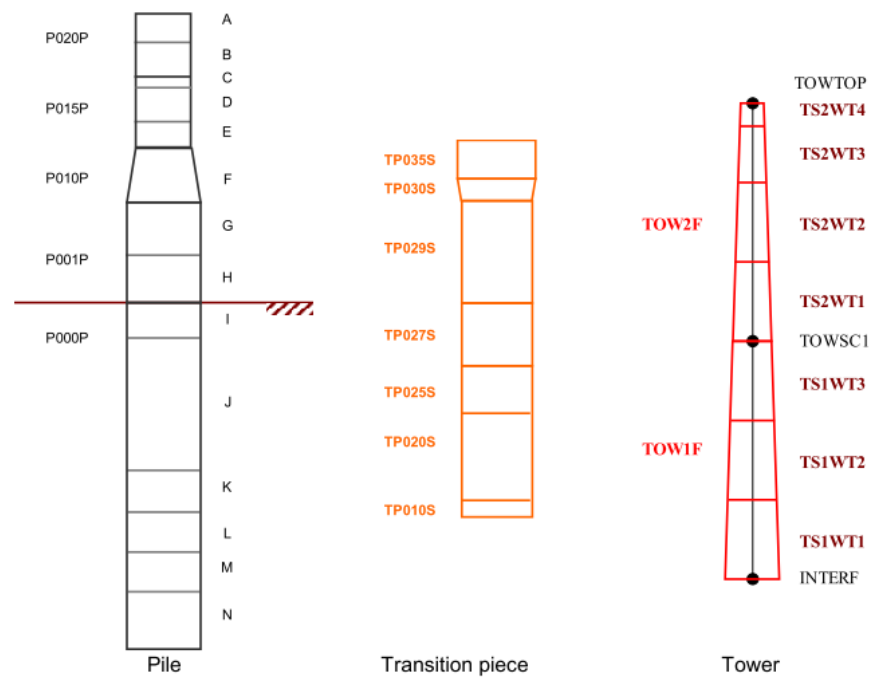
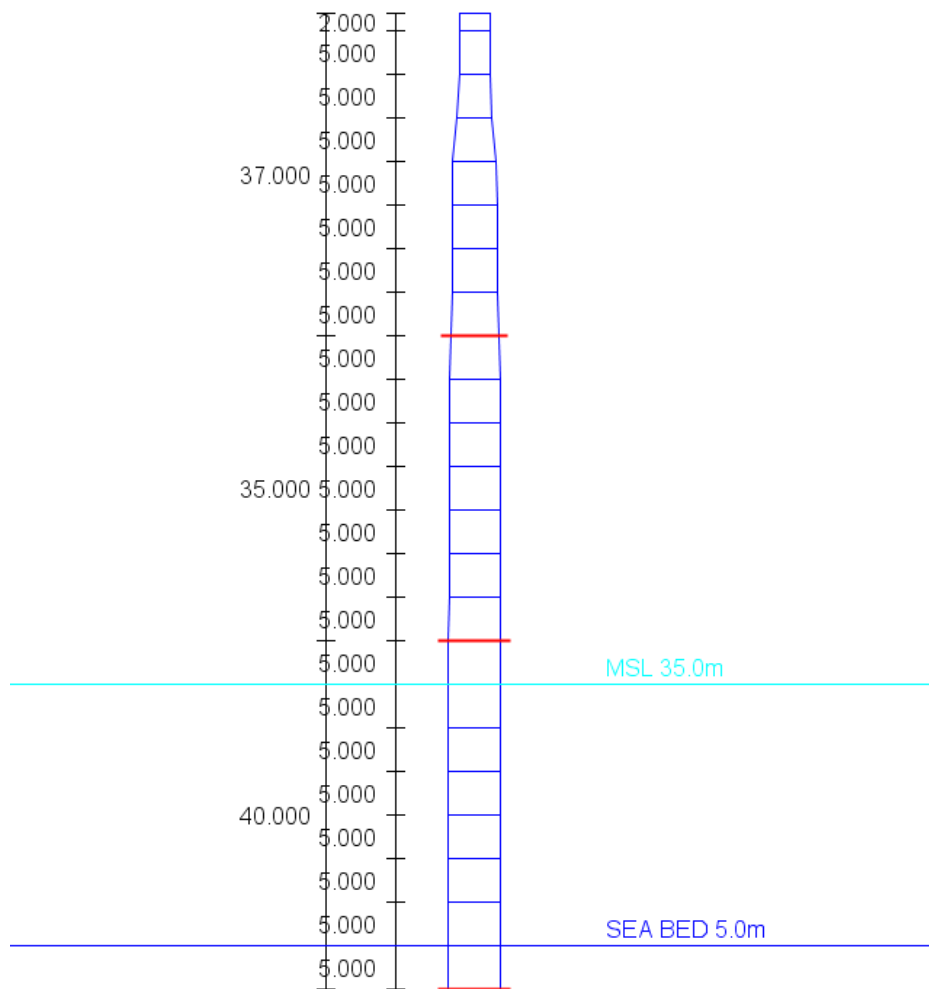


Figure V.5: Parameterization of the monopile support structure



c. Other secondary structures

Other secondary structures such as boat landing, ladders, platforms, J-tubes, anodes, and so on, will not be considered here though they may increase the vertical load for the pile foundation.

5.2.3. Corrosion

The additional thickness due to corrosion may increase the weight of structure in the foundation design. Within the splash zone, the following corrosion allowance should be used:

- Corrosion rate according to DNV standard: 0.3 mm/year
- Applicable corrosion period: 20 years
- Applicable corrosion allowance: $20 \times 0.3 \text{ mm} = 6.0 \text{ mm}$

Below the splash zone (submerged zone), the following corrosion allowance should be used:

- Applicable corrosion allowance:
 $20 \text{ years} \times 0.15 \text{ mm/year} = 3.0 \text{ mm}$

However, in this thesis, the additional wall thickness for corrosion will not be considered.

5.3. Environmental conditions

5.3.1. Site data

The water depth at the wind turbine location is 30 m. This depth is related to the mean still water level (MSL). Tide and storm elevations are not taken into account in this work.

5.3.2. Sea conditions

Sea state	Significant wave height HS (m)	Mean zero up-crossing period TZ (s)	Probability of the sea state (%)
0	0.25	2.0	20.47
1	0.25	4.0	21.76
2	0.75	3.4	8.62
3	0.75	5.3	13.25
4	1.25	5.2	10.66
5	1.75	6.0	4.83

5.3.3. Wind conditions

The dynamic pressure zone at the offshore site is IEC IA. Wind loads at tower top were evaluated thanks to the software AERODYN. The equivalent tower top load variations are given by:

Wind load spectrum	Number of loading cycles	F _x (kN)	M _y (kNm)
0	1.0E7	470.0	2800.0

5.3.4. Currents

Current effects will not be considered in this thesis.

5.3.5. Further meteorological – oceanographical parameters

Parameter	Value	Unit
Gravity acceleration	9.81	m/s ²
Sea water density	1025.0	kg/m ³

5.3.6. Soil conditions

a. Soil profiles

For design of pile foundations, detailed knowledge is required regarding strength and bearing capacity of the soil. This is usually gathered through in-situ sampling and analysis of drilled samples in the laboratory. The first property measured for all types is the buoyant density γ'_{soil} , usually for

submerged soil, which is the wet (or bulk) density minus the density of water. For clay, the undrained shear strength s_u and the strain at 50% of the maximum stress ε_{50} are measured.

For sand, the friction angle φ and the relative density of sand D_r are derived directly from in-situ measurements. The initial modulus of horizontal subgrade reaction, k , as in (4.29), can be derived from the friction angle using Figure IV.17 taken from (DNV-OS-J101, 2011) or from relative density D_r .

For this master thesis, soil conditions are taken from the Horns Rev offshore wind plant, Denmark.

Soil Layers	Name	Depth (m)	Young Modulus E kN/m ²	Density γ / γ' kN/m ³	Friction angle φ degree	Dilatancy angle ψ degree	Poisson's ratio ν	Relative density D_r
Layer 1	Sand	1.0	31800	20/10	37.8	10.8	0.3	65
Layer 2	Sand	3.5	57100	20/10	39.2	12.2	0.3	74
Layer 3	Sand	5.5	52534	20/10	38.3	11.3	0.3	69
Layer 4	Sand	6.5	44100	20/10	37.5	10.5	0.3	63
Layer 5	Sand	7.0	58200	20/10	38.9	11.9	0.3	73
Layer 6	Sand	8.5	72170	20/10	39.9	12.9	0.3	79
Layer 7	Sand	10.0	52950	20/10	38.8	11.8	0.3	72
Layer 8	Sand	11.5	35400	20/10	36.3	9.3	0.3	55
Layer 9	Sand	12.5	23530	20/10	33.5	6.5	0.3	37
Layer 10	Sand	13.5	13600	20/10	30.4	3.4	0.3	16
Layer 11	Org. sand	20.0	3135	17/7	19.4	0	0.3	1
Layer 12	Org. sand	21.04	12950	17/7	28.1	1.1	0.3	1
Layer 13	Sand	41.8	36800	20/10	34.0	7.0	0.3	40

b. Scour

If no scour protection is planned, an additional depth in relation to scour effects has to be assumed in accordance to the outer diameter of the foundation pile, D , to be $(2.5 \times D)$ according to (GL, 2005).

However, in this thesis, scour protection is assumed, by what no water depths variations due to scour are taken into account.

5.4. Load combination for ULS

Type	Label	Value	Unit
Tower top loads	Fx	1698.5	kN
	Fy	952.5	kN
	Mx	4318.0	kNm
	My	8888.0	kNm
	Mz	6190.0	kNm
Wind / wave misalignment		0.0	°
Wave conditions	Sea state	Regular	
	Wave height	10.0	m
	Wave period	14.0	s

5.5. Results of internal forces for foundation design

5.5.1. For ULS design

Id	F _x (kN)	F _y (kN)	F _z (kN)	M _x (kNm)	M _y (kNm)	M _z (kNm)
0	5701	1143	-15286	133198	378179	7428
1	5525	1143	-14513	127483	349884	7428
2	5168	1143	-13739	121768	322456	7428
3	4800	1143	-12966	116053	296787	7428
4	4411	1143	-12193	110338	273296	7428
5	4001	1143	-11457	104623	251716	7428
6	3624	1143	-10779	98908	231843	7428
7	3246	1143	-10159	93193	214086	7428
8	3177	1143	-9615	87478	198935	7428
9	3095	1143	-9161	81763	185044	7428
10	3004	1143	-8718	76048	171195	7428
11	2909	1143	-8311	70333	157403	7428
12	2817	1143	-7923	64618	143684	7428
13	2724	1143	-7553	58903	130047	7428
14	2660	1143	-7202	53188	116505	7428
15	2619	1143	-6875	47473	103082	7428
16	2583	1143	-6577	41758	89811	7428
17	2540	1143	-6290	36043	76720	7428
18	2490	1143	-6025	30328	63840	7428
19	2431	1143	-5779	24613	51210	7428
20	2370	1143	-5560	18898	38886	7428
21	2310	1143	-5378	13183	26886	7428
22	2249	1143	-5219	7468	15187	7428

Maximum internal loads at the seabed:

- Vertical load: $V = F_{z_1} = 14513 \text{ kN}$
- Horizontal load: $H_{\max} = \sqrt{F_{x_1}^2 + F_{y_1}^2} = \sqrt{5525^2 + 1143^2} = 5642 \text{ kN}$
- Moment:

$$M_{\max} = \sqrt{M_{x_1}^2 + M_{y_1}^2} = \sqrt{127483^2 + 349884^2} = 3.724 \times 10^5 \text{ kNm}$$

5.5.2. For SLS check

Loads for SLS analyses will be calculated in the next chapter.

5.6. Results of natural frequency analysis

Table V.2: Natural frequency of the support structure in EOL OS

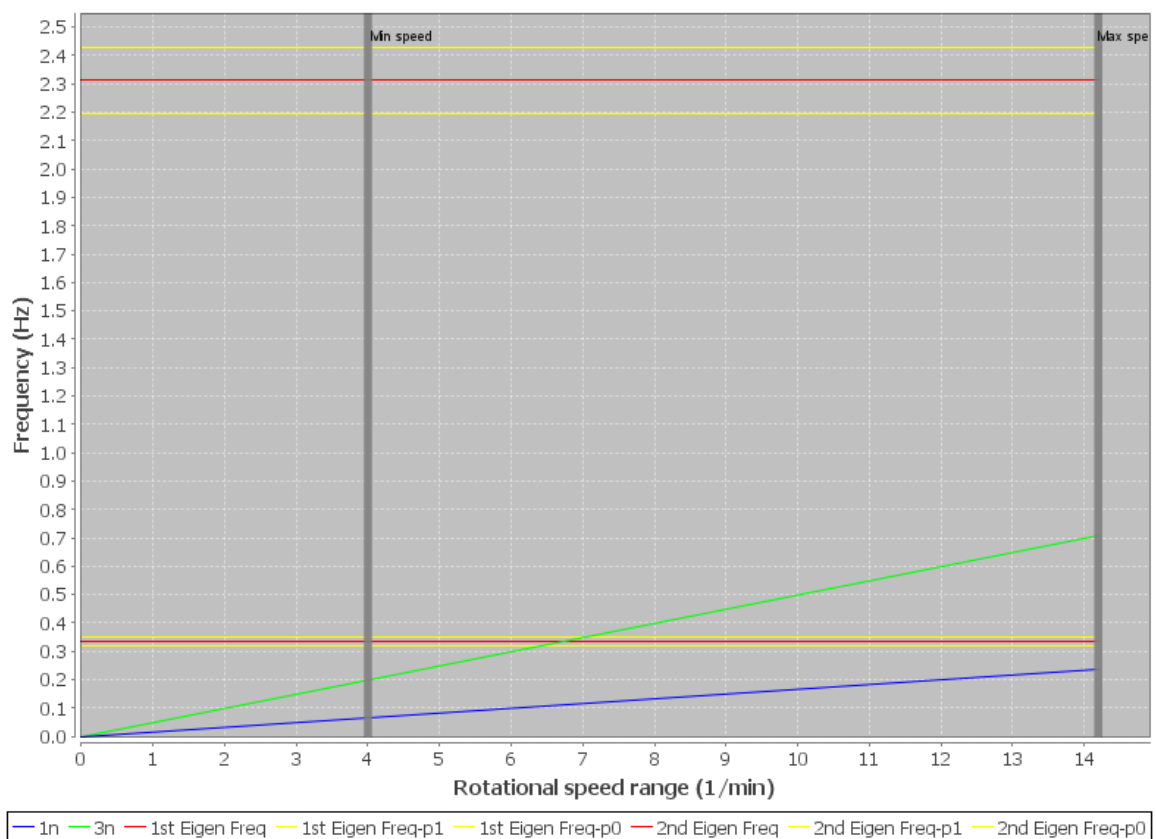
Resonance mode	Resonance frequency (Hz)	Upper limit (0.95 f)	Lower limit (1.05 f)
1	0.334	0.317	0.351
2	2.312	2.196	2.428

Table V.3: Excitation frequencies

Rotor speed	1P (or “1n”) excitation frequency	3P (or “3n”) Excitation frequency
4.0 (1/m) (minimum speed)	$f_{1P} = \frac{4.0}{60} = 0.067$	$f_{3P} = 3 \frac{4.0}{60} = 0.2$
12.2 (1/m) (rated speed)	$f_{1P} = \frac{12.2}{60} = 0.203$	$f_{3P} = 3 \frac{12.2}{60} = 0.61$
14.2 (1/m) (maximum speed)	$f_{1P} = \frac{14.2}{60} = 0.237$	$f_{3P} = 3 \frac{14.2}{60} = 0.71$

The Campbell diagram characterizing the offshore wind turbine shows the eigen frequencies with +/- 5% variance compared to the rotational speed range of the rotor.

Campbell diagram



The “1n” excitation frequency doesn’t meet the 1st natural frequency of the support structure.

The “1n” excitation frequency doesn’t meet the 2nd natural frequency of the support structure.

An intersection between the “3 n” excitation frequency and the 1st natural frequency of the support structure is found at the rotational frequency 6.68 (1/min).

The “3 n” excitation frequency doesn’t meet the 2nd natural frequency of the support structure.

Chapter VI. Foundation pile design



6.1. Introduction

The structure of this chapter is divided into three main parts:

- Preliminary design for the foundation pile. In this part, internal forces at the seabed getting from EOL-OS software is used for ULS design of the foundation pile. It is called preliminary design because the inputs for the calculation were taken from the EOL-OS which did not consider the presence of foundation part in its modeling.
- After having the dimensions of the foundation pile, a dynamic model for the foundation in SLS design will be considered.
- Finally the effect of foundation in dynamic behavior of the structure will be accessed.

6.2. Ultimate limit state design

The load-carrying capacity of piles shall be based on strength and deformation properties of the pile material as well as on the ability of the soil to resist pile loads.

As mentioned in Section 3.4.4, ULS design of the foundation pile will follow equation (3.2) and (3.1) with $\gamma_M = 1.25$ for axial capacity and 1.15 for lateral capacity. ULS design is carried out under the water level of MSL = 30 m.

As calculated from Section 5.5.1, maximum internal loads at the seabed elevation of the support structure are:

- Vertical load: $V = 14513 \text{ kN}$
- Horizontal load: $H_{\max} = 5642 \text{ kN}$
- Moment: $M_{\max} = 3.724 \times 10^5 \text{ kNm}$

From the results of EOL OS software, section of the foundation pile should not smaller than following values:

- Outside diameter: $D = 6.0 \text{ m}$
- Wall thickness: $t = 80 \text{ mm}$
- Steel material: S235 with $f_y = 235 \frac{\text{N}}{\text{mm}^2}$

6.2.1. Axial capacity

a. The design axial resistance

The pile resistance, R , is composed of two parts, one part being the accumulated skin resistance, R_s , and the other part is the tip resistance, R_p :

$$R = R_s + R_p - W = \sum f_{si} A_{si} + q_p A_p - W \quad (6.1)$$

where

- f_{si} = average unit skin friction along pile shaft in layer i.
 A_{si} = shaft area of pile in layer i.
 q_p = unit end resistance.
 A_p = gross end area of pile.
 W = weight of the foundation pile.

a.1). Accumulated skin resistance:

For piles in mainly cohesionless soils (sand), the average unit skin friction may be calculated according to:

$$f_s = K \cdot p_0' \tan \delta \leq f_1 \quad (6.2)$$

in which :

$K = 0.8$ for open-ended piles

p_0' is the effective overburden pressure

δ is the angle of soil friction on the pile wall as given in Table VI.1

f_1 is a limiting unit skin friction, see Table VI.1 for guidance.

**Table VI.1: Design parameters for axial resistance of driven piles
in cohesion less silicious soil (DNV-OS-J101, 2011)**

Density	Soil description	δ (degrees)	f_1 (kPa)	N_q (-)	q_1 (MPa)
Very loose Loose Medium	Silt Sand-silt ²⁾ Silt	15	48	8	1.9
Loose Medium Dense	Sand Sand-silt ²⁾ Silt	20	67	12	2.9
Medium Dense	Sand Sand-silt ²⁾	25	81	20	4.8
Dense Very dense	Sand Sand-silt	30	96	40	9.6
Dense Very dense	Gravel Sand	35	115	50	12.0
1) The parameters listed in this table are intended as guidelines only. Where detailed information such as in-situ cone penetrometer tests, strength tests on high quality soil samples, model tests or pile driving performance is available, other values may be justified. 2) Sand-silt includes those soils with significant fractions of both sand and silt. Strength values generally increase with increasing sand fractions and decrease with increasing silt fractions.					

a.2). Tip resistance:

The unit tip resistance of plugged piles in cohesionless soils can be calculated as:

$$q_p = N_q \cdot p_0' \leq q_1 \quad (6.3)$$

in which

N_q is the bearing factor, can be taken from Table VI.1

q_1 is a limiting tip resistance, see Table VI.1 for guidance.

From results of calculation as shown in Figure VI.1 to Figure VI.5, it is possible to find the sufficient length of the pile to satisfy equations (3.2). In Figure VI.5, the horizontal line is the design vertical load and all the pile length having design soil strength higher than this line is sufficient ($L_{\min} = 21 \text{ m}$, and $R_D(L_{\min}) = 21790 \text{ kN} > 14513 \text{ kN}$).

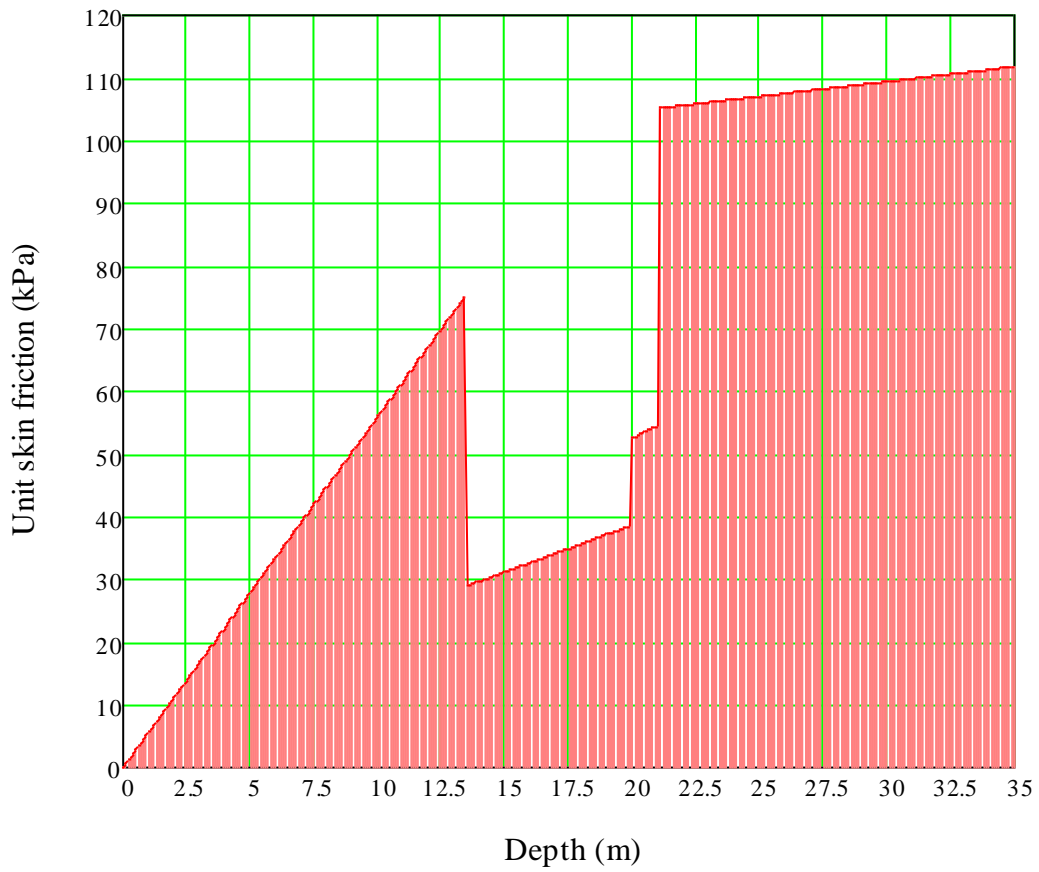


Figure VI.1: Unit skin friction along the pile

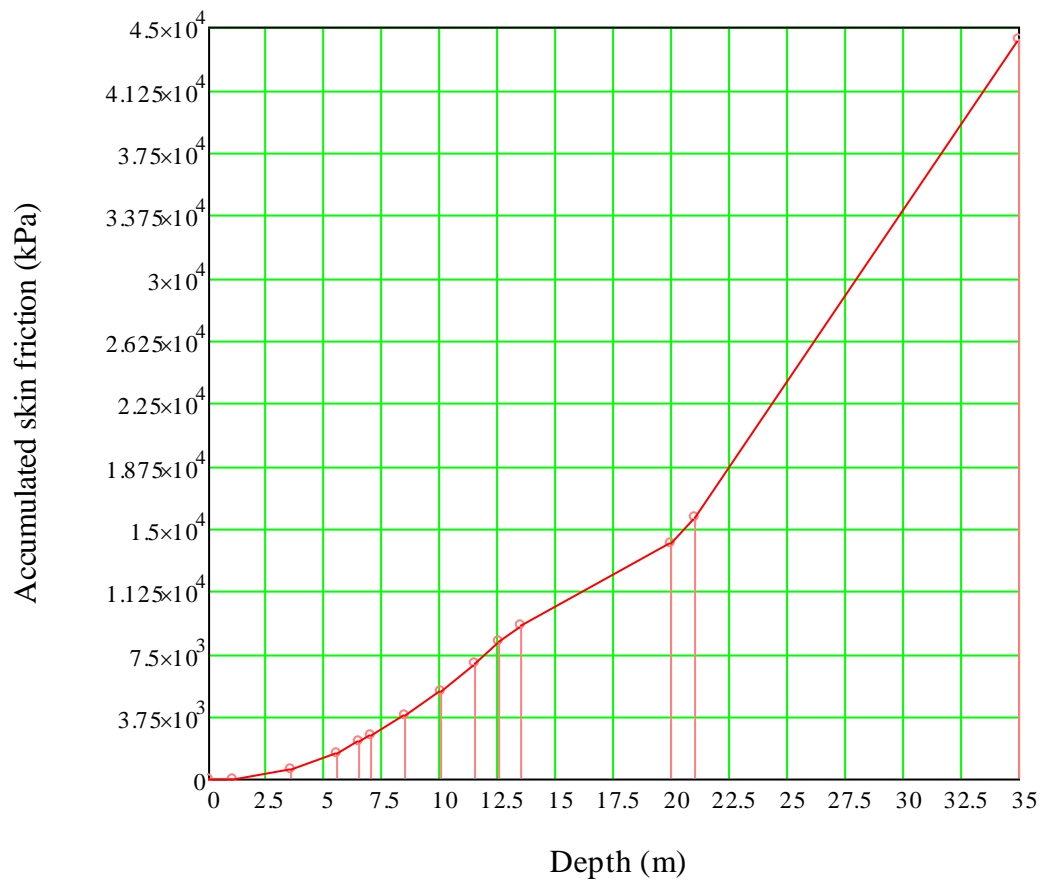


Figure VI.2: Accumulated skin friction vs. pile length

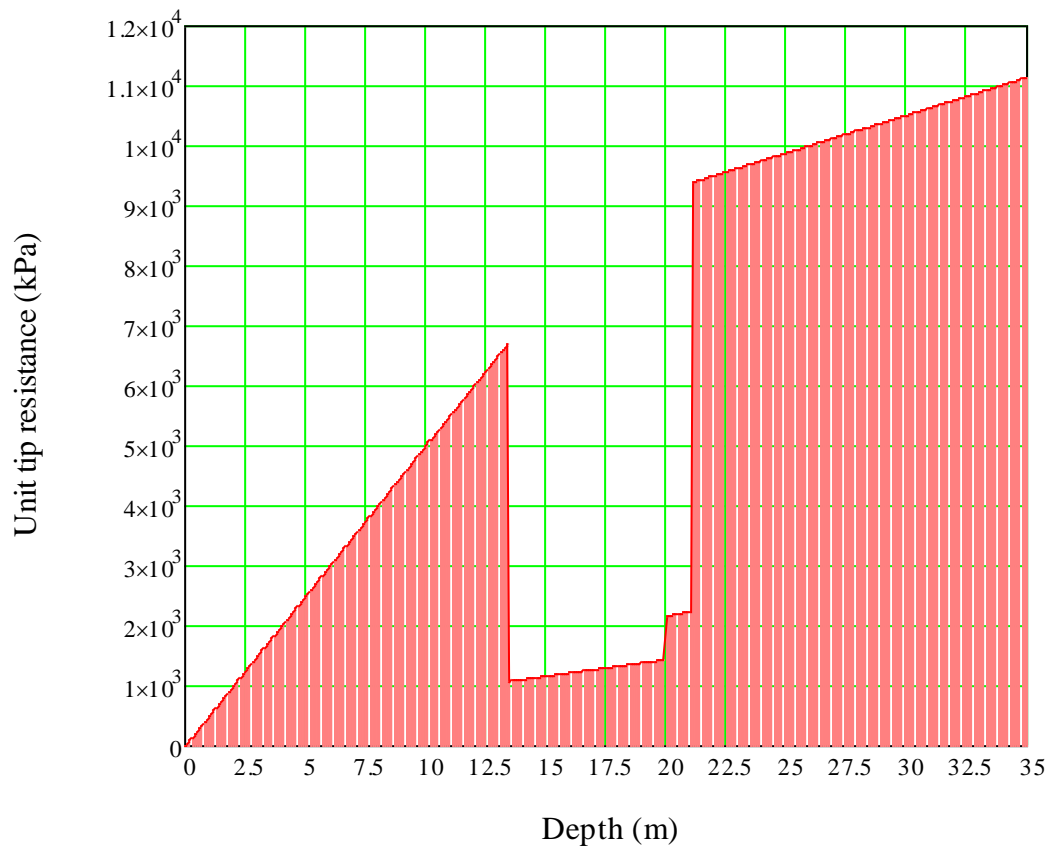


Figure VI.3: Unit tip resistance vs. pile length

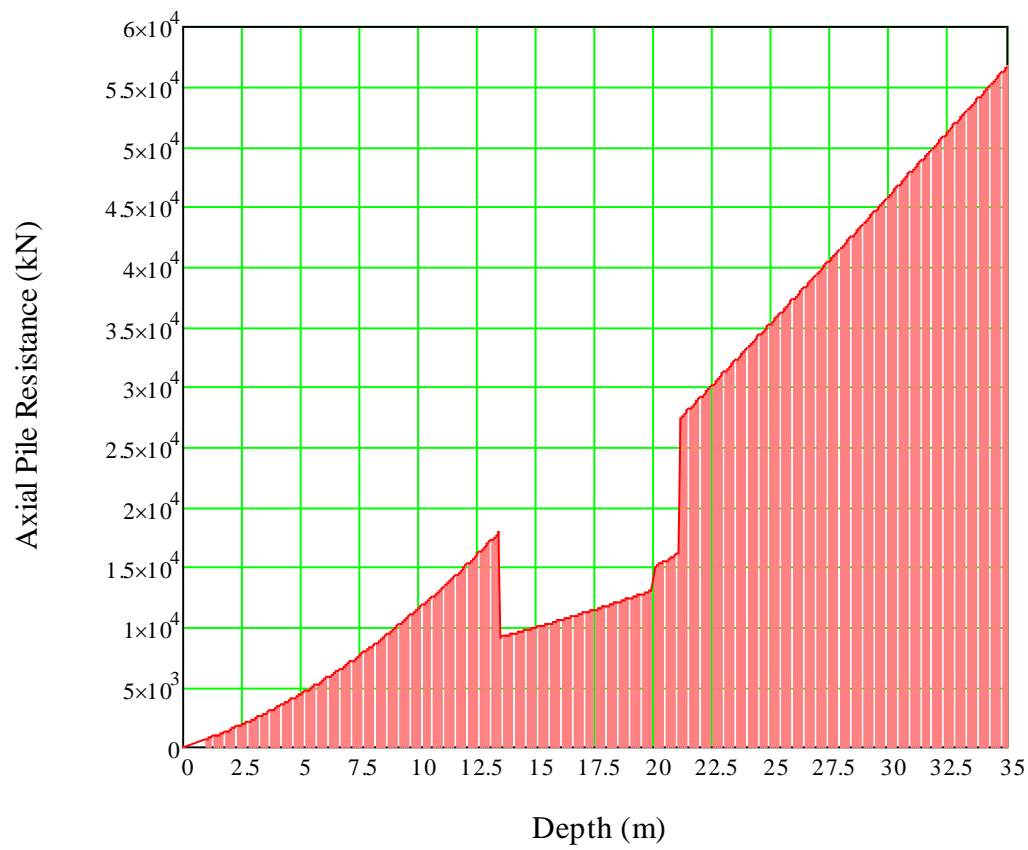


Figure VI.4: Axial pile resistance vs. pile length

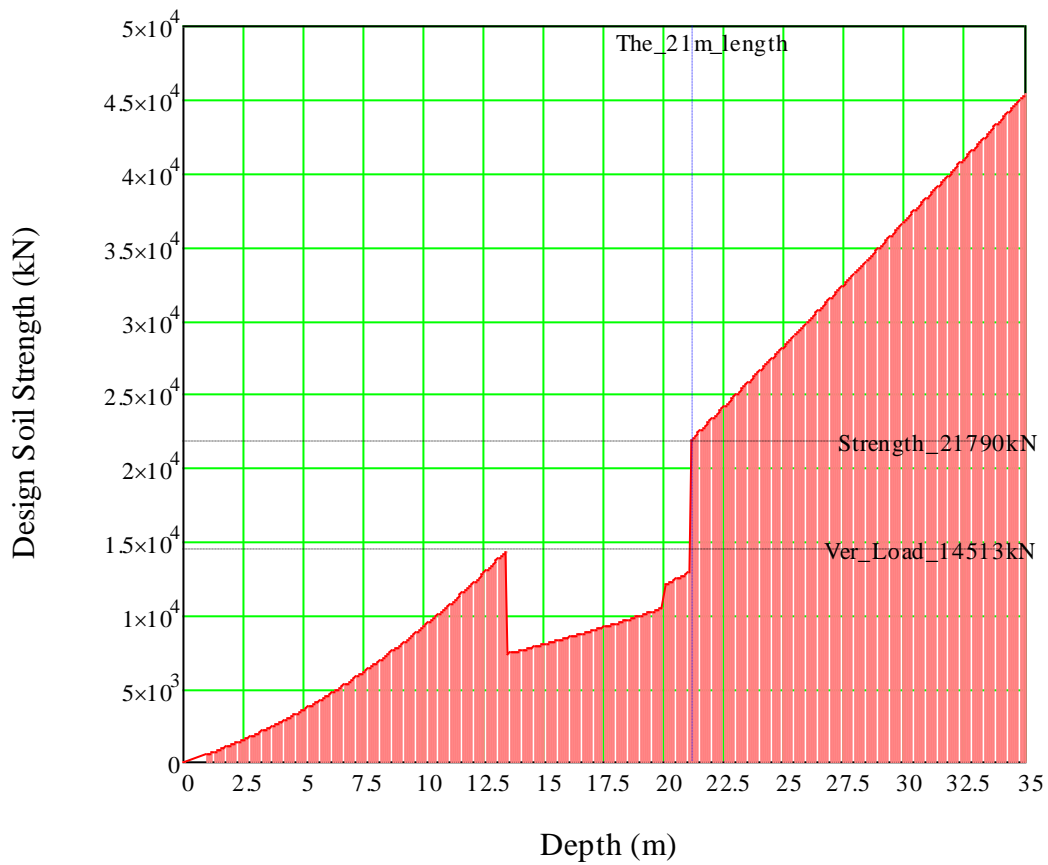


Figure VI.5: Design Soil Strength vs. Pile Length

b. Axial resistance in cyclic loading

The effects of cyclic loading on the axial pile resistance should be considered in design (see Section 4.10 Effect of cyclic loading to foundation). The main objective is to determine the shear strength degradation, i.e. the degradation of the unit skin friction, along the pile shaft for the appropriate prevailing loading intensities.

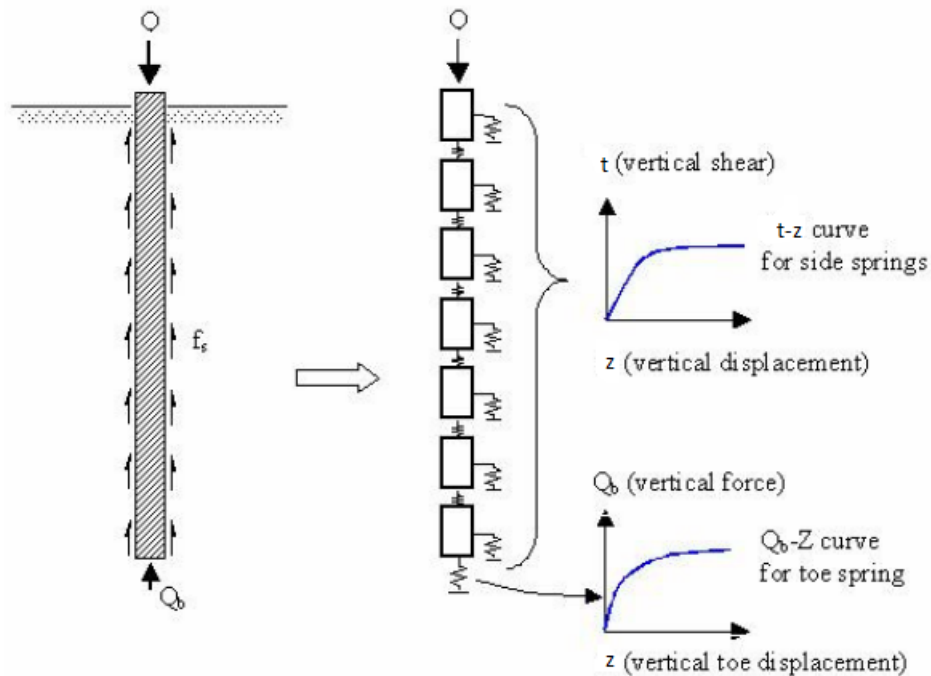


Figure VI.6: Illustration of the idealized model used in t-z load-transfer analyses

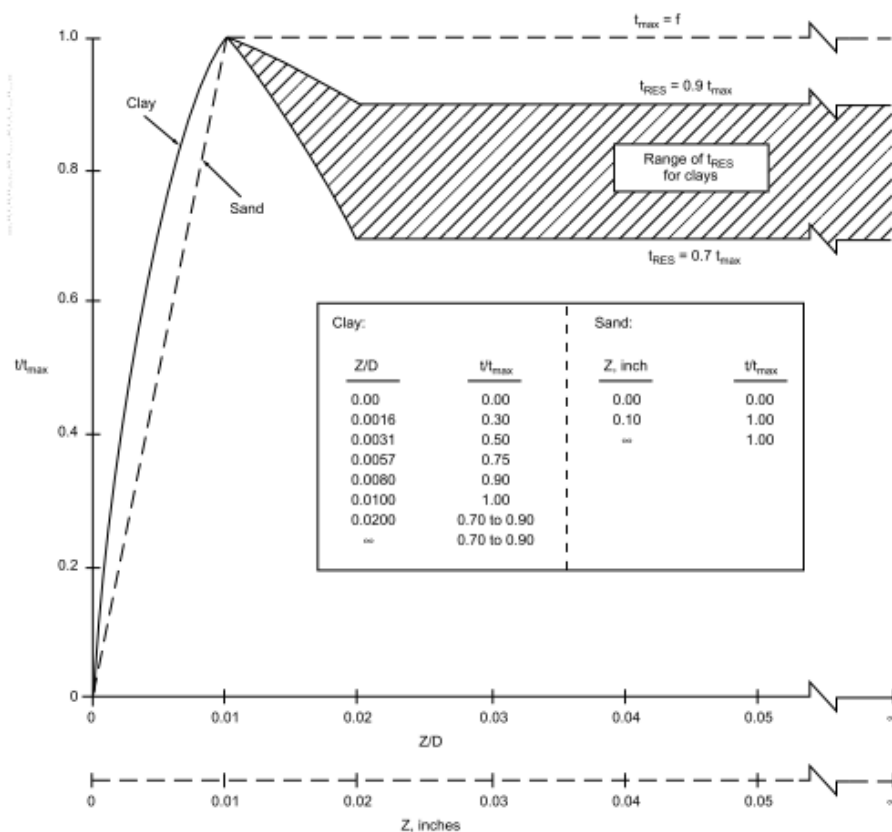


Figure VI.7: Illustration of the t-z curve according to API

b.1). The load-transfer (t-z) curves:

The load-transfer (t-z) method is probably the most widely used technique to study the problem of single axially loaded piles, and is particularly useful when the soil behavior is clearly nonlinear and/or when the soil surrounding the pile is stratified. This method involves modeling the pile as a series of elements supported by discrete nonlinear springs, which represent the resistance of the soil in skin friction (t-z springs). The soil springs are nonlinear representations of the soil reaction, t , versus displacement z as shown schematically in Figure VI.6.

For both clay and sandy soil, the t-z curve can be determined as illustrated in Figure VI.7. Note that for sand, after t_{\max} is reached, the curve is horizontal because $t_{\text{res}} = t_{\max}$ (API, 2000).

The t-z curves can also be generated according to a method by which a nonlinear relation applies between the origin and the point where the maximum skin resistance t_{\max} is reached (DNV-OS-J101, 2011):

$$z = t \frac{R}{G_0} \ln \frac{z_{IF} - r_f \frac{t}{t_{\max}}}{1 - r_f \frac{t}{t_{\max}}} \quad \text{for } 0 \leq t \leq t_{\max} \quad (6.4)$$

in which:

R denotes the radius of the pile,

G_0 is the initial shear modulus of the soil,

z_{IF} is a dimensionless zone of influence, defined as the radius of the zone of influence around the pile divided by R ,

r_f is a curve fitting factor.

For displacements z beyond the displacement where t_{\max} is reached, the skin resistance t decreases in linear manner with z until a residual skin resistance t_{res} is reached. For further displacements beyond this point, the skin resistance t stays constant.

Equation (6.4) will be used in this thesis to determine the nonlinear curve before t_{\max} is reached because it uses some important parameters of the soil and pile to define the relationship. The t-z curves in this thesis will be draw until the point where t_{\max} is reached, after that point, it is understood that $t = t_{\max}$ until z goes to infinity for sandy soil.

For sands, the initial shear modulus of the soil to be used for generation of t-z curves is to be taken as:

$$G_0 = \frac{m \sqrt{\sigma_a \cdot \sigma_v}}{2(1+\nu)} \quad \text{with } m = 1000 \tan \phi \quad (6.5)$$

In which $\sigma_a = 100$ kPa is a reference pressure and σ_v is the vertical effective stress, ν is the Poisson's ratio of the soil, and ϕ is the friction angle of the soil.

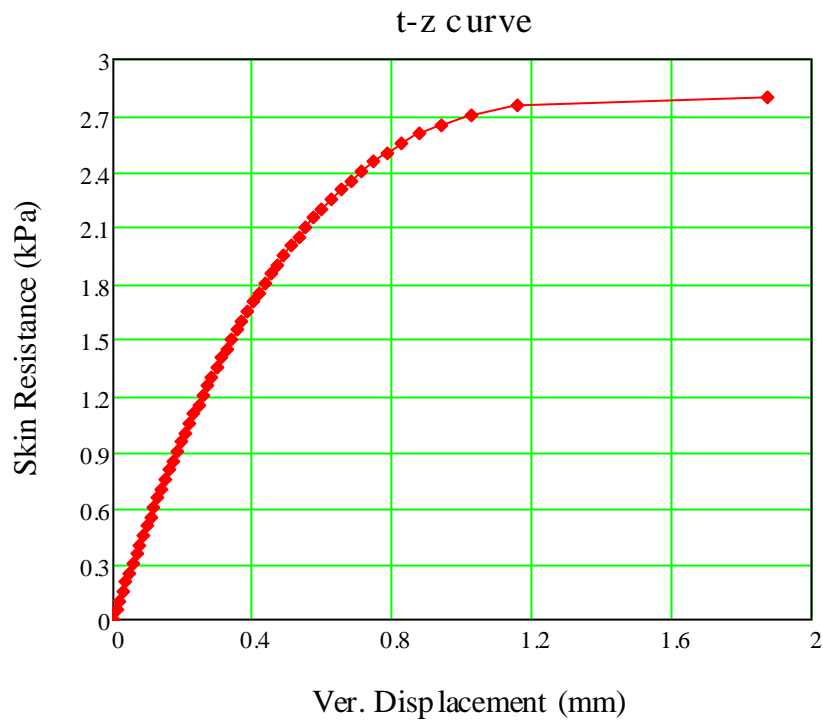


Figure VI.8: t-z curve at X=0.5 m

Figure VI.8 shows the t-z curve at X=0.5 m, for other elevation, t-z curves are shown in Appendix 1.

b.2). The Tip load Displacement (Q-z) curve

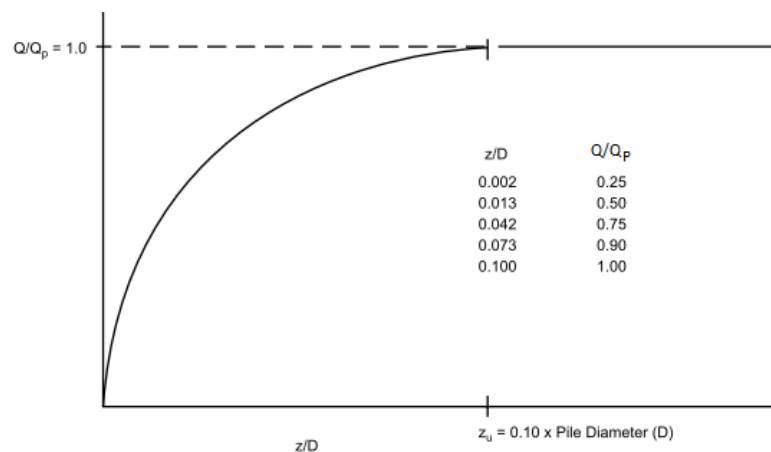


Figure VI.9: Generic pile Tip load - Displacement (Q-z) curve

According to API (API, 2000), relatively large pile tip movements are required to mobilize the full end bearing resistance that calculated from equation(6.3). A pile tip displacement up to 10 percent of the pile diameter may be required for full mobilization in both sand and clay soils. In the absence of more definitive criteria the following curve is recommended for both sands and clays.

$$\frac{z}{D} \quad \frac{Q}{Q_p}$$

0.002	0.25
0.013	0.50
0.042	0.75
0.073	0.90
0.100	1.00

Where

z = axial tip deflection, (mm)

D = pile diameter, (mm)

Q = mobilized end bearing capacity, (kN)

Q_p = total end bearing, (kN), as shown in Figure VI.3.

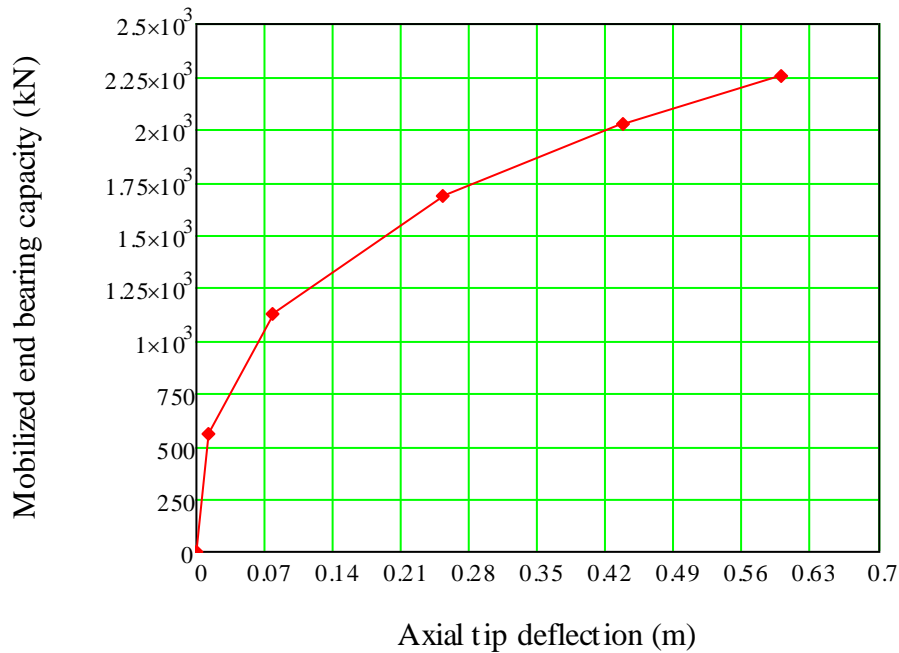


Figure VI.10: Q-z curve at depth X=21 m

Figure VI.10 shows the Q-z curve at X=21 m, for other elevation, Q-z curves are shown in Appendix

It should be mentioned here that Q-z curve in this thesis only drawn to the point where total end bearing is reached, after that point, the curve is in horizontal direction until axial tip deflection reaches infinity.

b.3). Settlement of foundation pile

As illustrated in Figure VI.6, the settlement of the foundation pile will be determined using that model. From the results of calculation, the settlement of the pile of less than or equal to 21 m cannot be obtained (because the solution cannot converge for these lengths). This is so because the mobilized resistance of the 21 m long pile is smaller than the applied load when the effects of cyclic loading are taken into account. Remember that it is only for a length larger than 21m that the foundation pile has a design axial resistance larger than the applied axial load (see Section 6.2.1). For other lengths, the settlement is reduced when the length is increased (see Table VI.2).

Table VI.2: Result of pile settlement calculation

Pile length (m)	Settlement (mm)	Pile length (m)	Settlement (mm)
22	-23.1	31	-10.5
23	-19.5	32	-10.0
24	-17.1	33	-9.6
25	-15.4	34	-9.2
26	-14.1	35	-8.9
27	-13.0	36	-8.6
28	-12.2	37	-8.3
29	-11.6	38	-8.0
30	-11.0		

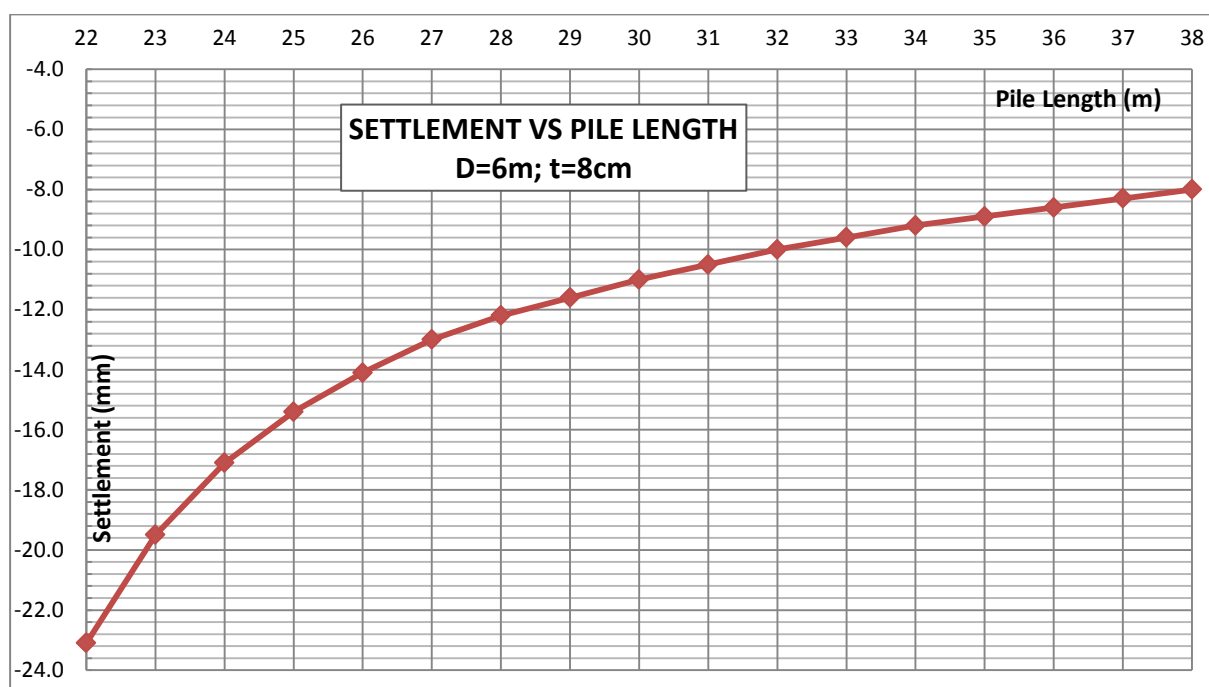


Figure VI.11: Settlement vs. pile lengths

6.2.2. Lateral capacity

For combined lateral loading and moment loading in the ULS, sufficient pile capacity against this loading shall be ensured. The pile capacity is formed by lateral pile resistance (DNV-OS-J101, 2011).

As mentioned in Section 3.4.4 Design criteria for monopile foundations, page 34, there are two requirements about pile capacity that have to be fulfilled:

- (1) The theoretical design total lateral pile resistance, which is found by vectorial integration of the design lateral resistance over the length of the pile, shall not be less than the design lateral load applied at the pile head.

- (2) The lateral displacement at the pile head shall not exceed some specified limit. The lateral displacement shall be calculated for the design lateral load and moment in conjunction with characteristic values of the soil resistance and soil stiffness.

a) Theoretical design total lateral pile resistance

The theoretical design total lateral pile resistance (ΣP_u), which is found by vectorial integration of the design lateral resistance over the length of the pile, shall not be less than the design lateral load applied at the pile head (H_{\max}):

$$\frac{\Sigma P_u}{\gamma_M} \geq H_{\max} \quad (6.6)$$

$$\Sigma P_u = \Sigma(p_{u_i} \cdot l_i) \quad (6.7)$$

in which $\gamma_M = 1.15$ taken Table III.1;

p_{u_i} = the static ultimate lateral resistance, determined by equation (4.24) or (4.28).

l_i = the thickness of soil layer used for integration.

As shown in Figure VI.13, the condition (denoted in equation(6.6)) is satisfied for pile lengths larger than 5.5 m. However, it is usually not enough to ensure that the lateral design load at the pile head does not exceed the design total lateral resistance that is theoretically available. This is so because long before the total available lateral resistance becomes mobilized by mobilization of all lateral soil resistance along the pile, excessive (and unacceptable) lateral pile displacements will take place at the pile head. So the pile length will be determined by considering the predicted pile head displacement as a function of pile length and making sure that the selected length corresponds to the flat part of the corresponding displacements-length curve (see Figure VI.17 and Figure VI.18).

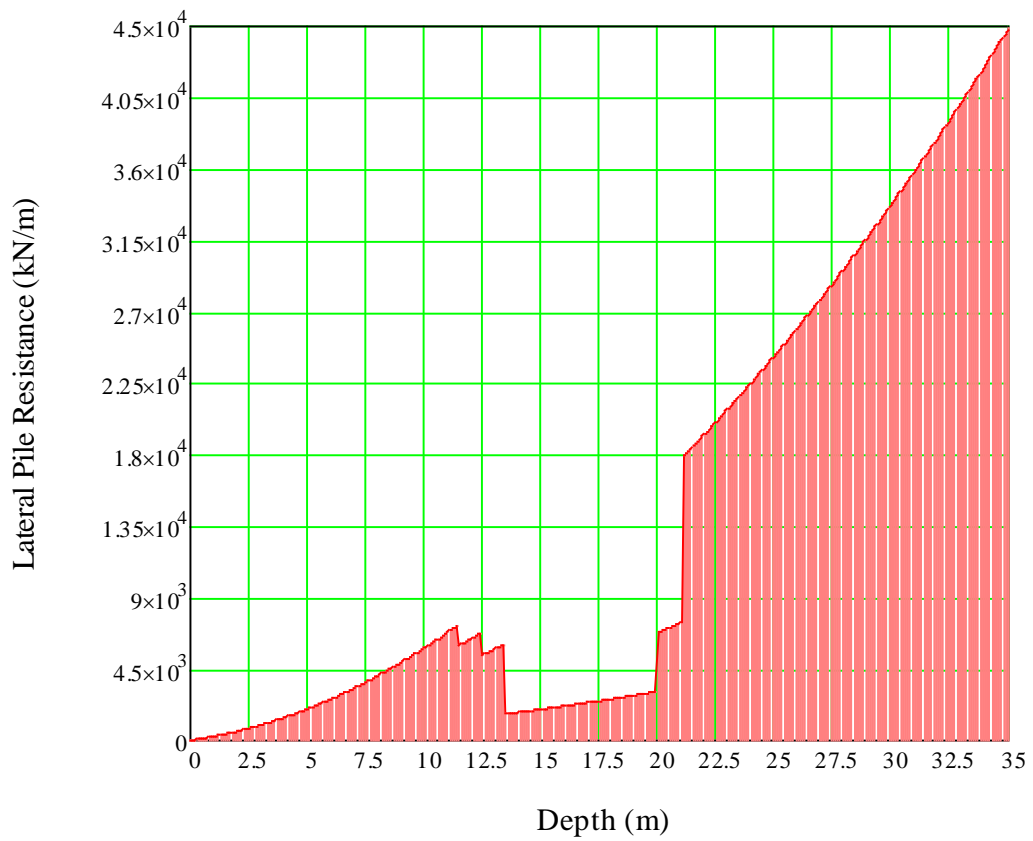


Figure VI.12: Lateral pile resistance vs. pile length (Diameter = 6m)

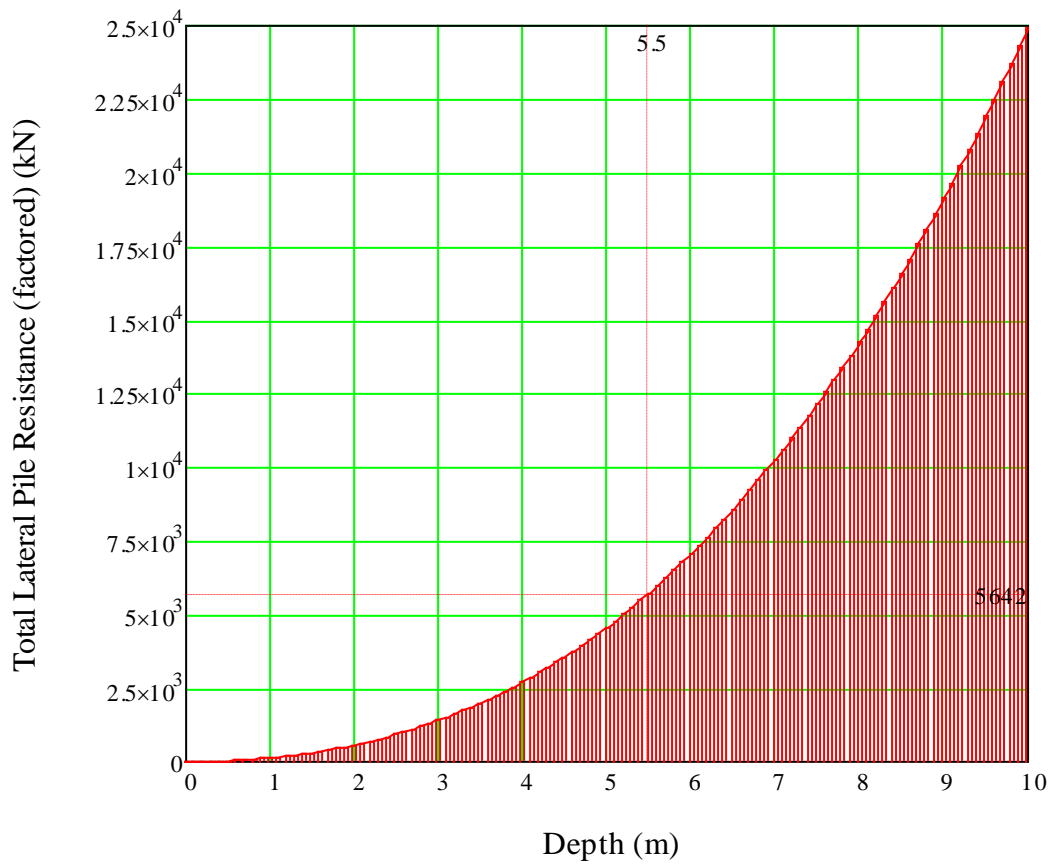


Figure VI.13: Total lateral pile resistance ($\gamma_m=1.15$) and the design lateral load (5642 kN)

b) The lateral displacement at the pile head

b.1). The p-y curves

The method recommended by DNV Standard (DNV-OS-J101, 2011) is used here to calculate the lateral capacity of the foundation pile under cyclic effects in ULS design. The procedure to produce these p-y curves has been introduced in Section 4.13.3 Load-displacement relationship, page 62. Figure VI.15 is the p-y curve at the depth 6.75 m, and Figure VI.14 is the database for that p-y curve. As shown in Figure VI.14, it is possible to see the ultimate lateral capacity of the soil at the depth 6.75 m under effects of cyclic loading. And this value is smaller than the theoretical value calculated from equation (4.24) or (4.28), shown in Figure VI.12 page 87.

Layer 5:

- Elevation of the top: top := 6.5 m
- Elevation of the bottom: bottom := 7 m
- Elevation of the middle: $x := 0.5 \cdot (\text{top} + \text{bottom}) = 6.75$ m
- Diameter of the pile: D := 6 m

Calculation of p-y curve:

Value _y =		Value _p =		Value _y =		Value _p =	
	0		0		0		0
43	-0.014	43	-2.872·10 ³	0	-0.1	0	-3.51059·10 ³
44	-0.012	44	-2.654·10 ³	1	-0.098	1	-3.51059·10 ³
45	-0.01	45	-2.374·10 ³	2	-0.096	2	-3.51059·10 ³
46	-8·10 ⁻³	46	-2.025·10 ³	3	-0.094	3	-3.510589·10 ³
47	-6·10 ⁻³	47	-1.604·10 ³	4	-0.092	4	-3.510589·10 ³
48	-4·10 ⁻³	48	-1.115·10 ³	5	-0.09	5	-3.510588·10 ³
49	-2·10 ⁻³	49	-572.113	6	-0.088	6	-3.510587·10 ³
50	0	50	0	7	-0.086	7	-3.510586·10 ³
51	2·10 ⁻³	51	572.113	8	-0.084	8	-3.510584·10 ³
52	4·10 ⁻³	52	1.115·10 ³	9	-0.082	9	-3.510581·10 ³
53	6·10 ⁻³	53	1.604·10 ³	10	-0.08	10	-3.510577·10 ³
54	8·10 ⁻³	54	2.025·10 ³	11	-0.078	11	-3.510572·10 ³
55	0.01	55	2.374·10 ³	12	-0.076	12	-3.510564·10 ³
56	0.012	56	2.654·10 ³	13	-0.074	13	-3.510554·10 ³
57	0.014	57	2.872·10 ³	14	-0.072	14	-3.51054·10 ³
58	...	58	...	15	...	15	...

Ultimate capacity at this depth

Figure VI.14: Database for the p-y curve at the depth 6.75 m

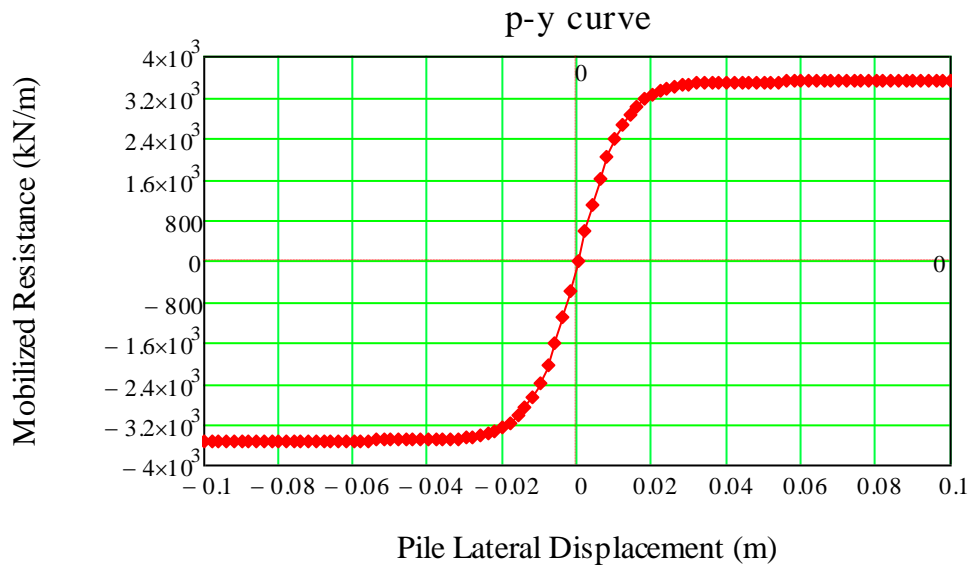


Figure VI.15: p-y curve at the depth 6.75m (layer 5)

b.2). Choosing pile length

Sufficient pile capacity against combined lateral loading and moment loading can be ensured by means of a single pile analysis in which the pile is discretized into a number of structural elements, interconnected by nodal points, and with soil support springs in terms of p-y and t-z curves attached at these nodes, at the pile tip the Q-z curve is used to find the mobilized tip resistance. Lateral forces and overturning moments are applied to the pile head. Also axial forces acting at the pile head need to be included because they may contribute to the bending moment and the mobilization of lateral soil resistance owing to second order effects.

Analysis is carried out for 19 pile lengths. Results of the calculation (using Sap2000 software) are shown in figures from Figure VI.16 to Figure VI.18 and

Table VI.3. Figure VI.16 shows the geometry model of that 19 piles and the nodal displacements of some pile heads from Sap2000 software.

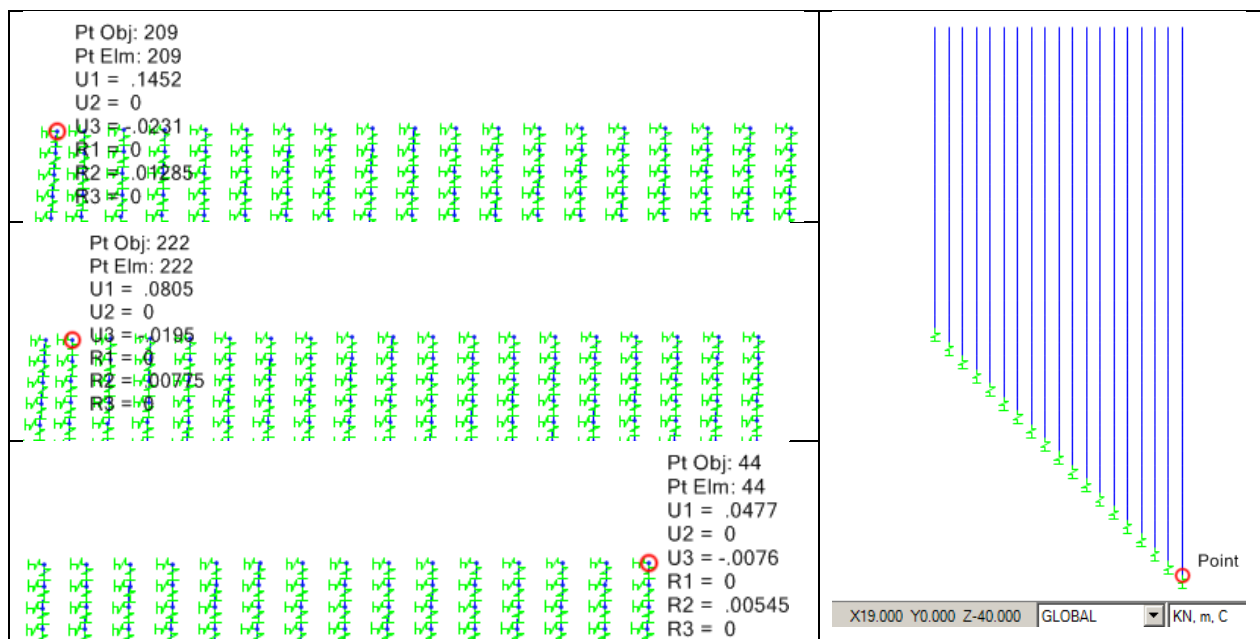


Figure VI.16: Results of lateral analysis

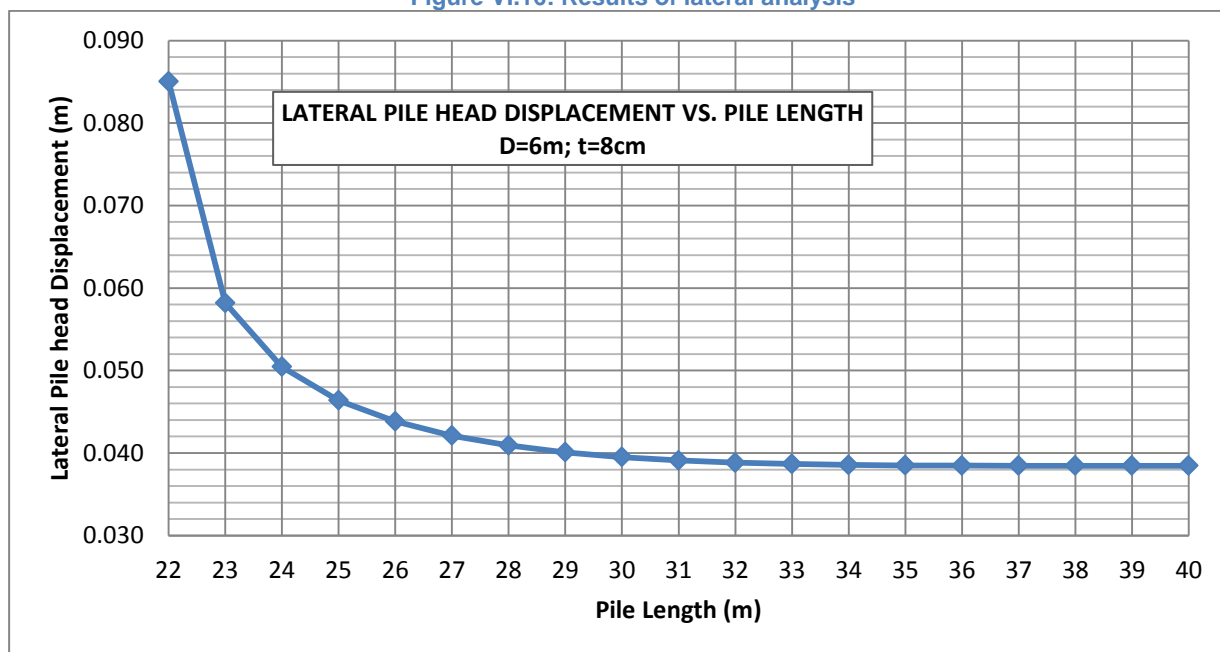


Figure VI.17: Lateral pile head displacement vs. Pile length

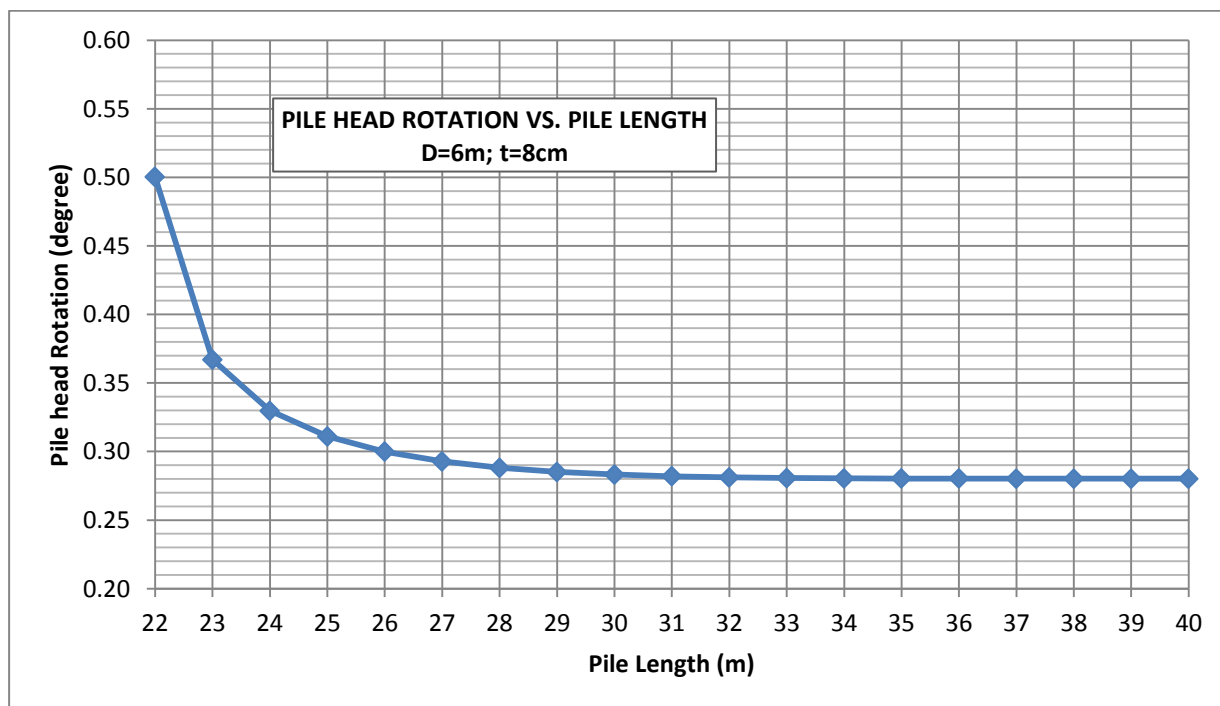


Figure VI.18: Pile head rotation vs. Pile length

Table VI.3: Displacement and Rotation of pile head with the length

Pile length (m)	Lateral pile head displacement (m)	Rotation of pile head (degree)
22	0.085	0.50
23	0.058	0.37
24	0.050	0.33
25	0.046	0.31
26	0.044	0.30

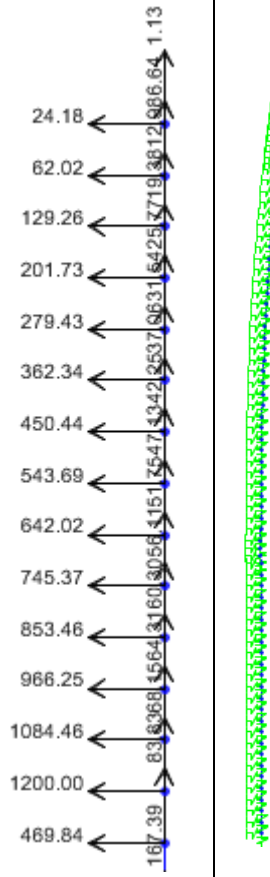
Pile length (m)	Lateral pile head displacement (m)	Rotation of pile head (degree)
27	0.042	0.29
28	0.041	0.29
29	0.040	0.29
30	0.040	0.28
31	0.039	0.28
32	0.039	0.28
33	0.039	0.28
34	0.039	0.28
35	0.038	0.28
36	0.038	0.28
37	0.038	0.28
38	0.038	0.28
39	0.038	0.28
40	0.038	0.28

From the results of calculation, the “specified limit” which is mentioned in the second requirement for ULS design for the lateral displacement is approximately 4 cm, and the minimum pile length that satisfies this requirement is 26 m.

b.3). Determining plastified soil zone of the chosen pile:

In order to find the length of the plastified soil zone, more springs need to be added near the pile head of the chosen pile. This length will be the distance from the ground to the first spring that works in Elasto-Plastic state. From the result of calculation (see Table VI.4), the plastified soil zone is about 75cm.

Table VI.4: Plastified soil zone of the chosen pile

Depth	p-y curve		Calculation		Conclusion		
	$[p_u]$ (kN)	$[y]$ (m)	Lateral Reaction (kN)	Lateral deflection (m)			
0.1	24.18	0.028	24.18	0.0384		Plastified	
0.25	62.02	0.034	62.02	0.0372		Plastified	
0.50	129.26	0.032	129.26	0.0360		Plastified	
0.75	201.74	0.036	201.73	0.0348			
1.00	279.45	0.038	279.43	0.0336		Not plastified	
1.25	362.39	0.040	279.43	0.0324		Not plastified	
1.50	450.56	0.042	362.34	0.0313		Not plastified	
1.75	543.96	0.042	450.44	0.0302		Not plastified	
2.00	642.60	0.048	543.69	0.0291		Not plastified	
2.25	746.47	0.056	642.02	0.0280		Not plastified	
2.50	855.56	0.050	745.37	0.0269		Not plastified	
2.75	969.89	0.054	853.46	0.0259		Not plastified	
3.00	1089.45	0.054	966.25	0.0249		Not plastified	
3.25	1214.24	0.058	1084.46	0.0239		Not plastified	

6.2.3. Structural Capacity of the steel pile

For the yield check, it is verified that the stress remains below the characteristic yield stress to avoid plastic deformations in the structure due to yielding of the steel. The check is performed by calculating the Von Mises stress at each node, taking the appropriate load factors into account and ascertaining that:

$$\sigma_{vi} \leq \frac{f_y}{\gamma_M} \quad (6.8)$$

where σ_{vi} is the Von Mises stress at node i ,

$$f_y \text{ is the yield stress, } f_y = 235 \frac{N}{mm^2}$$

γ_M is the material factor, $\gamma_M = 1.0$ for tabular structure, according to DNV Standard (DNV-OS-J101, 2011).

The foundation pile works as a beam-column structure, with the normal stresses (σ) acting normal to the cross section of the pile and the shear stresses (τ) acting in plane of the cross section.

Normal stresses, shear stresses, and Von Mises stresses are determined from equations (6.9) to (6.11) respectively:

$$\sigma = \frac{V}{A} + \frac{M.c}{I} \quad (6.9)$$

$$\tau = \frac{H.Q}{I.b} \quad (6.10)$$

$$\sigma_v = \sqrt{\sigma^2 + 3\tau^2} \quad (6.11)$$

Where:

V, M, H are internal axial force, moment, and shear force respectively,

I is the moment of inertia (or second moment) of the plane area (see Figure VI.20):

$$I = \frac{\pi}{4} (r_2^4 - r_1^4) \quad (6.12)$$

Q is the static moment (or first moment) of the calculated area, changing depends on the relative distance of the calculating point to the neutral axis of the cross section (see Figure VI.19). For each circular section as in Figure VI.19, the static moment is determined using the following equation:

$$Q = A_s \times \bar{y} \quad (6.13)$$

In

Figure VI.21, the area A_s is determined from:

$$A_s = \alpha \times r^2 \quad (6.14)$$

and the distance from gravity center of that shaded area to neutral axis :

$$\bar{y}_{s-r2} = \frac{2 \times r \times \sin \alpha}{3 \times \alpha} \quad (6.15)$$

A is the area of the hollow section of the foundation pile,

$$A = \pi (r_2^2 - r_1^2) \quad (6.16)$$

c is the distance from the calculating point to the neutral axis of the cross section,

b is the shear-width of the cross section at the elevation of calculating point (see

Figure VI.21).

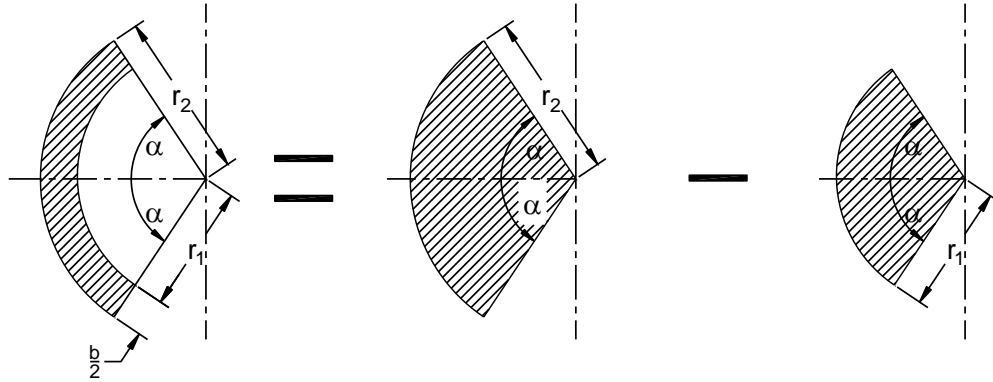


Figure VI.19: Process to calculate the static moment of a segment of hollow circular section

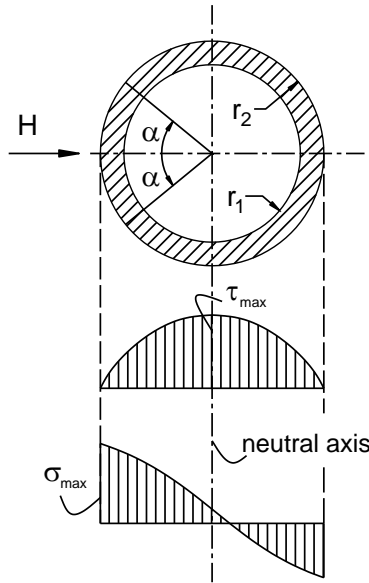


Figure VI.20: Normal stress and shear stress on the foundation pile

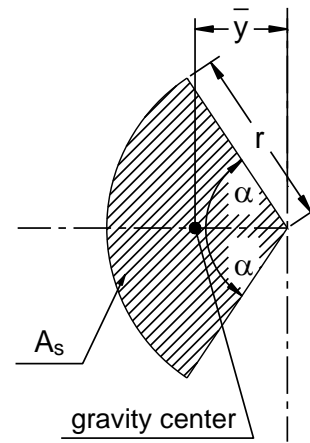


Figure VI.21: Parameters to determine static moment in a circular section

From the results of internal forces as shown in Figure VI.22 and Table VI.6, maximum Von Mises stress is calculated at each node based on the distributions of shear stress and normal stress on the corresponding section. Finally the utilization ratio, which is a ratio between the Von Mises stress and $\frac{f_y}{\gamma_M}$, is calculated at each node. This ratio must smaller than 1 to prevent yielding of steel, but should not be too small for economics reason. As shown in Figure VI.26, the utilization ratio is quite small at the depth of 10 m and beyond. It is possible to reduce the wall thicknesses of those locations as long as they are kept larger than the required minimum value for pile-driving (with soil having sustained hard driving (820 blows per meter) – according to API (API, 2000)):

$$t \geq 6.35 + \frac{D}{100} = 6.35 + \frac{6000}{100} = 66 \text{ mm} \quad (6.17)$$

with $D = 6000 \text{ mm}$ is the diameter of the foundation pile.

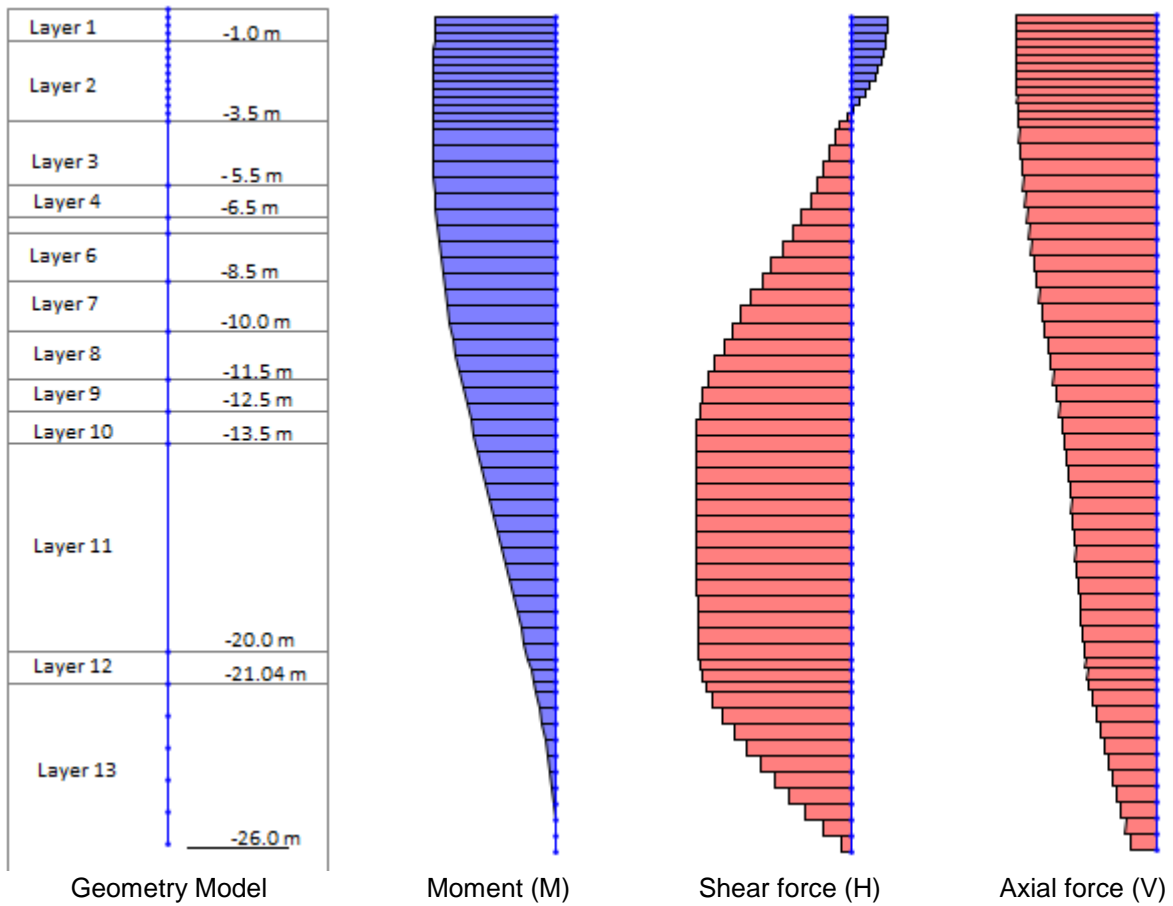


Figure VI.22: Internal forces of the 26m long pile

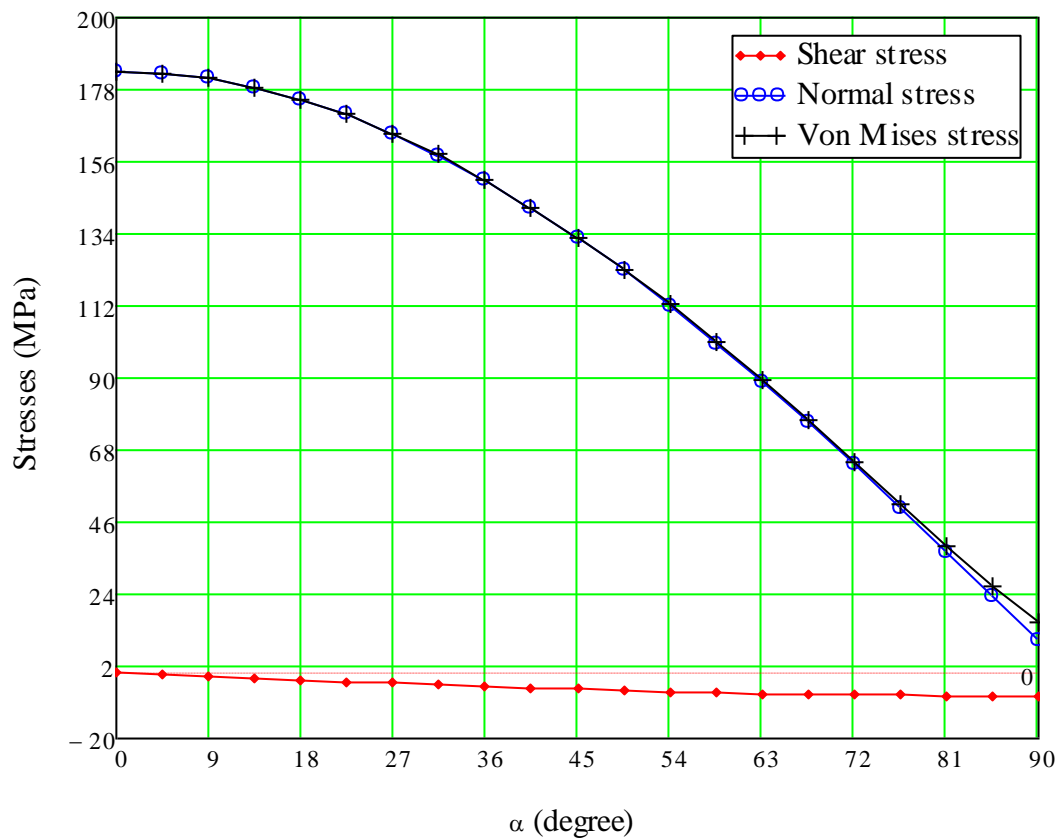


Figure VI.23: Stress distribution of foundation pile at the depth 1.0 m

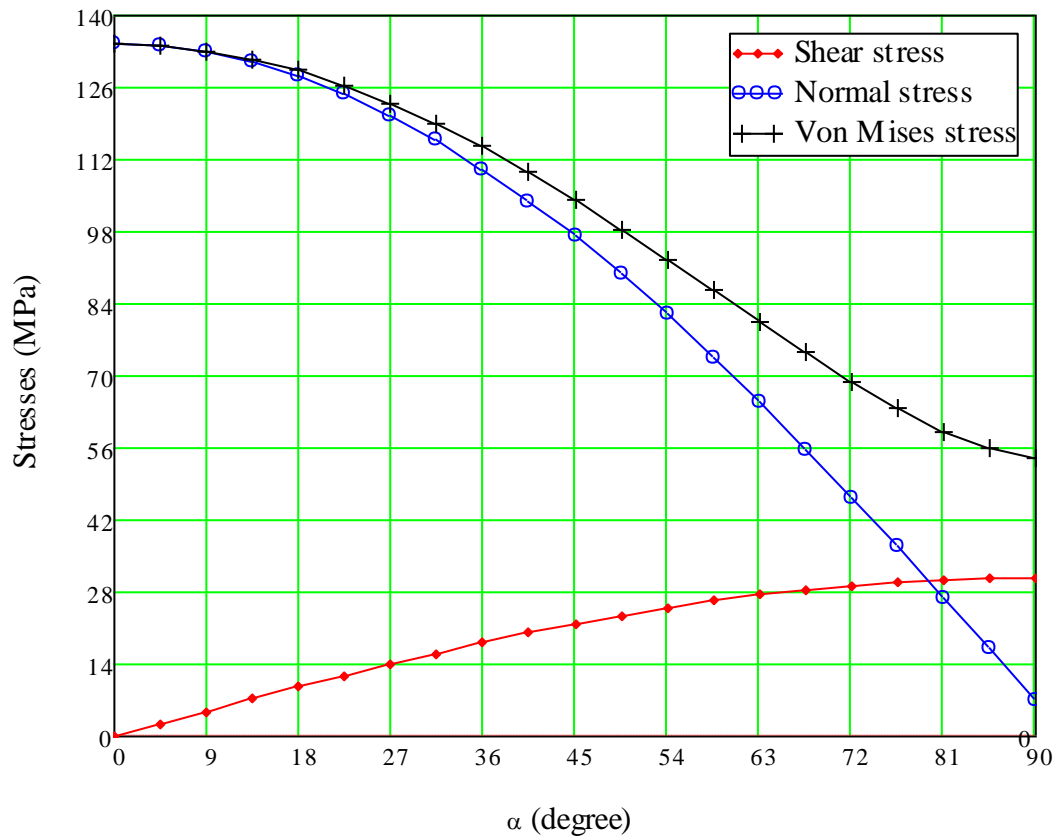


Figure VI.24: Stress distribution of foundation pile at the depth 12.0 m

Table VI.5: Values of stress distribution on the pile section at the depth 20.0 m

Angle (degree)	Normal stress σ (Pa)	Shear stress τ (Pa)	Von Mises σ_v (Pa)	Angle (degree)	Normal stress σ (Pa)	Shear stress τ (Pa)	Von Mises σ_v (Pa)
0.0	4.44E+07	0	4.44E+07	49.5	3.06E+07	2.41E+07	5.18E+07
4.5	4.42E+07	2.49E+06	4.44E+07	54.0	2.82E+07	2.57E+07	5.26E+07
9.0	4.39E+07	4.97E+06	4.47E+07	58.5	2.56E+07	2.71E+07	5.34E+07
13.5	4.33E+07	7.41E+06	4.51E+07	63.0	2.29E+07	2.83E+07	5.41E+07
18.0	4.24E+07	9.81E+06	4.57E+07	67.5	2.01E+07	2.93E+07	5.46E+07
22.5	4.14E+07	1.22E+07	4.64E+07	72.0	1.72E+07	3.02E+07	5.51E+07
27.0	4.01E+07	1.44E+07	4.72E+07	76.5	1.43E+07	3.09E+07	5.53E+07
31.5	3.86E+07	1.66E+07	4.81E+07	81.0	1.12E+07	3.14E+07	5.55E+07
36.0	3.69E+07	1.87E+07	4.90E+07	85.5	8.18E+06	3.16E+07	5.54E+07
40.5	3.49E+07	2.06E+07	5.00E+07	90.0	5.10E+06	3.17E+07	5.52E+07
45.0	3.29E+07	2.24E+07	5.09E+07				

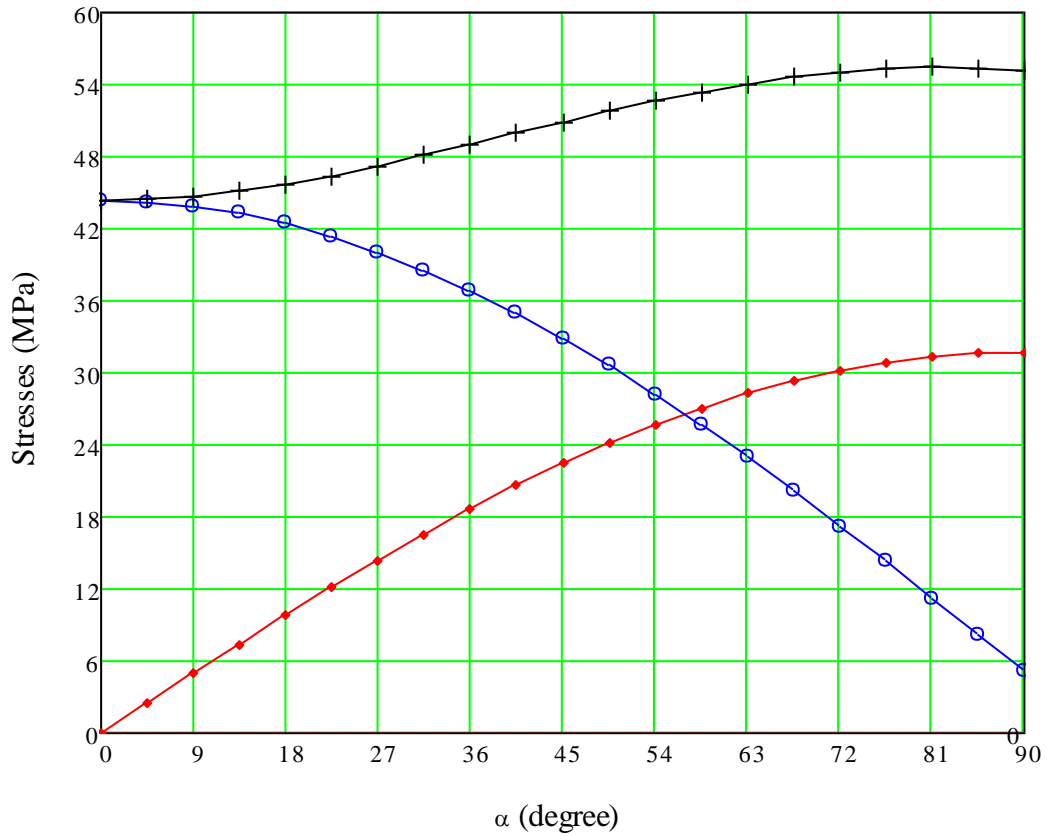


Figure VI.25: Stress distribution of foundation pile at the depth 20.0 m

Table VI.6: Internal forces, stresses and utilization of steel strength

Elev. (m)	Shear force (kN)	Axial force (kN)	Moment (kNm)	Max Normal stress (σ_{\max}) (Pa)	Max Shear stress (τ_{\max}) (Pa)	Max Von Mises Stress ($\sigma_{v\max}$) (Pa)	Utilization ratio $\frac{\sigma_{v\max} \times \gamma_M}{f_y}$
0.00	-5617.82	14511.80	-372400.00	1.81E+08	2.45E+07	1.81E+08	0.77
-0.25	-5617.82	14541.00	-373804.46	1.82E+08	2.45E+07	1.82E+08	0.77
-0.50	-5555.81	14563.41	-375193.41	1.82E+08	2.42E+07	1.82E+08	0.78
-0.75	-5426.54	14579.21	-376550.04	1.83E+08	2.36E+07	1.83E+08	0.78
-1.00	-5224.81	14588.66	-377856.24	1.84E+08	2.28E+07	1.84E+08	0.78
-1.25	-4945.36	14591.62	-379092.58	1.84E+08	2.15E+07	1.84E+08	0.78
-1.50	-4582.98	14588.30	-380238.33	1.85E+08	2.00E+07	1.85E+08	0.79
-1.75	-4132.45	14578.57	-381271.44	1.85E+08	1.80E+07	1.85E+08	0.79
-2.00	-3588.56	14562.40	-382168.58	1.86E+08	1.56E+07	1.86E+08	0.79
-2.25	-2946.12	14539.77	-382905.11	1.86E+08	1.28E+07	1.86E+08	0.79
-2.50	-2200.00	14511.16	-383455.11	1.86E+08	9.58E+06	1.86E+08	0.79
-2.75	-1345.11	14476.65	-383791.39	1.86E+08	5.86E+06	1.86E+08	0.79
-3.00	-376.48	14436.45	-383885.51	1.86E+08	1.64E+06	1.86E+08	0.79
-3.25	713.53	14390.68	-383707.13	1.86E+08	3.11E+06	1.86E+08	0.79
-3.50	1923.53	14339.57	-383226.24	1.86E+08	8.38E+06	1.86E+08	0.79
-4.00	2398.53	14294.19	-382026.98	1.85E+08	1.04E+07	1.85E+08	0.79

Elev. (m)	Shear force (kN)	Axial force (kN)	Moment (kNm)	Max Normal stress (σ_{\max}) (Pa)	Max Shear stress (τ_{\max}) (Pa)	Max Von Mises Stress ($\sigma_{v\max}$) (Pa)	Utilization ratio $\frac{\sigma_{v\max} \times \gamma_M}{f_y}$
-4.50	3346.17	14145.19	-380353.90	1.85E+08	1.46E+07	1.85E+08	0.79
-5.00	4286.60	13996.36	-378210.60	1.83E+08	1.87E+07	1.83E+08	0.78
-5.50	5217.60	13847.69	-375601.80	1.82E+08	2.27E+07	1.82E+08	0.78
-6.00	6362.47	13675.78	-372420.57	1.81E+08	2.77E+07	1.81E+08	0.77
-6.50	7699.86	13480.66	-368570.63	1.79E+08	3.35E+07	1.79E+08	0.76
-7.00	9110.50	13270.24	-364015.39	1.76E+08	3.97E+07	1.76E+08	0.75
-7.50	10707.62	13026.50	-358661.58	1.74E+08	4.66E+07	1.74E+08	0.74
-8.00	12350.77	12765.00	-352486.19	1.71E+08	5.38E+07	1.71E+08	0.73
-8.50	13887.55	12503.83	-345542.42	1.67E+08	6.05E+07	1.67E+08	0.71
-9.00	15466.66	12226.10	-337809.09	1.64E+08	6.74E+07	1.64E+08	0.70
-9.50	17054.47	11931.83	-329281.85	1.60E+08	7.43E+07	1.60E+08	0.68
-10.00	18464.21	11637.88	-320049.75	1.55E+08	8.04E+07	1.55E+08	0.66
-10.50	19818.94	11337.72	-310140.28	1.50E+08	8.63E+07	1.50E+08	0.64
-11.00	21087.69	11031.37	-299596.43	1.45E+08	9.18E+07	1.45E+08	0.62
-11.50	22158.08	10725.33	-288517.39	1.40E+08	9.65E+07	1.40E+08	0.60
-12.00	22957.30	10421.03	-277038.74	1.34E+08	1.00E+08	1.34E+08	0.57
-12.50	23527.67	10118.55	-265274.90	1.29E+08	1.02E+08	1.29E+08	0.55
-13.00	23894.39	9824.86	-253327.71	1.23E+08	1.04E+08	1.23E+08	0.52
-13.50	24105.69	9539.89	-241274.86	1.17E+08	1.05E+08	1.17E+08	0.50
-14.00	24181.10	9324.47	-229184.31	1.12E+08	1.05E+08	1.12E+08	0.48
-14.50	24190.12	9178.42	-217089.26	1.06E+08	1.05E+08	1.06E+08	0.45
-15.00	24186.10	9032.55	-204996.21	1.00E+08	1.05E+08	1.00E+08	0.43
-15.50	24170.02	8886.84	-192911.19	9.47E+07	1.05E+08	9.47E+07	0.40
-16.00	24142.79	8741.29	-180839.80	8.91E+07	1.05E+08	8.91E+07	0.38
-16.50	24105.24	8595.90	-168787.18	8.34E+07	1.05E+08	8.34E+07	0.36
-17.00	24058.18	8450.68	-156758.09	7.78E+07	1.05E+08	7.78E+07	0.33
-17.50	24002.37	8305.61	-144756.91	7.22E+07	1.05E+08	7.22E+07	0.31
-18.00	23938.47	8160.69	-132787.67	6.66E+07	1.04E+08	6.66E+07	0.28
-18.50	23867.12	8015.92	-120854.11	6.10E+07	1.04E+08	6.10E+07	0.26
-19.00	23788.92	7871.30	-108959.65	5.54E+07	1.04E+08	5.68E+07	0.24
-19.50	23704.36	7726.82	-97107.47	4.99E+07	1.03E+08	5.59E+07	0.24
-20.00	23613.93	7582.49	-85300.50	4.43E+07	1.03E+08	5.54E+07	0.24
-20.69	22984.83	7218.74	-69228.42	3.67E+07	1.00E+08	5.38E+07	0.23
-21.04	22579.06	7030.43	-61401.01	3.30E+07	9.83E+07	5.29E+07	0.22
-21.52	21582.95	6742.25	-51041.20	2.80E+07	9.40E+07	5.05E+07	0.21
-22.00	19941.77	6338.82	-41469.15	2.33E+07	8.69E+07	4.66E+07	0.20
-23.00	16213.99	5492.68	-24284.34	1.49E+07	7.06E+07	3.79E+07	0.16
-23.50	14141.96	5057.64	-17213.36	1.13E+07	6.16E+07	3.31E+07	0.14
-24.00	11930.30	4617.91	-11248.21	8.28E+06	5.20E+07	2.79E+07	0.12
-25.00	7054.37	3724.21	-2935.56	3.85E+06	3.07E+07	1.66E+07	0.07
-25.50	4369.08	3270.18	-751.02	2.54E+06	1.90E+07	1.04E+07	0.04
-26.00	1502.04	2811.33	0.00	1.89E+06	6.54E+06	3.97E+06	0.02

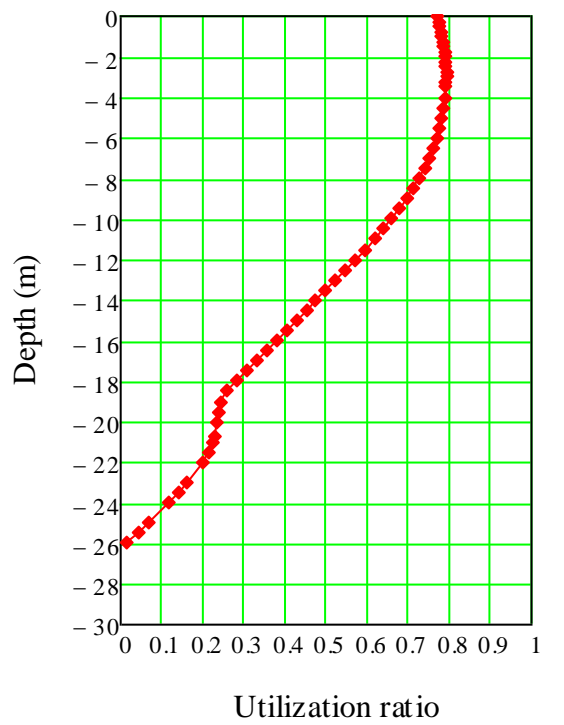
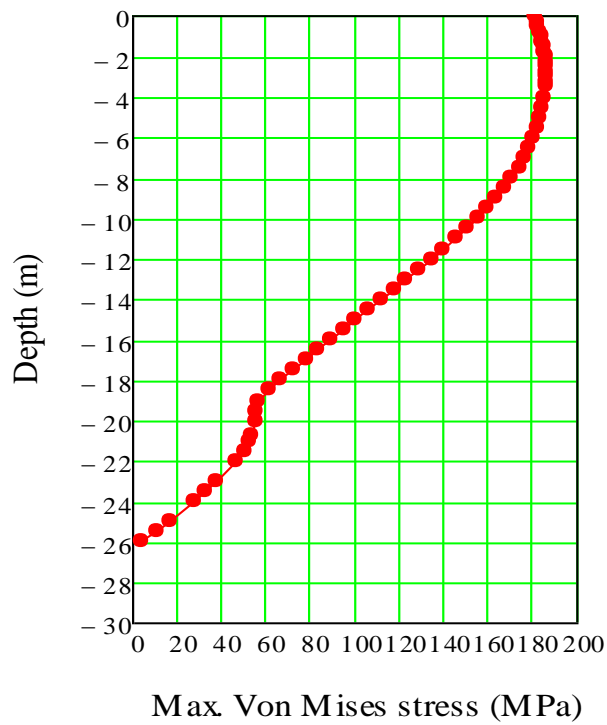
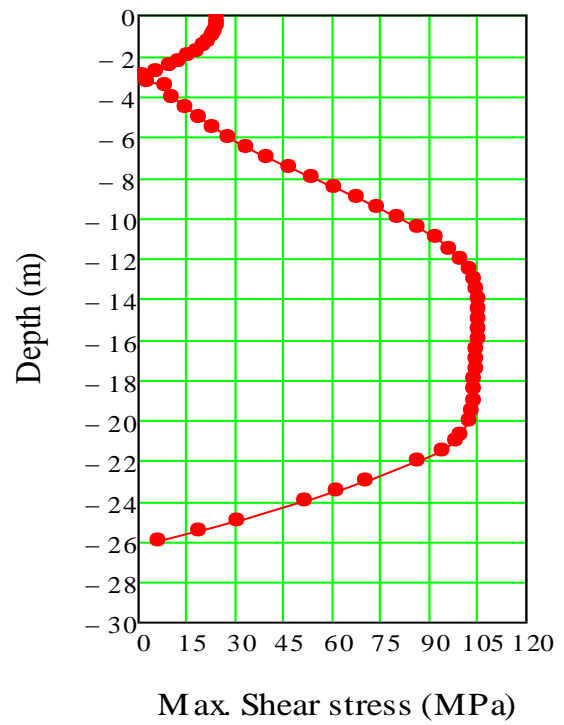
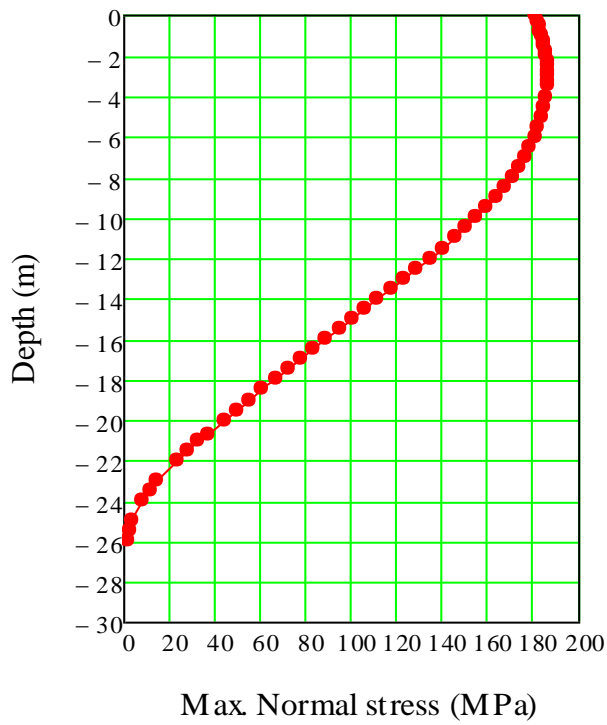


Figure VI.26: Maximum stresses and utilization ratios along the pile length

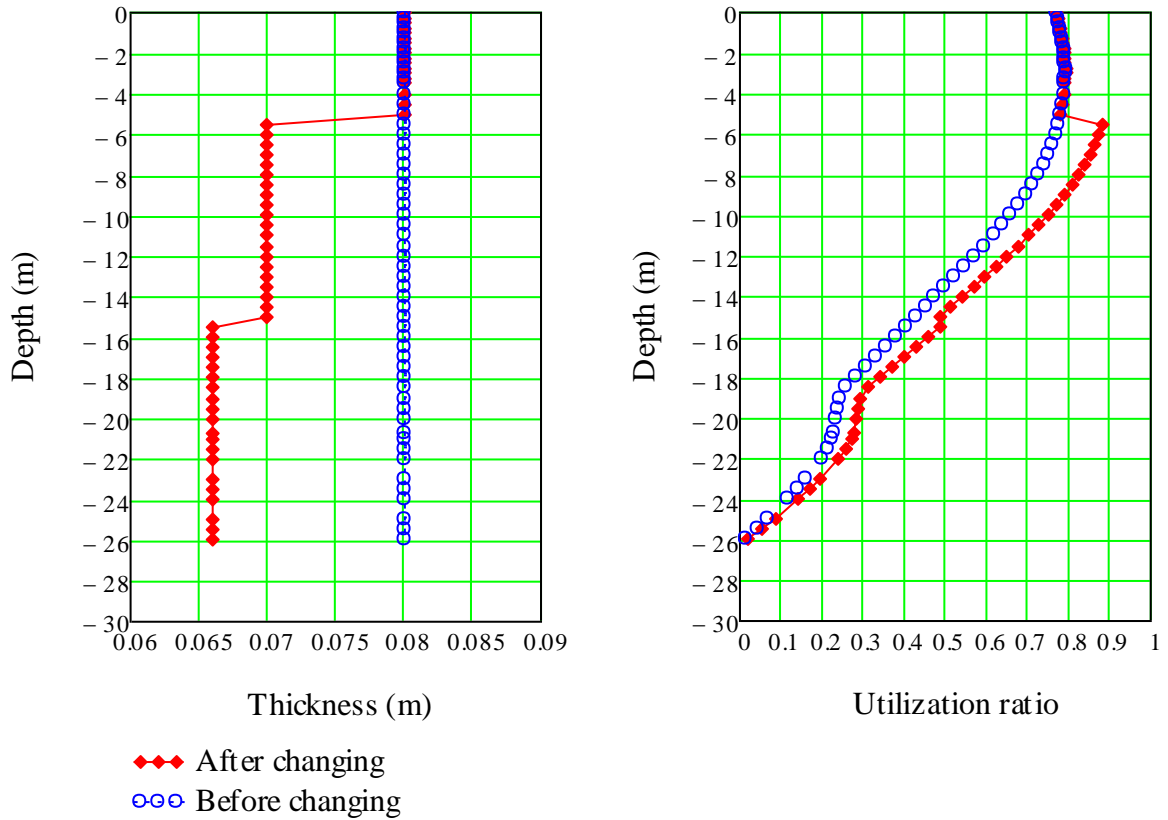


Figure VI.27: The utilization ratio after changing wall thickness

An attempt has been made to reduce the wall thickness. As shown in Figure VI.27, the utilization ratio increase significantly when the thickness reduced from 8 cm to 7 cm at the depth of 5m. However, the final wall thickness should be given after doing a sensitivity analysis of the wall thickness to the accumulated displacement of the foundation pile in SLS check.

6.3. Serviceability limit state check

6.3.1. General

For design of the serviceability limit state, characteristic soil strength values are to be used for the soil strength. Characteristic loads are to be used for the loads. The loading shall be representative of loads that will cause permanent deformations of the soil in the long term, and which in turn will lead to permanent deformations of the pile foundation, e.g. a permanent accumulated tilt of the pile head. For this purpose, the behavior of the soil under cyclic loading needs to be represented in such a manner that the permanent cumulative deformations in the soil are appropriately calculated as a function of the number of cycles at each load amplitude in the applied history of SLS loads.

For design in the serviceability limit state, it shall be ensured that deformation tolerances are not exceeded. The deformation tolerances refer to permanent deformations (DNV-OS-J101, 2011). With the chosen wind turbine, the permanent tilting must be smaller than 0.5 degree. Assume that 0.25 degree is the maximum tilting angle used for construction errors then the permanent tilting angle of the foundation pile must be smaller than 0.25 degree.

6.3.2. Geometry model

Dynamic behavior of the entire structure is totally different from the model used in EOL-OS software which considers the pile foundation is rigid (see Section 6.4). So after having the preliminary dimension of the foundation pile, it is necessary to model a fully dynamic behavior of the structure in order to get a reliable internal forces as well as displacement of the tower top. In the limited time for this thesis, recalculation the internal forces for ULS design will be ignored and only accumulated displacements due to loads in SLS check will be calculated.

When a soil is subjected to a sequence of cyclic loads, both cyclic strains and residual or permanent strains develop. The latter are the strains that remain at the end of each cycle of load and represent a cumulative effect that must be added to the effects of previous storms. Both the peak cyclic displacement that occurs during a storm as well as the permanent displacement will be considered in this SLS analysis.

As explained in Section **4.13.2 Pile-soil interface**, and because all the layers of the chosen site are sandy soil, it is possible to use the Kinematic model for hysteretic response of the soil (CSI, 2011) (see Figure VI.28 and Figure VI.30). The backbone curves are taken from the p-y curves recommended by DNV (DNV-OS-J101, 2011).

These p-y curves are already calculated in the section 6.2 Ultimate limit state design (page 88). The modification for them to use in this SLS check is merely the way of imposing a sufficiently fine discretization near the origin of the p-y curves in order to get a correct representation of the initial slopes (see Figure VI.29).

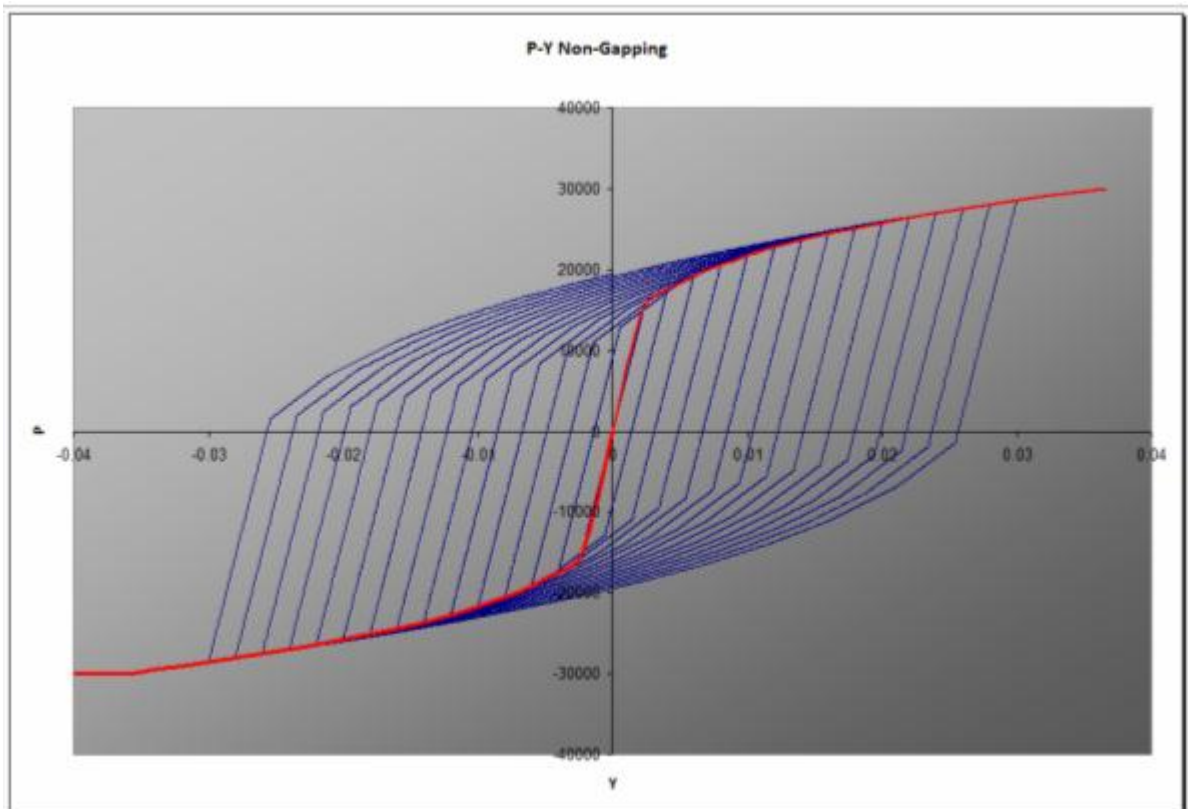


Figure VI.28: Kinematic model simulates non-gapping behavior

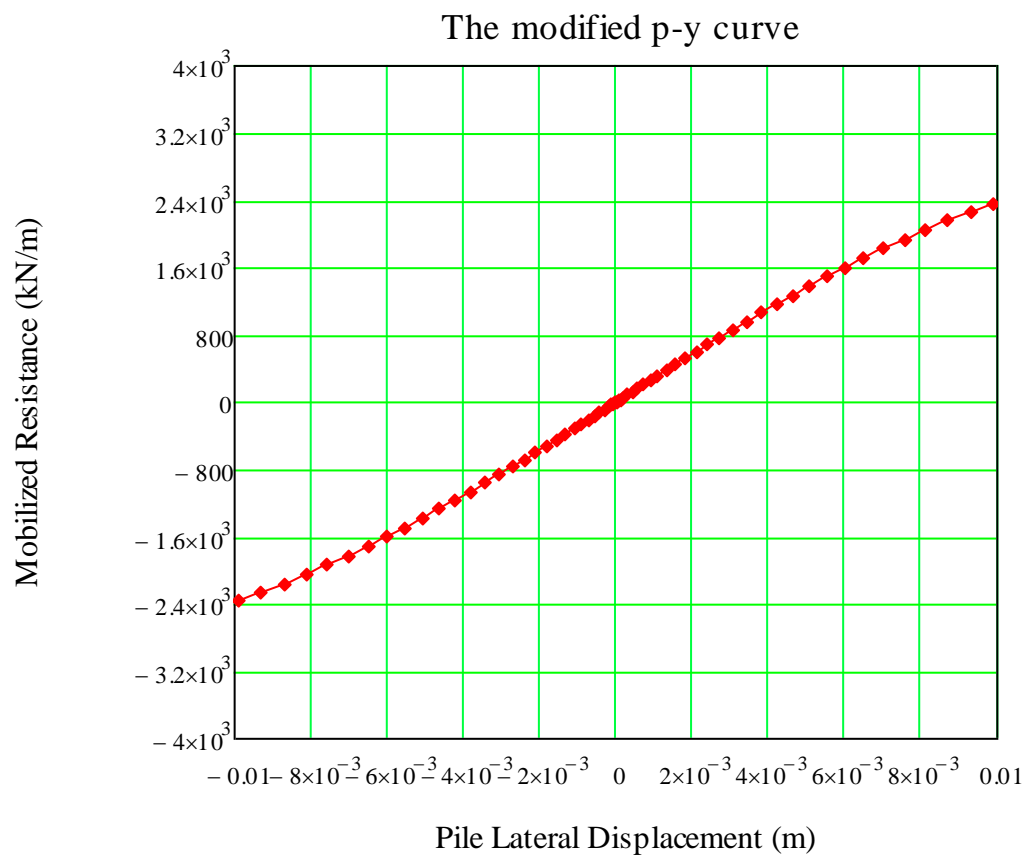


Figure VI.29: An example of the modified p-y curve for SLS analysis

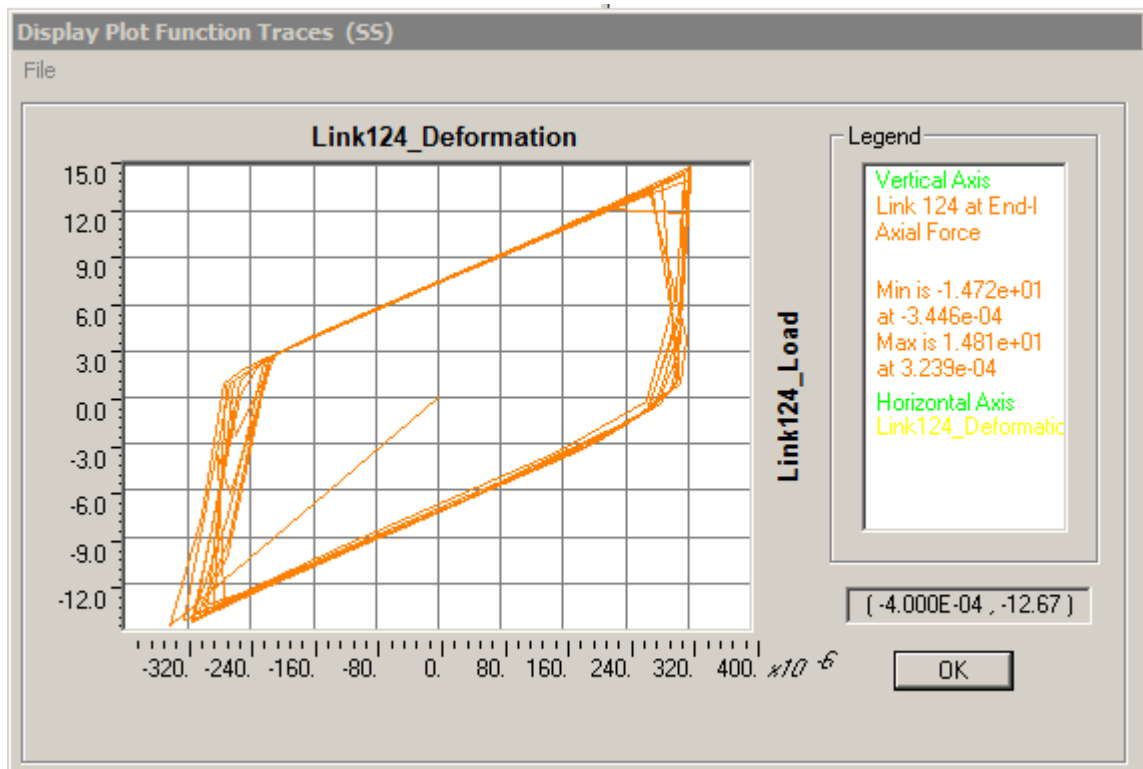


Figure VI.30: An example of hysteretic behavior of Link 124 in the model

6.3.3. Loads

Monopile offshore wind turbine developments are sited in very shallow water and therefore the wave loads are much reduced (because the large waves will have already broken and the lever arm for moments is small). In these circumstances, wind loads may begin to dominate. However, the aim of this master thesis is to study the behavior of the tower with foundation under cyclic loadings, and then wind load determination will not be paid any attention.

Typically onshore wind turbine load simulations have 10 minute duration, whereas the offshore industry has used 3 hour simulations (Watson, Structure and Foundations Design of Offshore Wind Installations, 2000). As shown in Figure VI.31 to Figure VI.34, the magnitude of maximum wave load is varied significantly when changing simulation duration (in 10 minute simulation it is 200N instead of 150N in 100 second simulation).

An attempt has been made to calculate the displacement of the whole structure under a cyclic wave load in 10 minute simulation. It took about 100 hours of computation to complete this analysis. In order to save time for analyzing the behavior of the whole structure with foundation, simulation time of 100 seconds will be chosen in this master thesis.

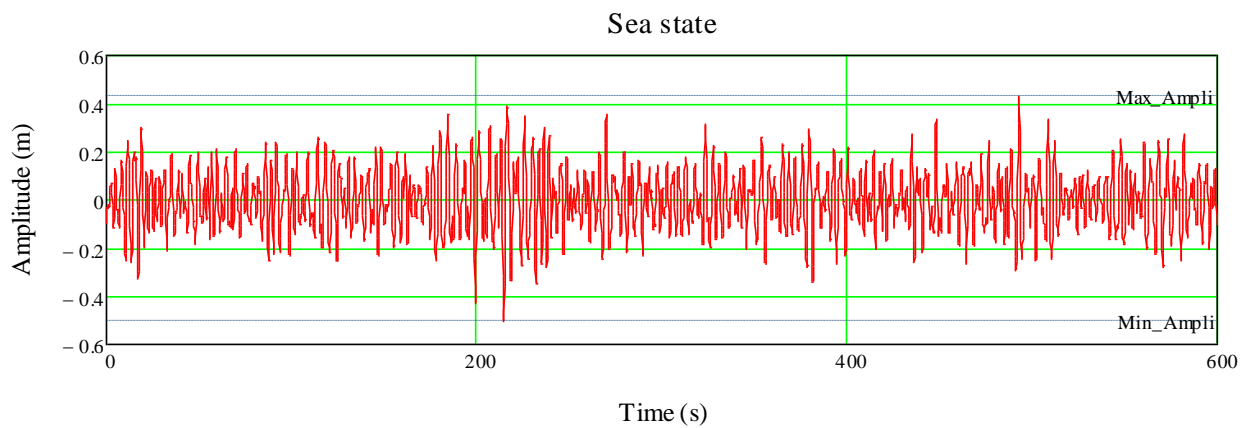


Figure VI.31: Wave height of Sea-state 0 in a 10 minute simulation

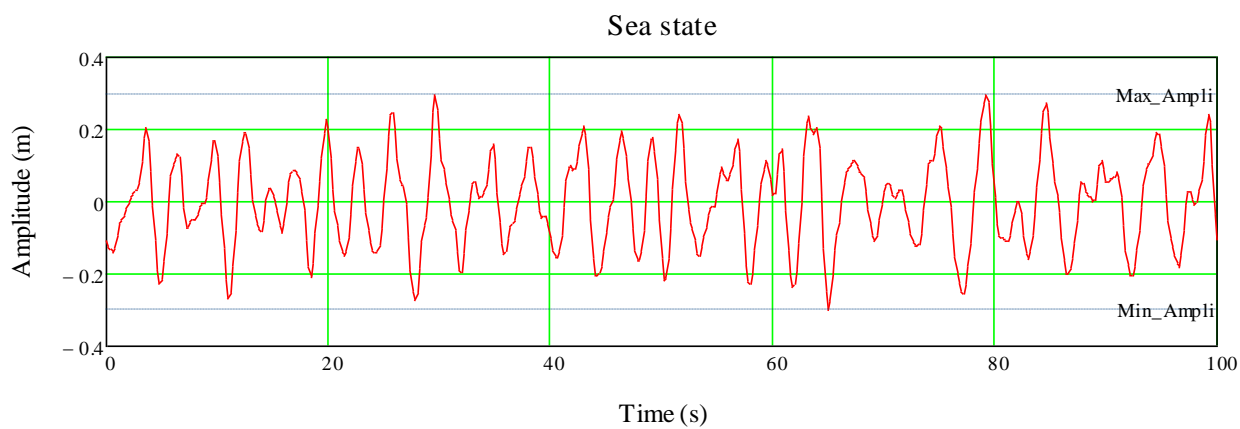


Figure VI.32: Wave height of Sea-state 0 in a 100 second simulation

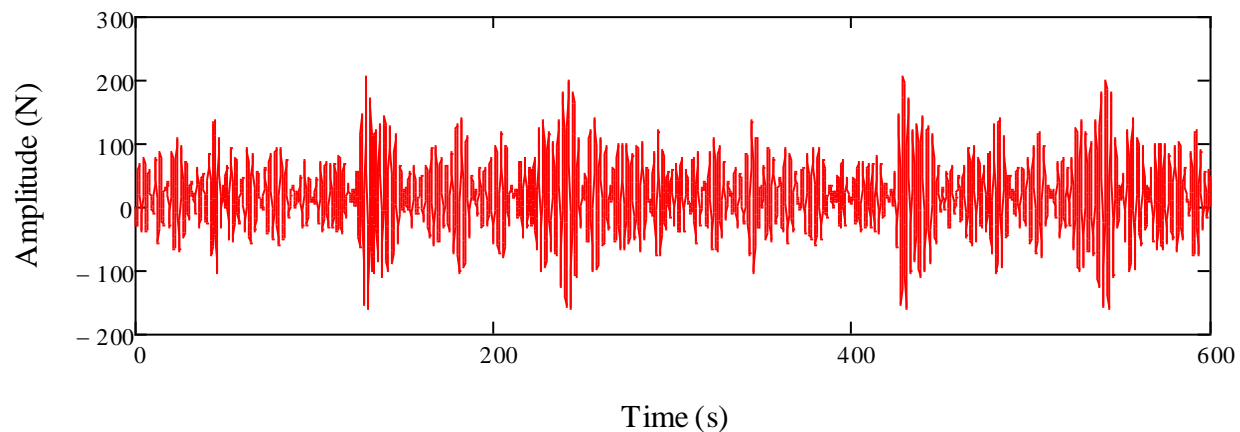


Figure VI.33: Wave load of Sea-state 0 in a 10 minute simulation (at seabed level)

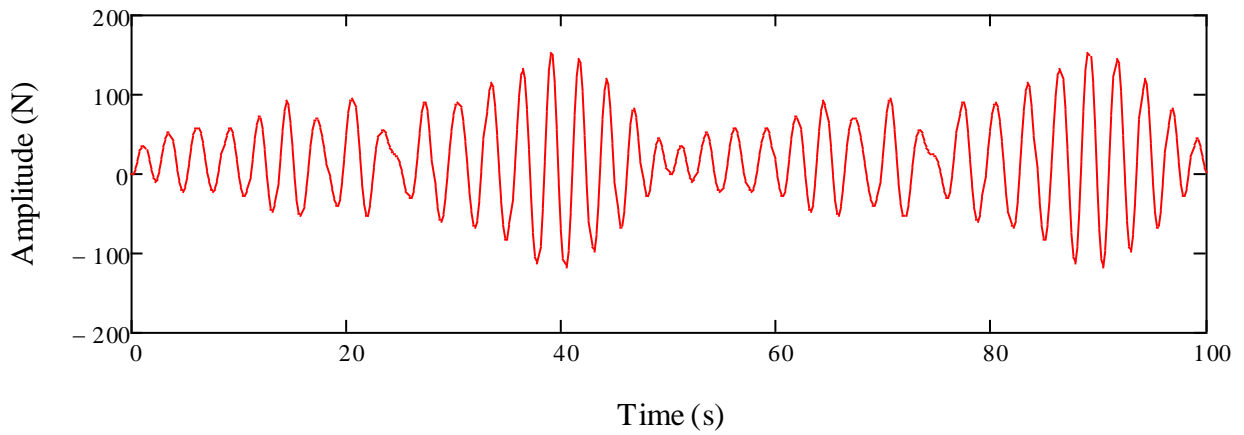


Figure VI.34: Wave load of Sea-state 0 in a 100 second simulation (at seabed level)

Three sea states will be used in the following calculation of the thesis (see Table VI.7):

Table VI.7: Sea states for SLS check – taken from 112 states (TEMPEL, 2006)

Sea state	Wind velocity at hub V_w (m/s)	Significant wave height H_s (m)	Mean zero up-crossing period T_z (s)	Probability of the sea state (%)
0	8	0.50	3	10.572
1	10	1.00	4	8.955
2	24	3.5	5	0.080

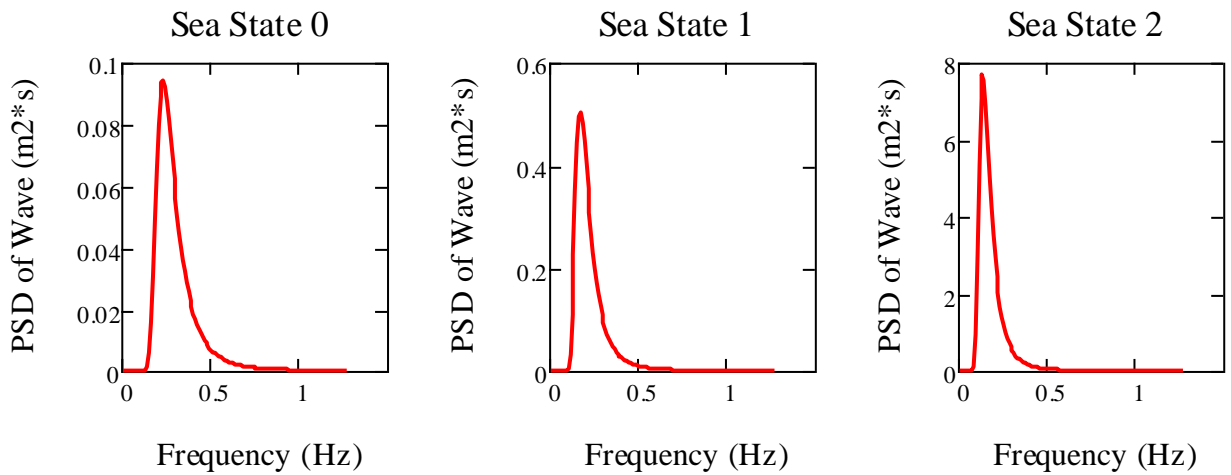


Figure VI.35: Wave Spectrum of Sea States

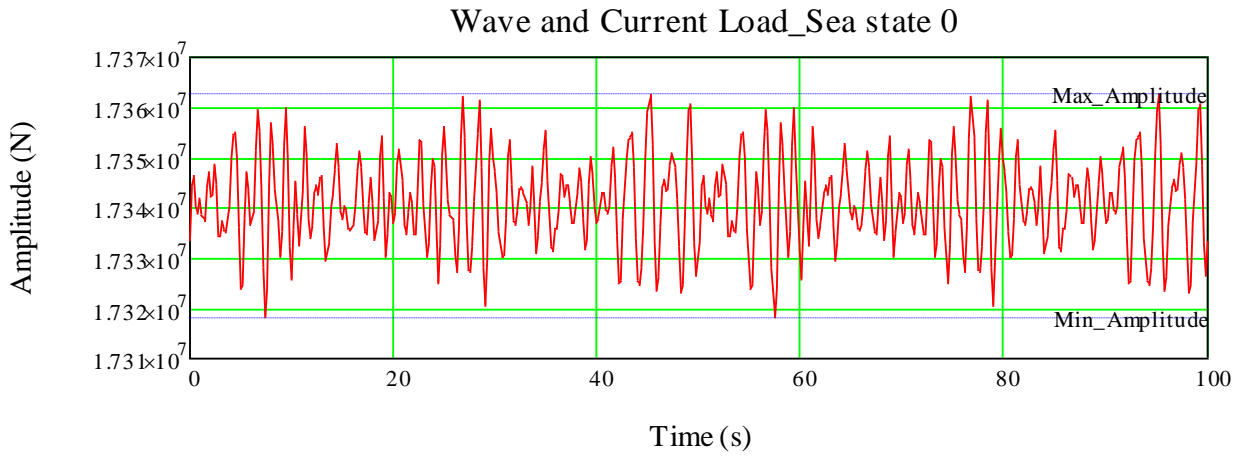


Figure VI.36: Time domain of Wave and Current Load from Sea State 0 at MSL

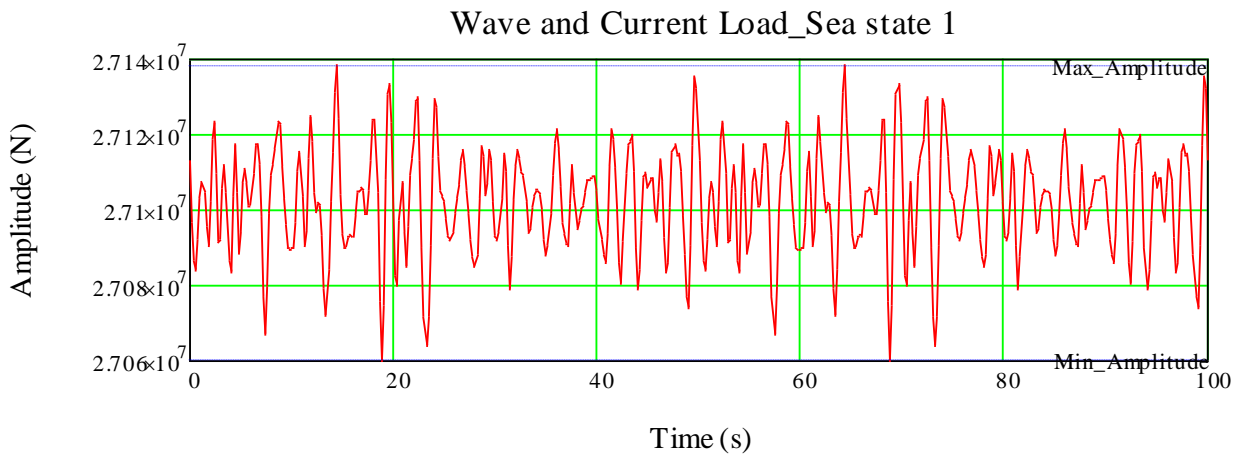


Figure VI.37: Time domain of Wave and Current Load from Sea State 1 at MSL

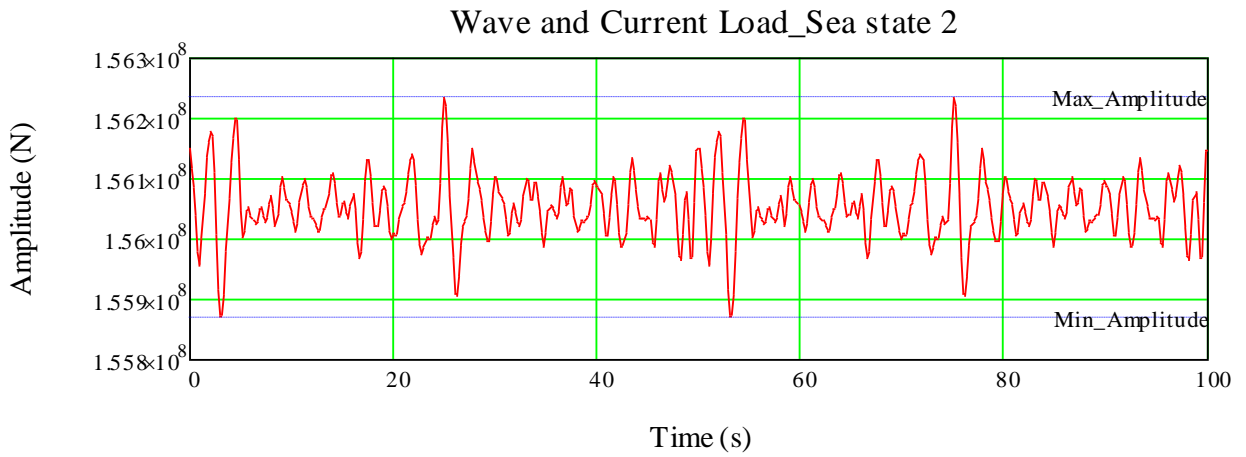


Figure VI.38: Time domain of Wave and Current Load from Sea State 2 at MSL

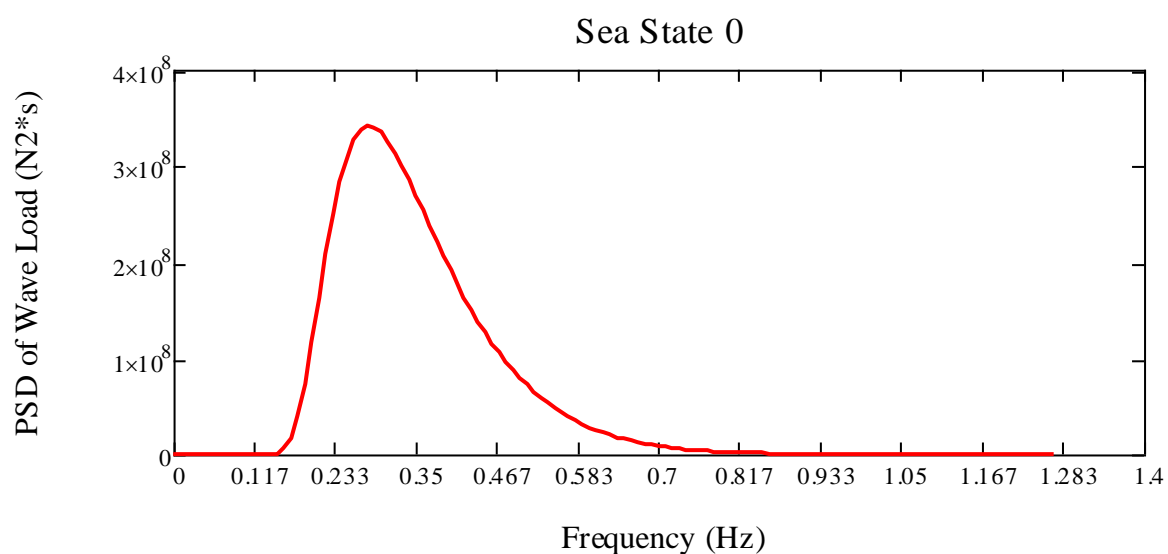


Figure VI.39: Frequency domain of Wave Load from Sea State 0 at MSL

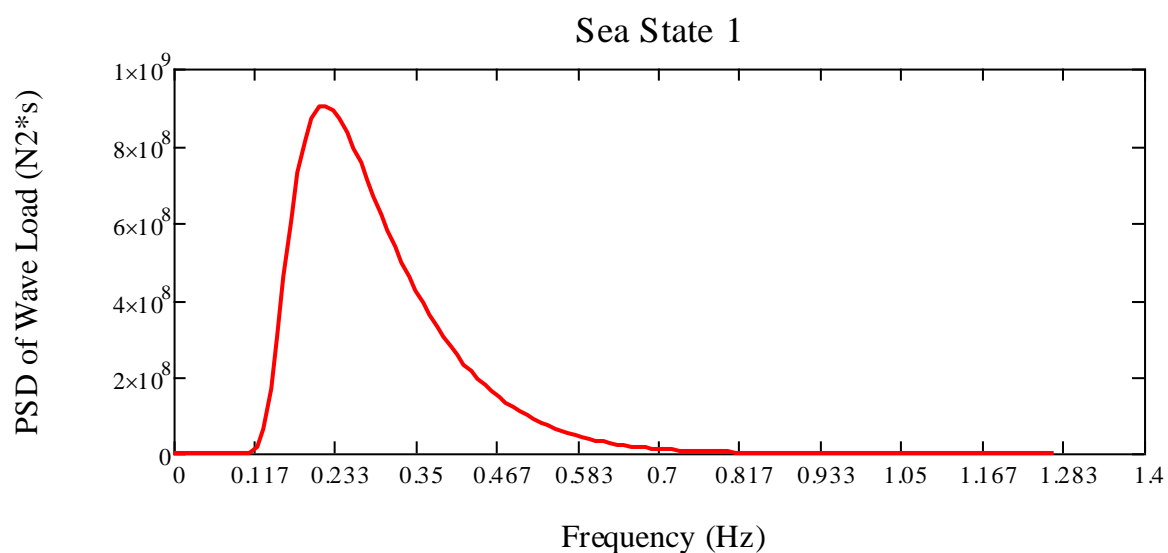


Figure VI.40: Frequency domain of Wave Load from Sea State 1 at MSL

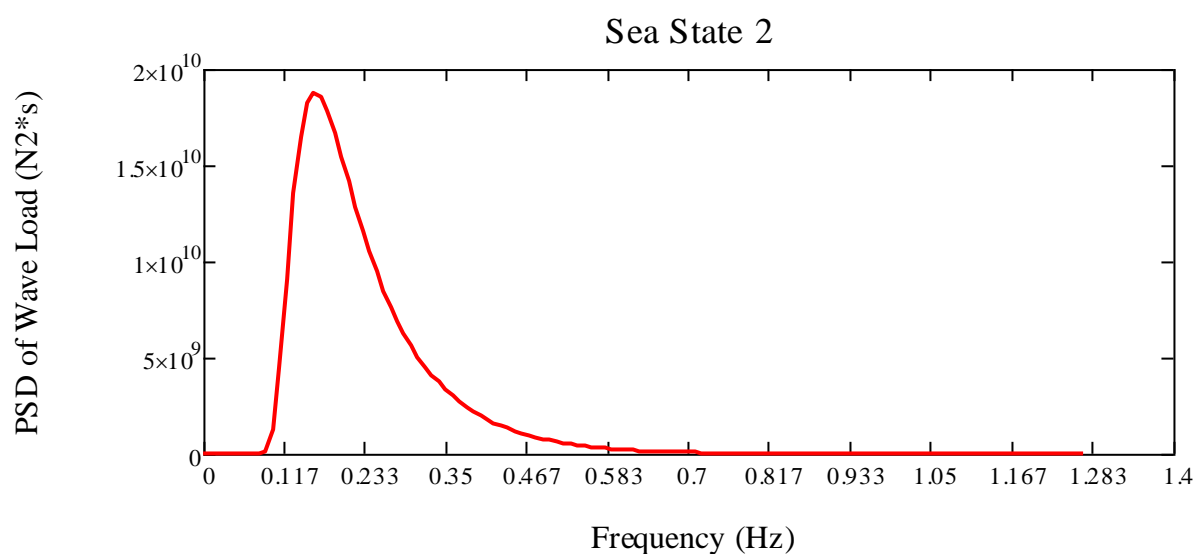


Figure VI.41: Frequency domain of Wave Load from Sea State 2 at MSL

6.3.4. Results of calculation

a. Single storm

In order to see the permanent displacement as well as the maximum displacement caused by a single storm, these analyses will assume that after one single storm wave load will be zero while the structure goes to its new equilibrium position.

As shown in Figure VI.42, Figure VI.44, Figure VI.46 and Figure VI.48, at the beginning structure stays at an equilibrium position (when $t=0$ s). During the storm, it oscillates around a new equilibrium position (when $0s < t < 100s$). And finally, when the storm had gone, its vibration damps out ($100s < t < 200$ s) and a new equilibrium position is defined ($t > 200$ s). This new equilibrium position is different from the original one, their distance gives the permanent displacement caused by the storm.

Table VI.8: Results of SLS calculations in single storm

SS	Elev.	Horizontal Displacement (Ux)					Rotation Displacement (Ry)				
		Max. (mm)	Mean (mm)	Stdev. during loading	Per. (mm)	Stdev. After damp out	Max. (deg)	Mean Ry (deg)	Stdev. During loading	Per. (deg)	Stdev. After damp out
(1)	(2)	(3)	(4)	(5)	(6)	(7)	(8)	(9)	(10)	(11)	(12)
1	Tower top	289.9	75.1	92.2	13.8	10.0	0.21	0.04	1.2e-3	6.38e-3	1.3e-4
	Seabed	10.4	5.5	1.55	1.9	0.29	0.07	0.028	2.5e-4	6.41e-3	2.2e-5

Note

(1):	Sea states	(7):	Standard deviation after damp out
(2):	Elevation	(8):	Maximum rotation displacements
(3):	Maximum horizontal displacements	(9):	Mean rotation displacements
(4):	Mean horizontal displacements	(10):	Standard deviation during loading
(5):	Standard deviation during loading	(11):	Permanent rotation displacements
(6):	Permanent horizontal displacements	(12):	Standard deviation after damp out

Because the cyclic loading used for SLS calculation consists only wave loads, so it is impossible to judge whether the pile foundation is sufficient or not in working conditions. However, for a practical project, the magnitude of cyclic loading will be larger but the dynamic behavior of the structure is almost the same.

In SLS analysis, the most important information need to be considered is the permanent tilting of the wind turbine because it will affect the yield energy. From the results of calculation, under the cyclic loading caused by Sea state 1, the permanent rotation displacements at the seabed and at the tower top are almost the same, about 6.4×10^{-3} degree (this value should be smaller than the allowable value of 0.25 degree).

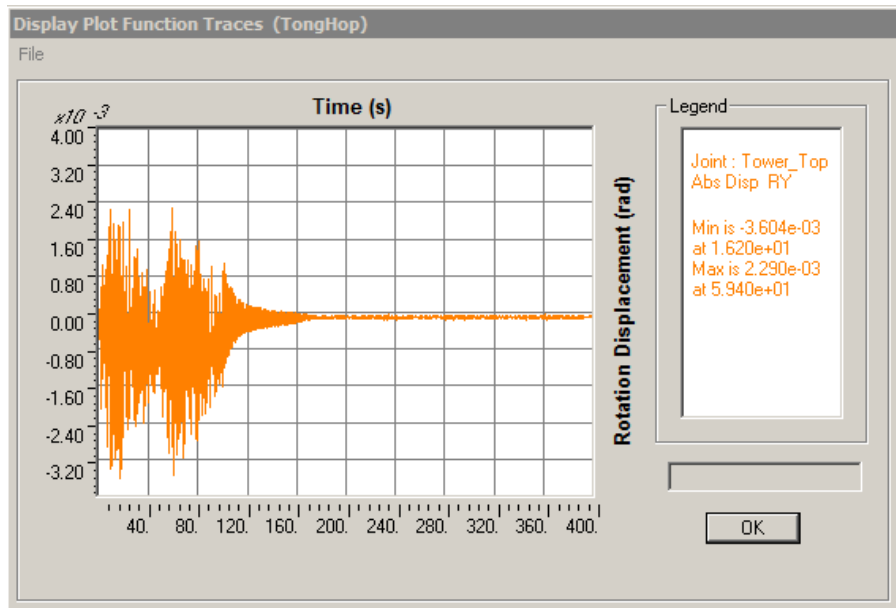


Figure VI.42: Rotation Displacement at tower top – Sea State 1

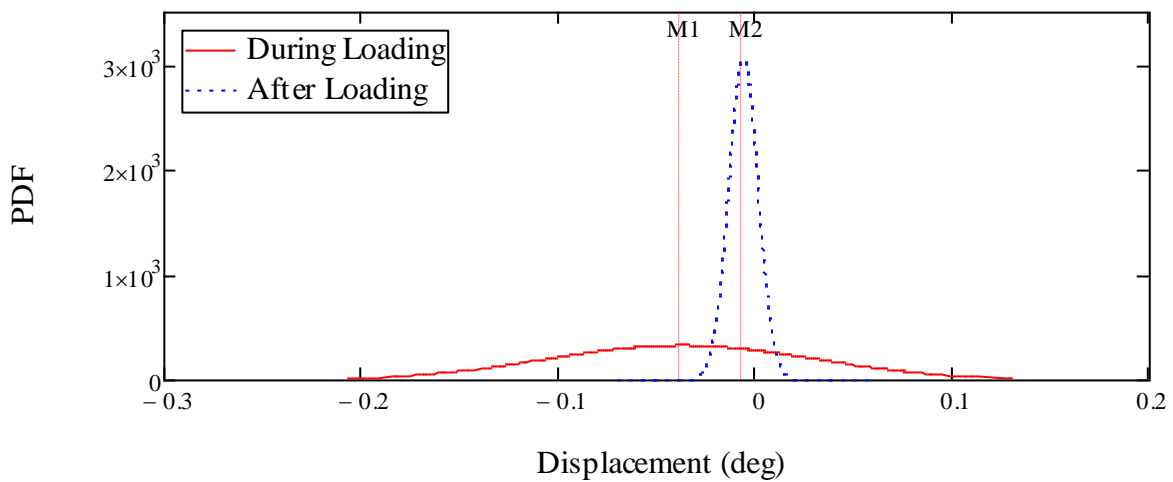


Figure VI.43: PDF of Rotation Displacement at tower top - Sea state 1

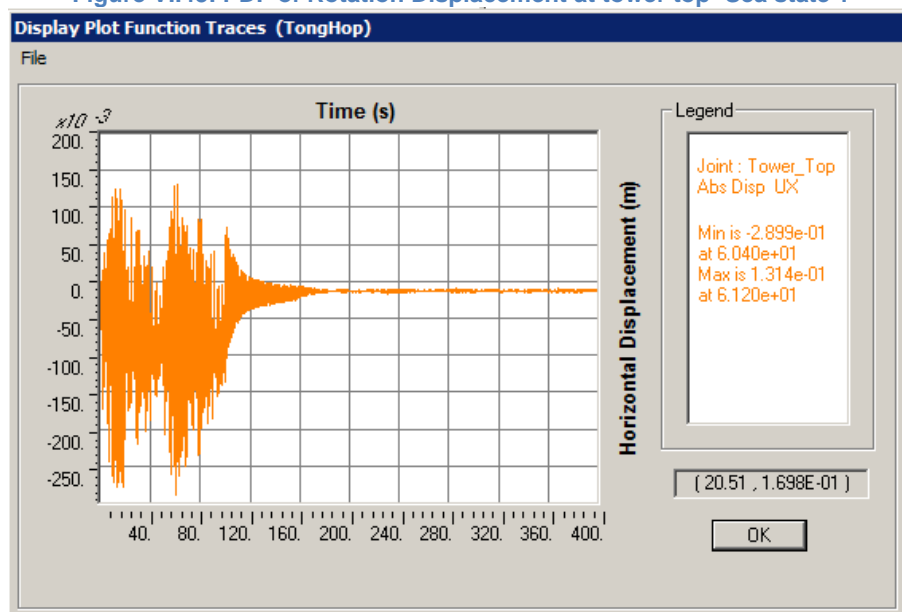


Figure VI.44: Horizontal Displacement at tower top - Sea State 1

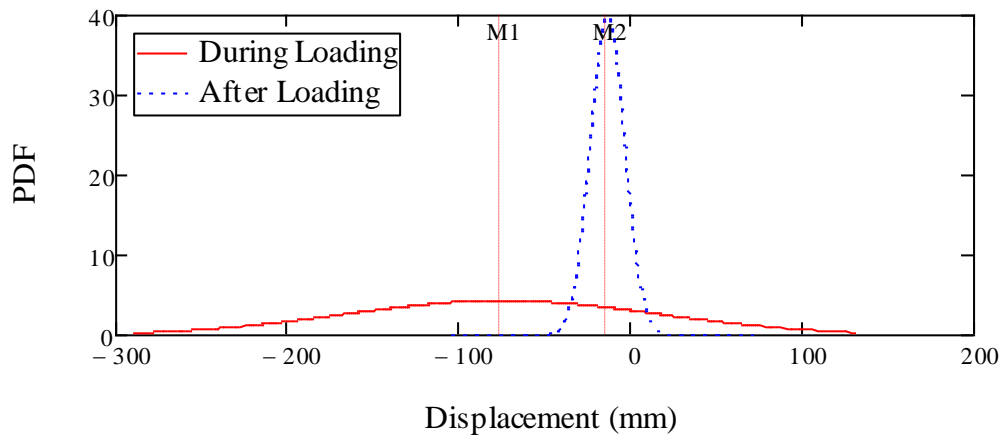


Figure VI.45: PDF of Horizontal Displacement at tower top- Sea state 1

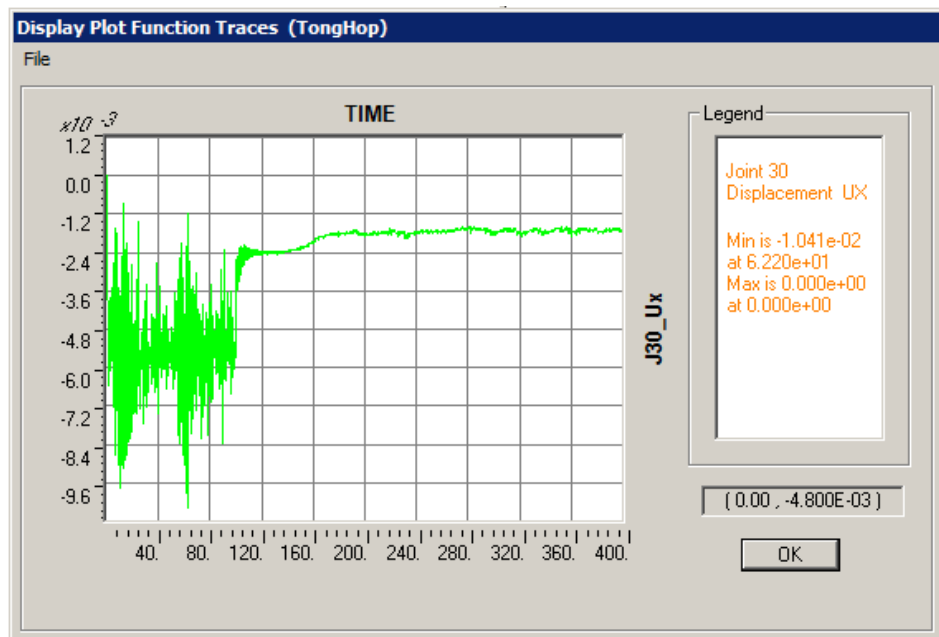


Figure VI.46: Horizontal Displacement at seabed - Sea State 1

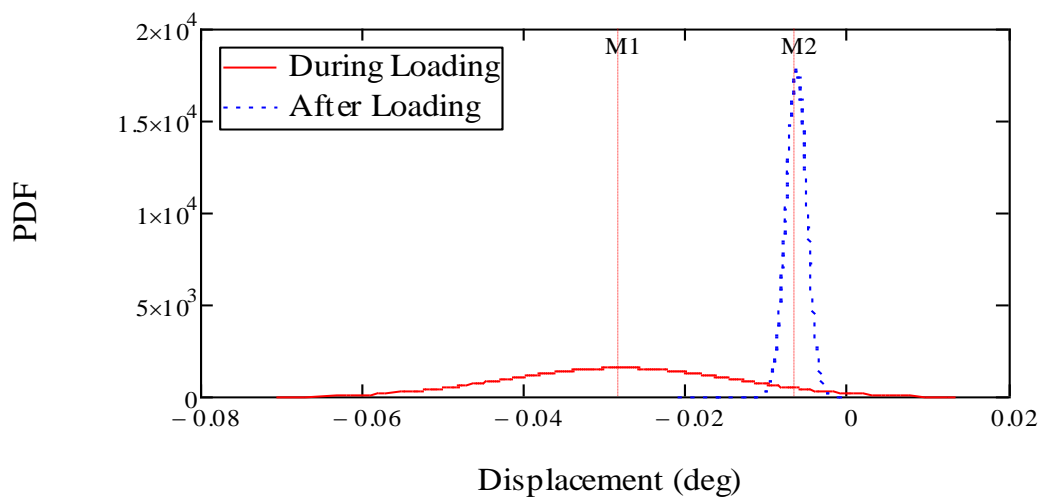


Figure VI.47: PDF of Horizontal Displacement at seabed - Sea state 1

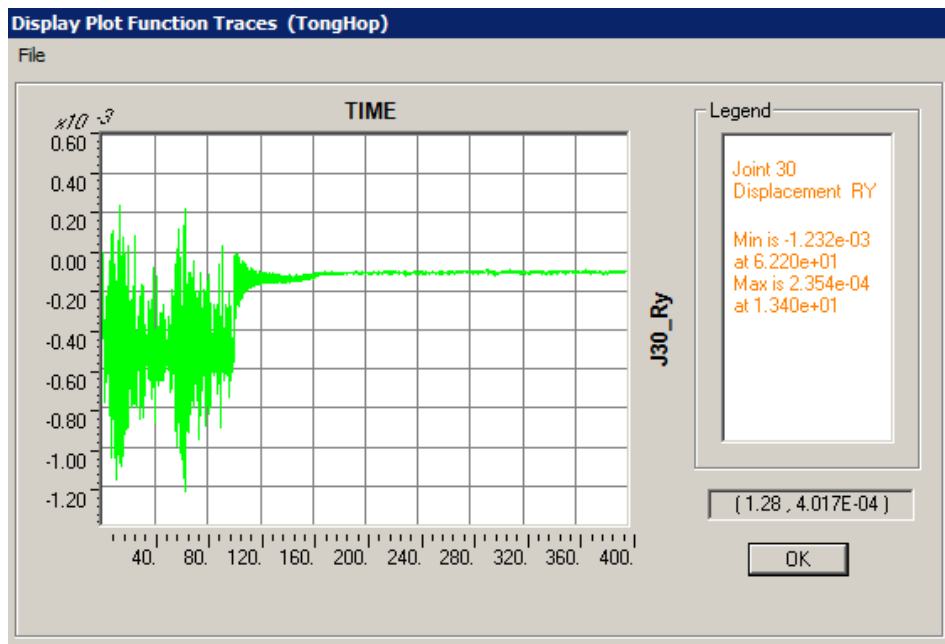


Figure VI.48: Rotation Displacement at seabed – Sea State 1

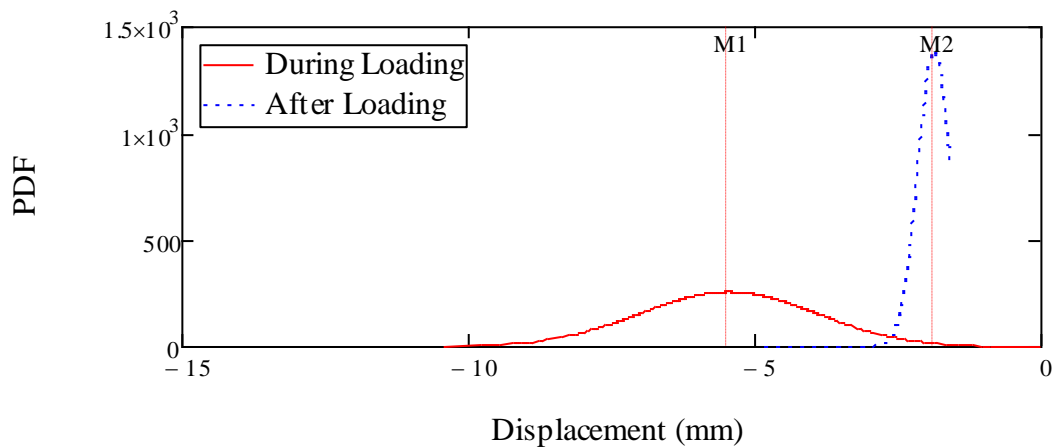


Figure VI.49: PDF of Rotation Displacement at seabed- Sea state 1

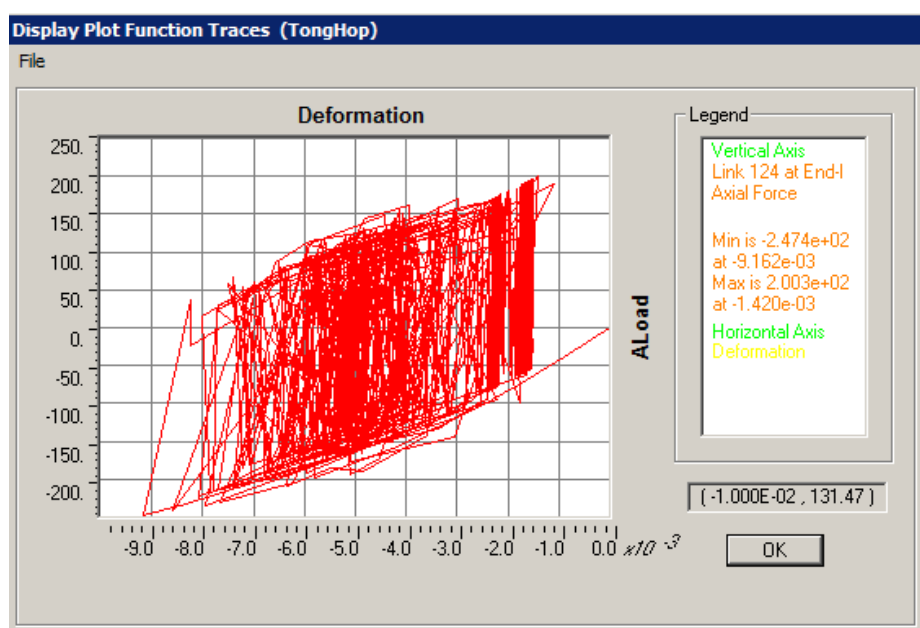


Figure VI.50: Behavior of one of the springs during and after the storm – Sea State 1

b. Effect of previous storm

As shown in Figure VI.44, after suffering from one storm, the new equilibrium position of the tower is defined. So at a certain time, this new equilibrium position will depends on the accumulated displacement that caused by previous storms.

c. Two successive storms

As shown in Figure VI.51 to Figure VI.53 and Table VI.9, the maximum horizontal displacement U_x in case of two successive storms is higher than it is in case of single storm. That means the new equilibrium positions of the tower in case of two successive storms is further than in case of single storm (because the origin of the p-y curve is moved further)

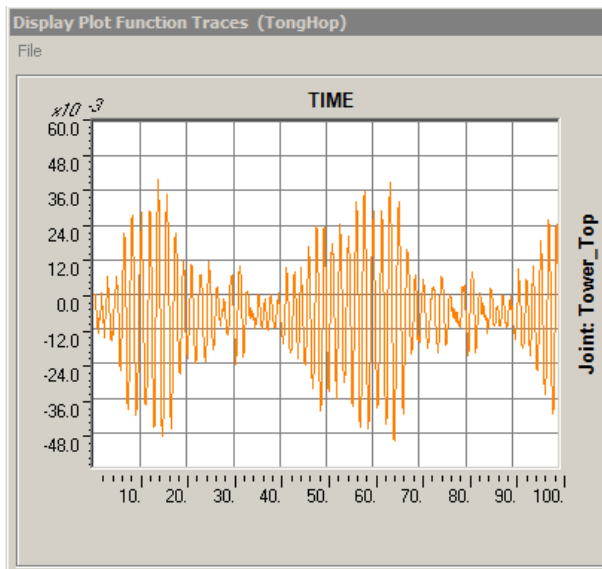


Figure VI.51: U_x of the tower top-single storm

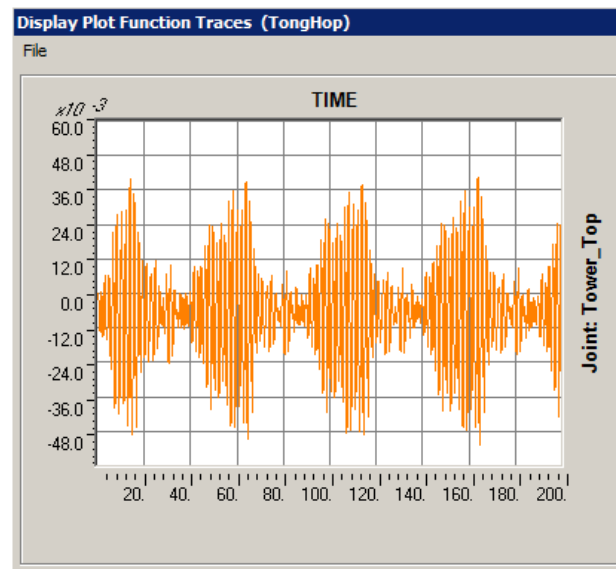


Figure VI.52: U_x of the tower top-two successive storms

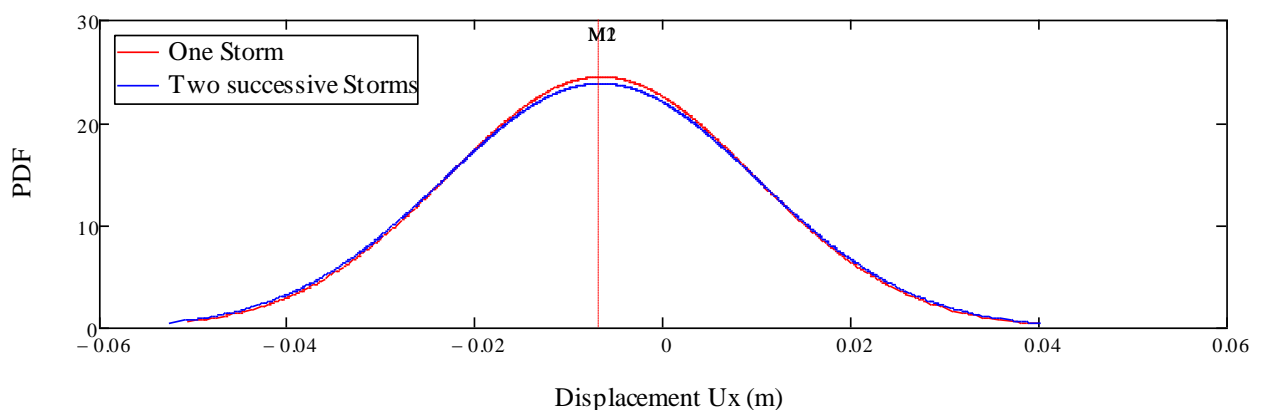


Figure VI.53: Comparing U_x at the tower top between Single storm and two successive storms

Table VI.9: Parameters of the two normal distributions

Models	Single storm	Two successive storms
Mean values (mm)	6.68	6.75
Standard deviations (mm)	16	17
Maximum values (mm)	51	53

6.3.5. Conclusions of SLS calculation

There is not any conclusion that is given for the chosen foundation pile about its validation in working conditions because of the lack of wind loads and not enough sea states. However, from the result of calculations, some important comments have been made:

- The “permanent accumulated tilt of the pile head” which is required by DNV standard (DNV-OS-J101, 2011) to compare with “the deformation tolerances” can be calculated using hysteretic behavior of the soil.
- The hysteretic behavior using in this thesis is non-degraded hysteresis type, which is only suitable for problems with the medium range of soil strain, approximately below the level of 10^{-3} (elasto-plastic behavior). For the shear strain level larger than about 10^{-2} , soil properties tend to change appreciably not only with shear strain but also with the progression of cycles. It is termed degraded hysteresis type, and need further researches.
- To assess the validation of the foundation pile in SLS design, the permanent displacement of each sea state should be calculated and put on the probability distribution diagram (as shown in Figure VI.54). Based on that diagram, the probability of the accumulated displacement will be calculated. Finally, if the probability of the accumulated displacement which equals to the allowable displacement value (for example 0.25 degrees for the tilt of the tower) is small enough then the chosen dimension of the foundation pile is sufficient. Otherwise, the stiffness of the foundation pile need to be increased until that condition is met.

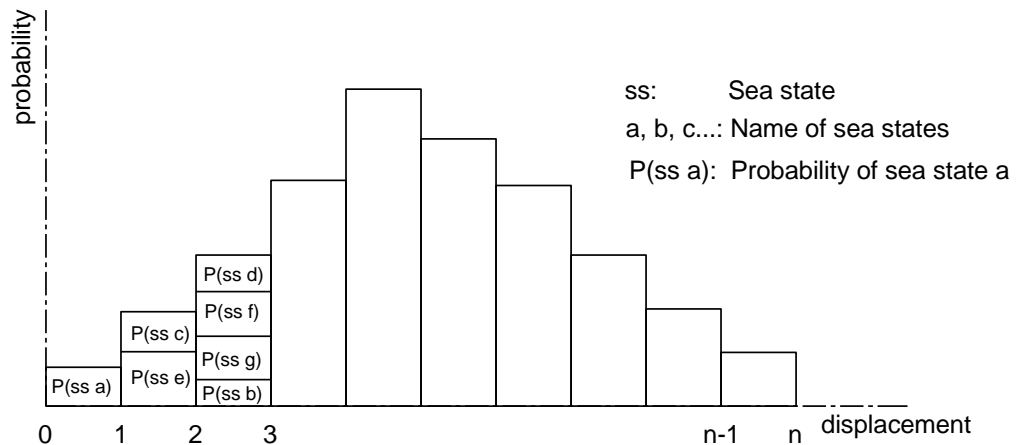


Figure VI.54: Probability distribution diagram of displacements

6.4. Effect of foundation in dynamic behavior of the structure

6.4.1. Reconsidering the model

When considering the foundation pile as a part of the model in analyses of offshore wind turbine structures the behavior of the structures will be softer than the one fixed at the seabed which is used in ELO-OS software. In order to see the differences in their behaviors, the steady-state analyses of both models are carried out. It is of interest to point out that steady-state analysis seeks the response of the structure at one or more frequencies to loading. And because the response characteristics of the structures themselves are concerned, a constant frequency function will be used.

Of course, a conservative assumption must be made in order to do the steady-state analysis. That is all the springs are linear with their initial stiffness (see Table VI.10). In fact, each of them is a nonlinear spring with an arbitrary stiffness that is smaller than the initial value.

Table VI.10: Linear stiffness of springs

Layer	Elevation (m)	Linear stiffness (at the middle of the layer) (kN/m)
Layer 1	0 – 1	2.138×10^4
Layer 2	1 – 3.5	9.621×10^4
Layer 3	3.5 – 5.5	1.924×10^5
Layer 4	5.5 – 6.5	2.566×10^5
Layer 5	6.5 – 7.0	2.886×10^5
Layer 6	7.0 – 8.5	3.314×10^5
Layer 7	8.5 – 10.0	3.955×10^5
Layer 8	10.0 – 11.5	4.597×10^5
Layer 9	11.5 – 12.5	3.683×10^5
Layer 10	12.5 – 13.5	2.562×10^5
Layer 11	13.5 – 20.0	4.623×10^4
Layer 12	20.0 – 21.04	2.633×10^5
Layer 13	21.04 – 26.0	7.827×10^5

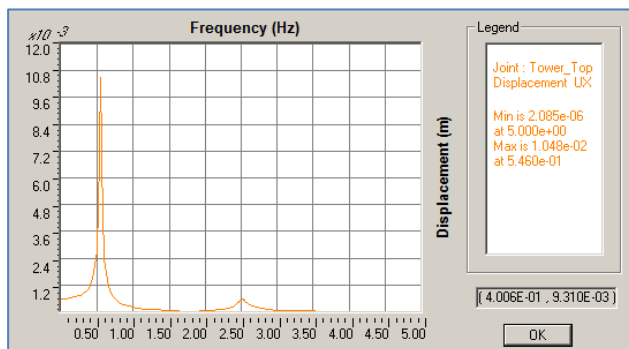


Figure VI.55: Response of structure in spring model – displacement at the tower top

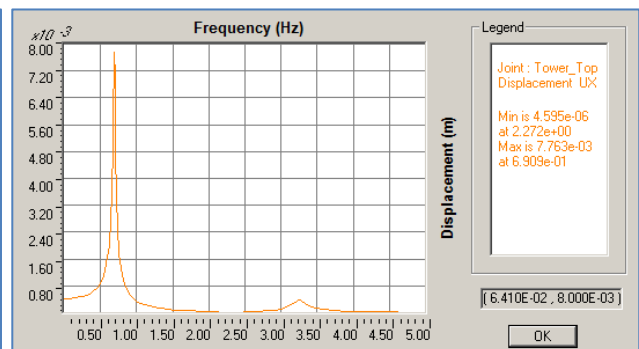


Figure VI.56: Response of structure in fixed-at-seabed model – displacement at the tower top

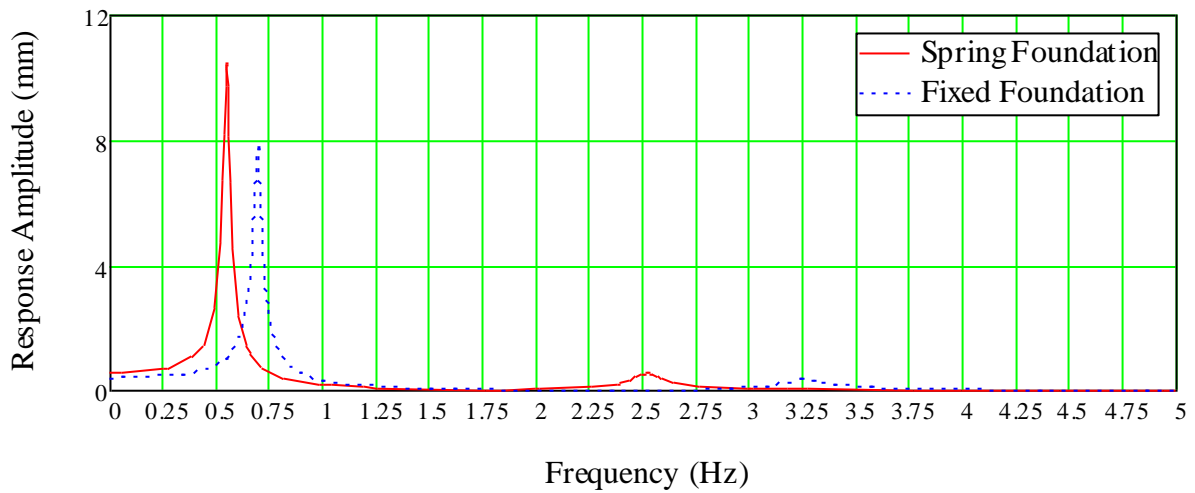


Figure VI.57: Compare the responses of two models at tower top

Using three wave loads as in Figure VI.39, Figure VI.40 and Figure VI.41 in page 107, calculated from the given sea states to calculate the corresponding responses, results are shown in Figure VI.58, Figure VI.59, and Figure VI.60 respectively.

From the results of modal applied loads, it is obvious that in reality the behavior of the nonlinear spring system is much softer, and then modal applied loads would be much larger and it implies that displacements of the structure in this model will be larger than they are in a fixed foundation model.

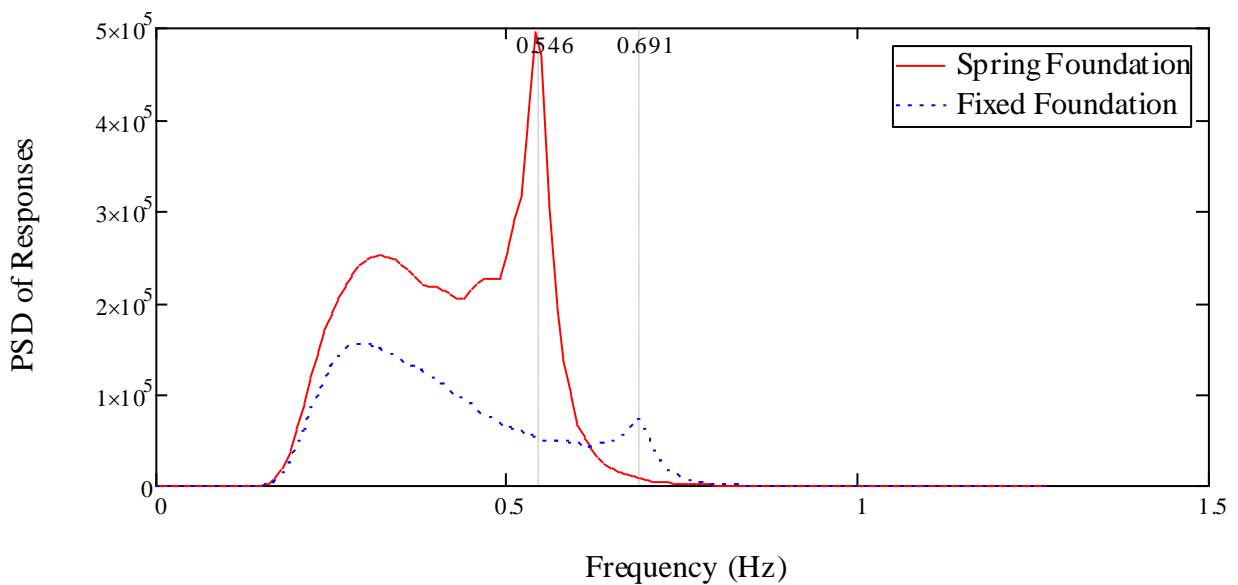


Figure VI.58: PSD of Responses at tower top caused by sea state 0

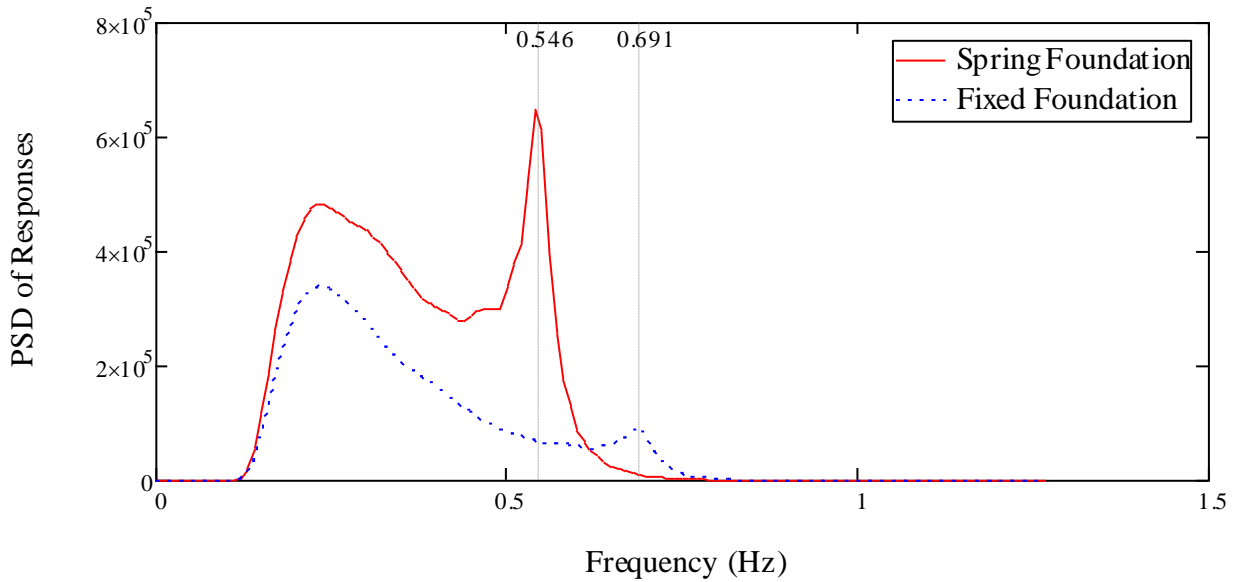


Figure VI.59: PSD of Responses at tower top caused by sea state 1

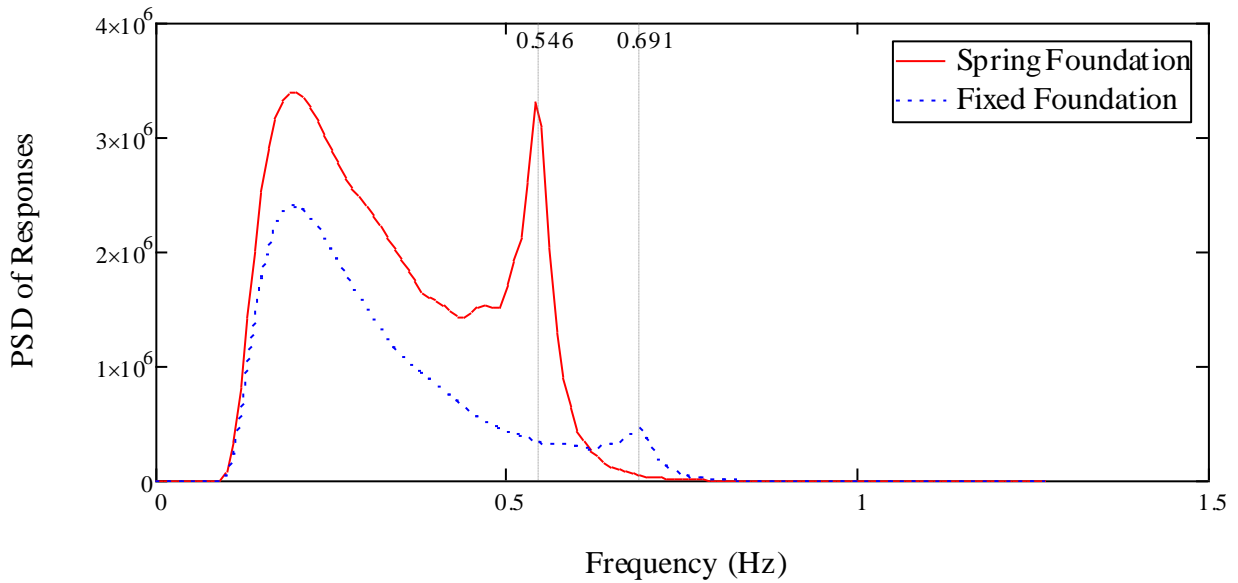


Figure VI.60: PSD of Responses at tower top caused by sea state 2

6.4.2. Spring foundation vs. fixed foundation

In order to see clearly the final effect of the foundation in behavior of the whole structure, this section will be devoted to calculating rotation displacements of the tower top in both models.

Wave loads will be calculated from Sea state 0, and this is the only dynamic load acting on the structure. Time-history wave loads are calculated at each 1m distance from MSL downward.

Nonlinear springs are used to represent the behavior of the foundation in the spring foundation model.

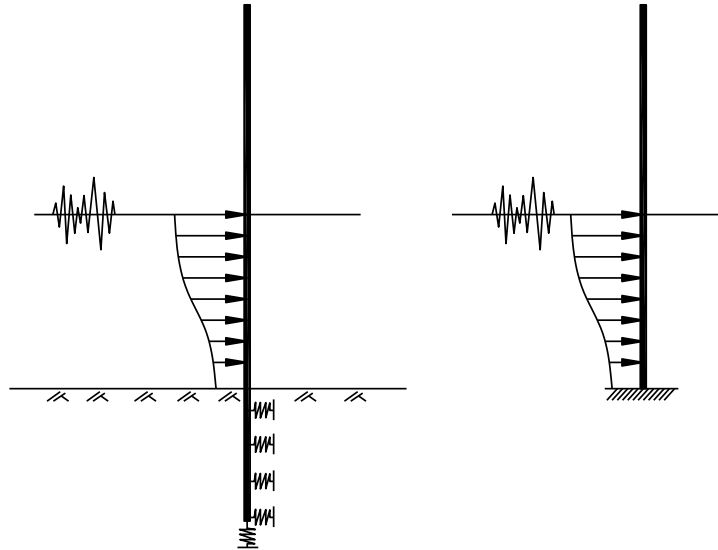


Figure VI.61: Calculating models of offshore wind turbine structure
a) Spring foundation and b) Fixed foundation

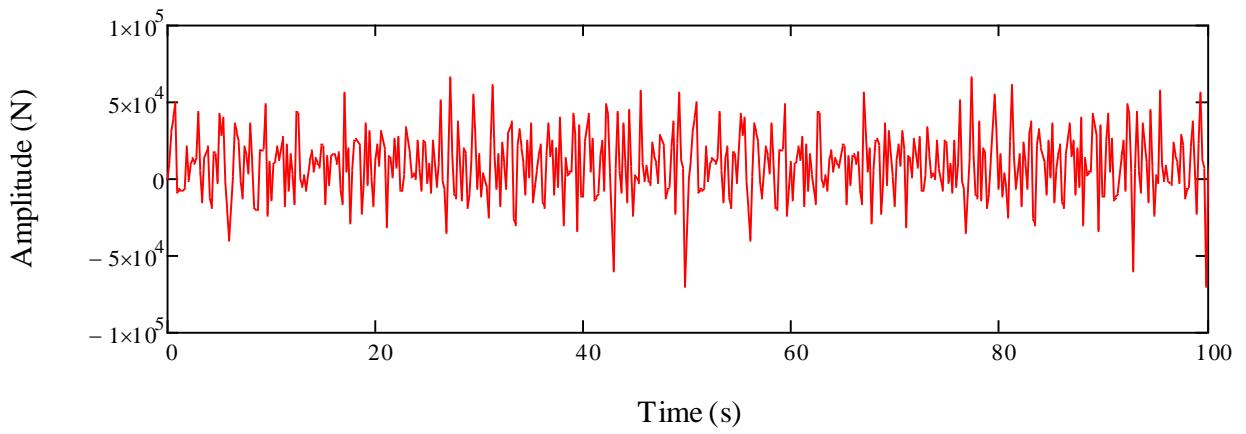


Figure VI.62: Wave load at sea water level (MSL)

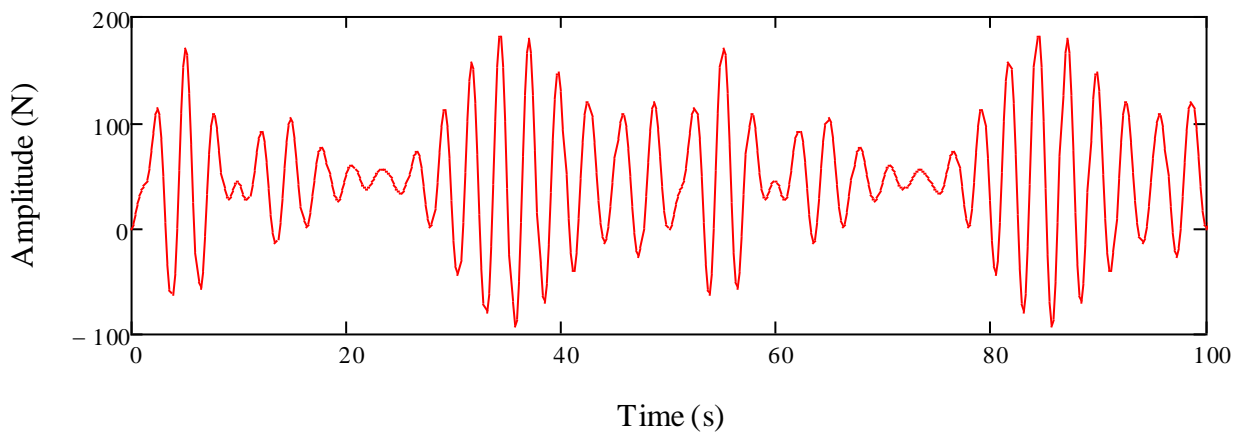


Figure VI.63: Wave load at seabed level

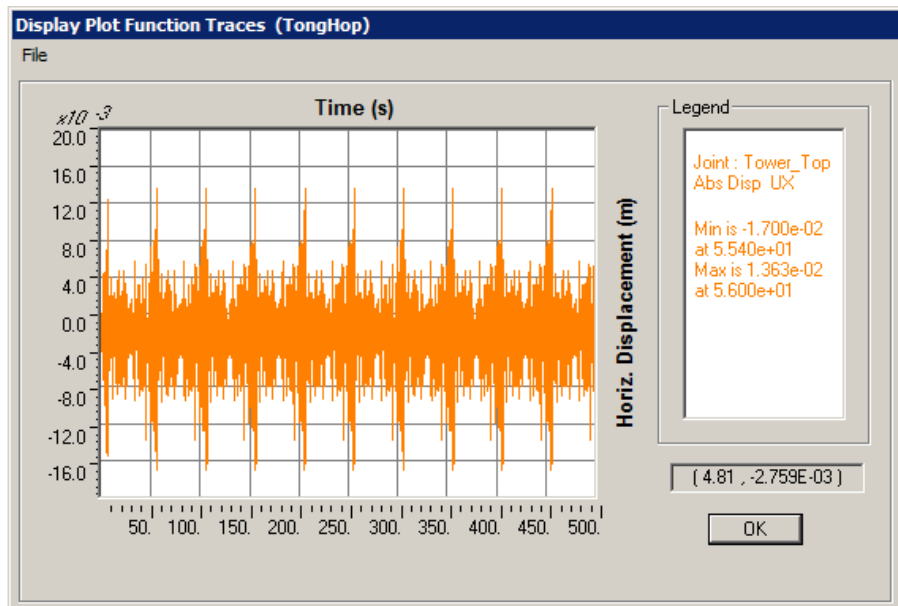


Figure VI.64: Horizontal displacement of the tower top in the fixed foundation model

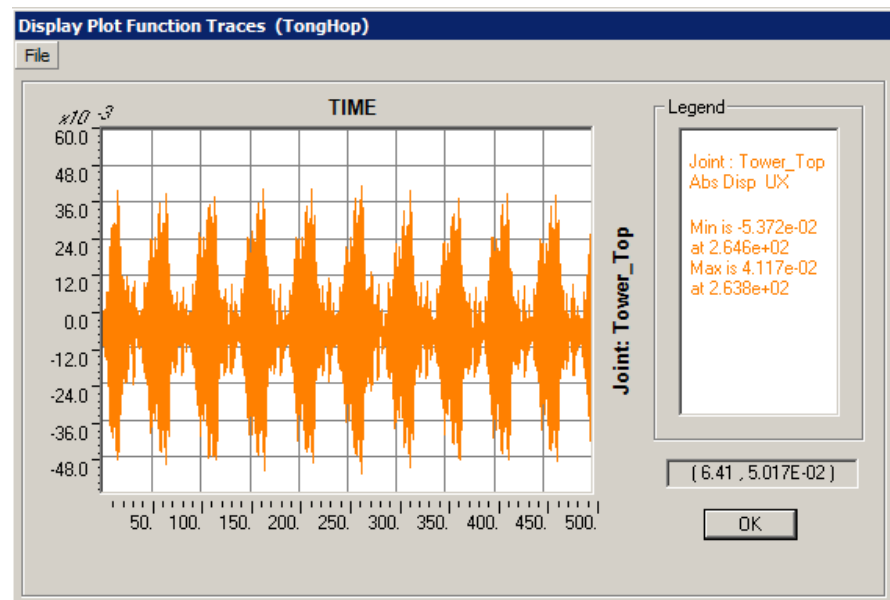


Figure VI.65: Horizontal displacement of the tower top in the spring foundation model

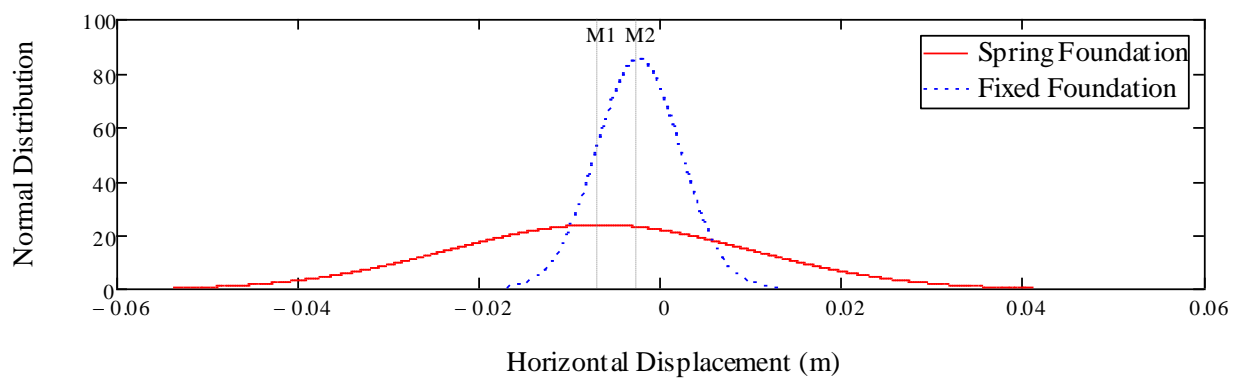


Figure VI.66: Normal distribution of horizontal displacements at tower top

Table VI.11: Tower top displacement in two models

Models	Spring Foundation	Fixed Foundation
Mean values (mm)	6.8	2.5
Standard deviations (mm)	17	4.7
Maximum values (mm)	54	17

From the results in Table VI.11, maximum horizontal displacement at the tower top is three times larger in Nonlinear Spring Foundation Model than in Fixed Foundation Model.

6.4.3. Linear spring vs. nonlinear spring foundation

In order to see the differences between nonlinear and linear spring model, the model with linear spring foundation under cyclic loading caused by Sea state 0 had been calculated.

From the result of calculation, it is obvious that having the same wave load input but the amplitude of displacements in the linear spring model are much larger than they are in the nonlinear spring model. This is because internal damping is not included in the linear spring model of the soil.

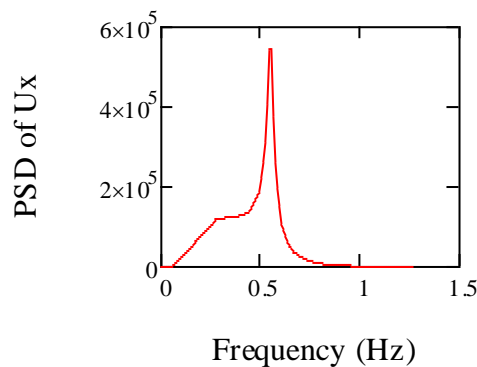


Figure VI.67: Power Spectral Density of horizontal displacements at the tower top - linear spring model

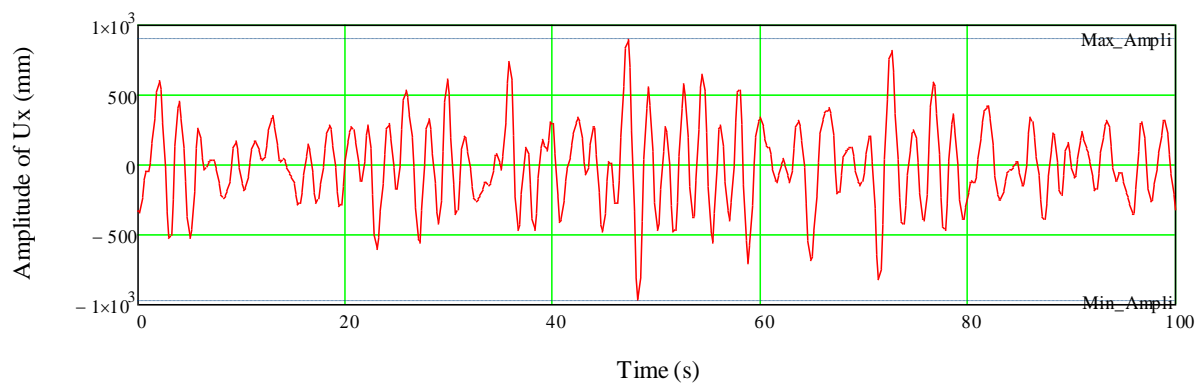


Figure VI.68: Result of Ux at the tower top in time domain

Models	Non-linear Spring Foundation	Linear Spring Foundation
Mean values (mm)	6.8	0.644
Standard deviations (mm)	17	290
Maximum values (mm)	54	967

6.5. Effect of p-y curve on the dynamic behavior of structure

In order to see the effect of the initial subgrade reaction in the dynamic behavior of the structure, the relationship between Damping Coefficient and Horizontal Displacement are drawn for different values of initial subgrade reaction of the soil. Figure VI.69 shows three curves named DNV, 140%DNV and 60%DNV. They correspond to the relationships when the initial subgrade reaction gets the value from DNV standard, increases 40% and decrease 40% respectively. From the result, it is obvious that with a higher initial subgrade reaction, the internal damping of the soil will be higher.

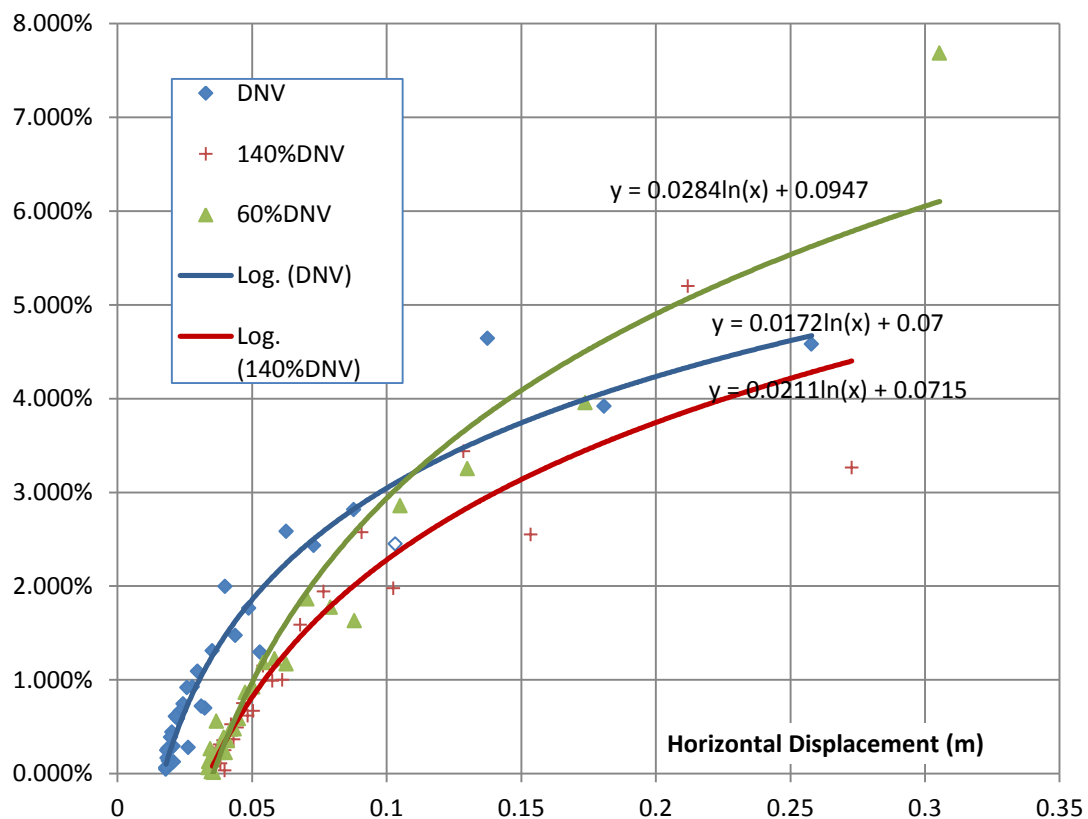


Figure VI.69: Damping Coefficient vs. Horizontal Displacement

Chapter VII. Conclusions and Future works

7.1. Conclusions

- Determining the dimensions of foundation pile for monopile foundations of offshore wind turbines can be done using DNV Standard (DNV-OS-J101, 2011) using Beam Nonlinear Winkler Foundation (BNWF) model.
- Pile-Soil Interface in cyclic loading can be modeled using nonlinear spring on both sides of the foundation pile with Kinematic behavior for cohesionless soils and Takeda behavior for cohesive soil.
- Behaviors of the tower in the fixed-at-seabed model and in the model with foundation pile are totally different. Displacements of the structure are larger in the model with the presence of foundation pile.
- Damping of the offshore wind turbine structure mostly comes from internal damping of the soil, which can be modeled using nonlinear springs and hysteresis behaviors. It is possible to use nonlinear springs and dashpots instead of modeling hysteresis behaviors however the permanent accumulated displacements cannot be observed in that case.

7.2. Future works

- Degradation of soil stiffness makes the permanent displacements become more serious. Including this kind of behavior in BNWF model would be useful in practical design.
- Hysteretic behaviors need to be calculated in Step-by-step solution method in a dynamic analysis. This will be a challenge job in integrating the foundation pile into design optimization of the tower because it is time consuming.

Bibliography

- API. (2000). *Recommended Practice for Planning, Designing and Constructing Fixed Offshore Platforms*. Washington, D.C: American Petroleum Institute.
- Atkinson, J. (n.d.). *An Introduction to the mechanics of soils and foundations*.
- Bhushan K., and Askari S. (1984). Lateral load tests on drilled pier foundations for solar plant heliostats. *Laterally loaded piles*. Edited by J.A. Langer. ASTM, STP 835, 141-155.
- Bhushan K., Haley S.C., and Fong P.T. (1979). Lateral load tests on drilled piers in stiff clays. *Journal of the Geotechnical Engineering Division, ASCE*, 105(GT8): 969-985.
- Bhushan K., Lee L.J., and Grime D.B. (1981). Lateral load tests on drilled piers in sand. *Proceedings of a Session on Drilled Piers and Caissons, Geotechnical Engineering Division, American Society of Civil Engineers, National Convention*, (pp. 131-143). St. Louis, Mo.,.
- Bowles, J. E. (1997). *Foundation Analysis and Design*. McGraw-Hill.
- BSH. (2007). *Design Standard of Offshore Wind Turbines*.
- CSI. (2011). *CSI Analysis Reference Manual*. Berkeley: University Avenue, California, USA.
- Dikmen, U. (2009). Statistical correlations of shear wave velocity and penetration resistance for soils. *Journal of Geophysics and Engineering*, 61-72.
- DNV-OS-J101, D. N. (2011). *Design of offshore wind turbine structures*.
- DNV-RP-C205. (2007). *Environmental Conditions and Environmental Loads*.
- GL. (2005). *Guideline for the Certification of Offshore Wind Turbines*. Germanischer Lloyd WindEnergie GmbH.
- Graff, K. F. (1975). *Wave Motion in Elastic Solids*. Courier Dover Publications.
- GWEC, G. W. (2011). *Annual market update 2010*. 1040 Brussels: Global Wind Energy Council.
- H.G.Poulos. (n.d.). Influence of cyclic loading on axial pile response.
- IEC, I. E. (2009). *IEC 61400-3, Wind turbines - part 3: Design requirements for offshore wind turbines*. Geneva, Switzerland.
- Jachary J. Westgate and Jason T. DeJong. (2005). *Geotechnical Considerations for Offshore Wind Turbines*.
- Jan van der Tempel and David-Pieter Molenaar. (2004). Wind Turbine Structural Dynamics - A Review of the Principles for Modern Power Generation, Onshore and Offshore. *Wind Engineering Volume 26, No.4*, pp 211-220.
- M. Hesham El Naggar and Kevin J. Bentley. (2000). Dynamic analysis for laterally loaded piles and dynamic p-y curves. *NRC Canada*, 1166-1183.
- Matlock, H. (1970). Correlations for design of laterally loaded piles in soft clay. *Proceedings of the 2nd Offshore Technology Conference Vol.1*, (pp. 577-588). Houston, Tex.
- Meyer B.J., and Reese L.C. (1979). Analysis of single piles under lateral loading. *Research Report 2441, Center for Highway Research, The University of Texas at Austin*, 1-145.
- Micheal F. Cook and J. Kim Vandiver. (1982). Measured and Predicted Dynamic Response of a Single Pile Platform to Random Wave Excitation. *Offshore Technology Conference*, 637-647.
- Ray W. Clough & Joseph Penzien. (2003). *Dynamics of structures*. Berkeley, CA 94704 USA: McGraw-Hill, Inc.
- Reese, L. C.; Cox, W. R.; Koop, F.D. (1974). Analysis of Laterally Loaded Piles in Sand. *Proceedings of the VI Annual Offshore Technology Conference*. Dallas.

- TEMPEL, J. V. (2006). *Design of Support Structures for Offshore Wind Turbines*.
- Vries, W. d. (2011). *Final report WP 4.2 "Support Structure Concepts for Deep Water Sites"*. Delft, The Netherlands: Delft University of Technology.
- Watson, G. (2000). *Structure and Foundation Design of Offshore Wind Installations*. Final Report from the Offshore Wind Energy Network Workshop.
- Watson, G. (2000). *Structure and Foundations Design of Offshore Wind Installations*. Offshore Wind Energy Network.
- Zaaijer, M. (2002). Foundation models for the dynamic response of offshore wind turbines.

Honor Statement

I pledge that this Master Thesis, entitled “Design monopile foundations for offshore wind turbines” has not been submitted for academic credit in any other capacity, and that this Master Thesis has not yet been published.

I further pledge that I have written this Master Thesis myself, on my own. I have not employed any sources or aids other than those listed. I have appropriately identified and acknowledged all words and ideas taken from other works.

Liege, the 30th July 2012

Mai Anh Quang

Appendix 1. T-Z curves

Layer 5:

- Elevation of the top: $\text{top} := 6.5 \quad \text{m}$
- Elevation of the bottom: $\text{bottom} := 7.0 \quad \text{m}$
- Elevation of the middle: $x := 0.5 \cdot (\text{top} + \text{bottom}) = 6.75 \quad \text{m}$
- Diameter of the pile: $D := 6 \quad \text{m}$
- Effective depth of the spring: $h := 1 \quad \text{m}$

$$t_{\max}(x) = 37.811 \quad \text{kN/m}^2$$

$$t := 0, 0.4 \dots t_{\max}(x) \quad \text{kPa}$$

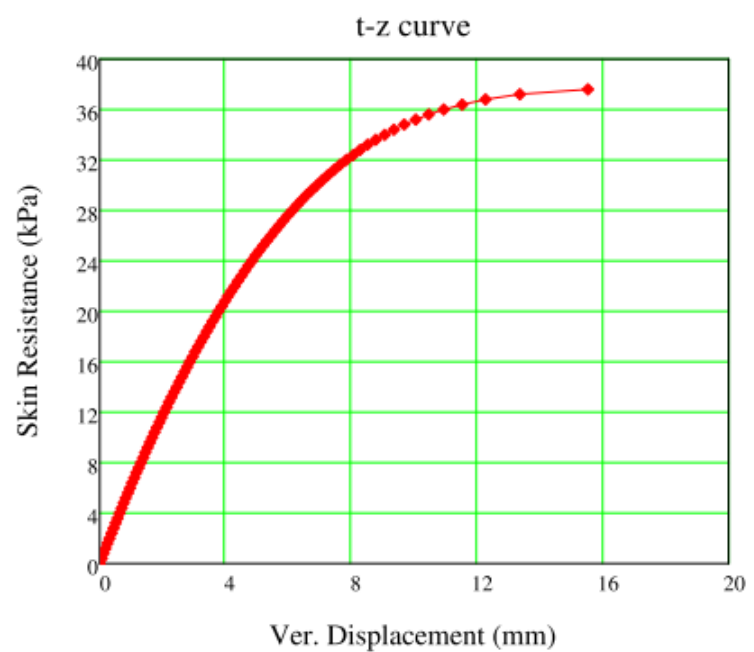
$$T_{\text{load}}(t) := t \cdot \pi \cdot D \cdot h \quad \text{kN}$$

$z(x, D, t) =$

$7.638 \cdot 10^{-3}$
$7.842 \cdot 10^{-3}$
$8.056 \cdot 10^{-3}$
$8.283 \cdot 10^{-3}$
$8.523 \cdot 10^{-3}$
$8.78 \cdot 10^{-3}$
$9.055 \cdot 10^{-3}$
$9.355 \cdot 10^{-3}$
$9.683 \cdot 10^{-3}$
0.01
0.01
0.011
0.012
0.012
0.013
...

$T_{\text{load}}(t) =$

0
7.54
15.08
22.619
30.159
37.699
45.239
52.779
60.319
67.858
75.398
82.938
90.478
98.018
105.558
...



Layer 10:

- Elevation of the top: $\text{top} := 12.5 \quad \text{m}$
- Elevation of the bottom: $\text{bottom} := 13.5 \quad \text{m}$
- Elevation of the middle: $x := 0.5 \cdot (\text{top} + \text{bottom}) = 13 \quad \text{m}$
- Diameter of the pile: $D := 6 \quad \text{m}$
- Effective depth of the spring: $h := 1 \quad \text{m}$

$$t_{\max}(x) = 72.822 \quad \text{kN/m}^2$$

$$t := 0, 0.5 \dots t_{\max}(x) \quad \text{kPa}$$

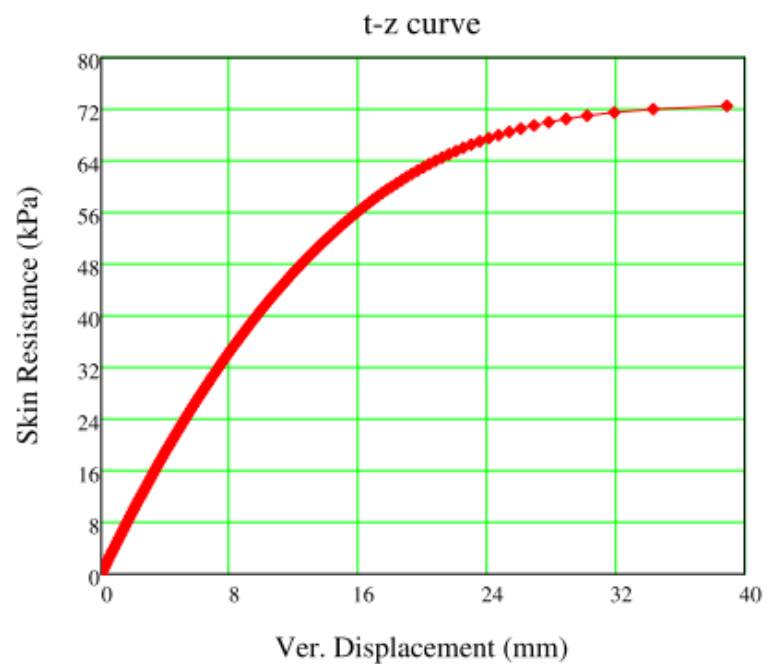
$$T_{\text{load}}(t) := t \cdot \pi \cdot D \cdot h \quad \text{kN}$$

 $z(x, D, t) =$

0
$9.6282 \cdot 10^{-5}$
$1.9299 \cdot 10^{-4}$
$2.9012 \cdot 10^{-4}$
$3.8769 \cdot 10^{-4}$
$4.8569 \cdot 10^{-4}$
$5.8413 \cdot 10^{-4}$
$6.8302 \cdot 10^{-4}$
$7.8237 \cdot 10^{-4}$
$8.8217 \cdot 10^{-4}$
$9.8243 \cdot 10^{-4}$
$1.0832 \cdot 10^{-3}$
$1.1844 \cdot 10^{-3}$
$1.2861 \cdot 10^{-3}$
$1.3882 \cdot 10^{-3}$
...

 $T_{\text{load}}(t) =$

0
9.425
18.85
28.274
37.699
47.124
56.549
65.973
75.398
84.823
94.248
103.673
113.097
122.522
131.947
...



Layer 12:

- Elevation of the top: $\text{top} := 20 \quad \text{m}$
- Elevation of the bottom: $\text{bottom} := 21.04 \quad \text{m}$
- Elevation of the middle: $x := 0.5 \cdot (\text{top} + \text{bottom}) = 20.52 \quad \text{m}$
- Diameter of the pile: $D := 6 \quad \text{m}$
- Effective depth of the spring: $h := 1 \quad \text{m}$

$$t_{\max}(x) = 53.617 \quad \text{kN/m}^2$$

$$t := 0, 0.5 \dots t_{\max}(x) \quad \text{kPa}$$

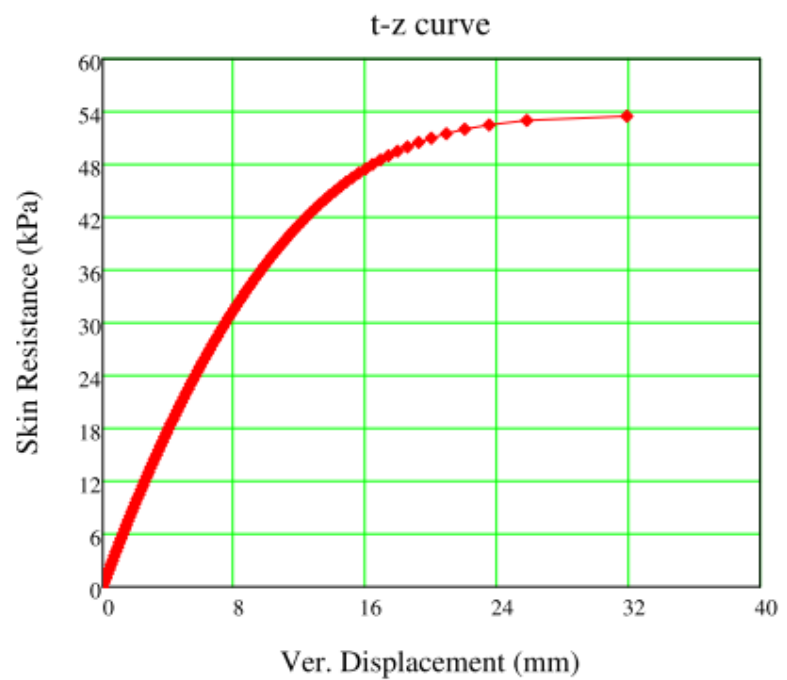
$$T_{\text{load}}(t) := t \cdot \pi \cdot D \cdot h \quad \text{kN}$$

 $z(x, D, t) =$

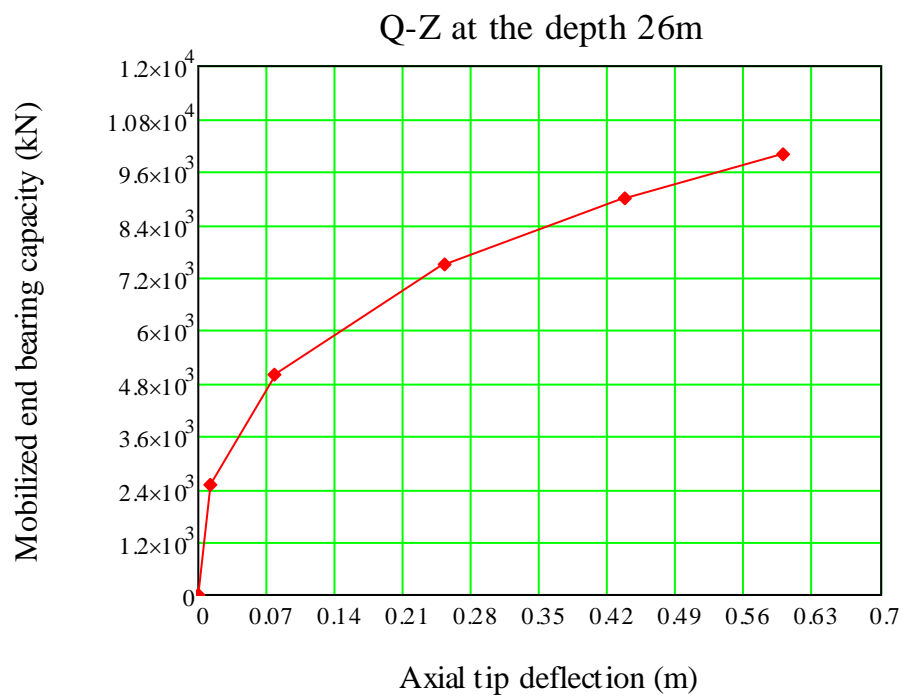
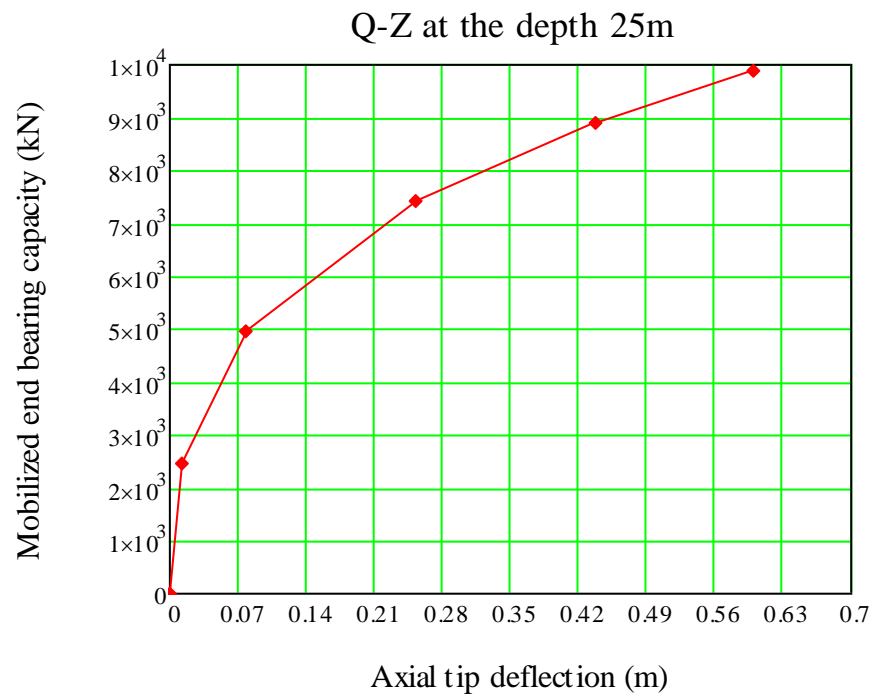
0
$9.8721 \cdot 10^{-5}$
$1.9803 \cdot 10^{-4}$
$2.9794 \cdot 10^{-4}$
$3.9847 \cdot 10^{-4}$
$4.996 \cdot 10^{-4}$
$6.0137 \cdot 10^{-4}$
$7.0377 \cdot 10^{-4}$
$8.0683 \cdot 10^{-4}$
$9.1054 \cdot 10^{-4}$
$1.0149 \cdot 10^{-3}$
$1.12 \cdot 10^{-3}$
$1.2257 \cdot 10^{-3}$
$1.3322 \cdot 10^{-3}$
$1.4393 \cdot 10^{-3}$
...

 $T_{\text{load}}(t) =$

0
9.425
18.85
28.274
37.699
47.124
56.549
65.973
75.398
84.823
94.248
103.673
113.097
122.522
131.947
...



Appendix 2. Q-Z curves



Appendix 3. P-Y curves

Layer 5:

- Elevation of the top: $\text{top} := 6.5 \quad \text{m}$
- Elevation of the bottom: $\text{bottom} := 7 \quad \text{m}$
- Elevation of the middle: $x := 0.5 \cdot (\text{top} + \text{bottom}) = 6.75 \quad \text{m}$
- Diameter of the pile: $D := 6 \quad \text{m}$

Calculation of p-y curve:

Value_y =

	0
43	-0.014
44	-0.012
45	-0.01
46	$-8 \cdot 10^{-3}$
47	$-6 \cdot 10^{-3}$
48	$-4 \cdot 10^{-3}$
49	$-2 \cdot 10^{-3}$
50	0
51	$2 \cdot 10^{-3}$
52	$4 \cdot 10^{-3}$
53	$6 \cdot 10^{-3}$
54	$8 \cdot 10^{-3}$
55	0.01
56	0.012
57	0.014
58	...

Value_p =

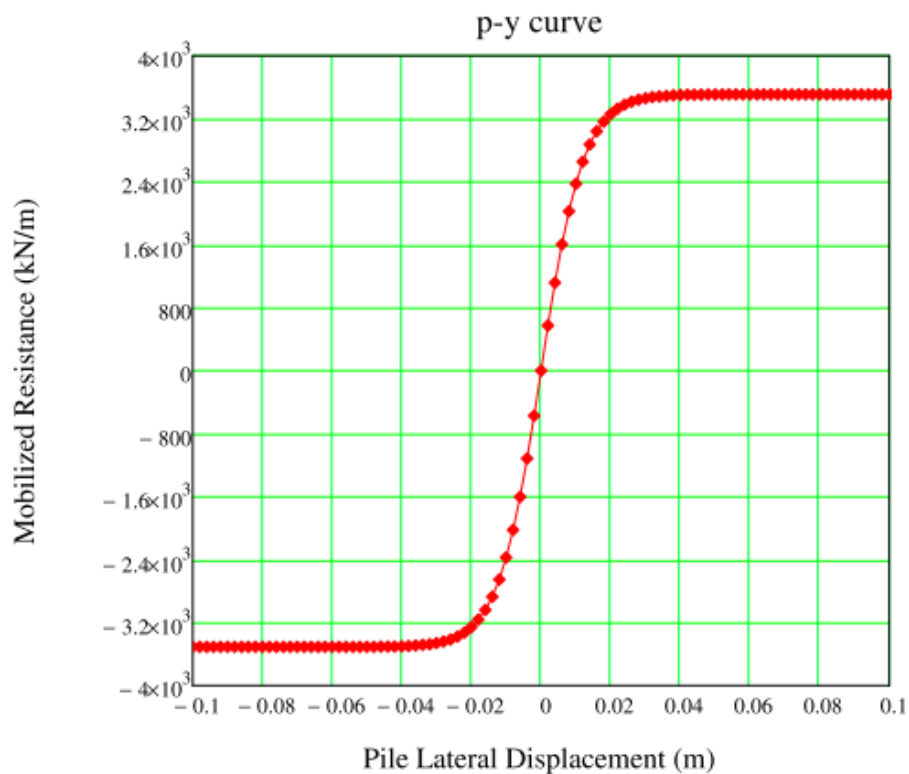
	0
43	$-2.872 \cdot 10^3$
44	$-2.654 \cdot 10^3$
45	$-2.374 \cdot 10^3$
46	$-2.025 \cdot 10^3$
47	$-1.604 \cdot 10^3$
48	$-1.115 \cdot 10^3$
49	-572.113
50	0
51	572.113
52	$1.115 \cdot 10^3$
53	$1.604 \cdot 10^3$
54	$2.025 \cdot 10^3$
55	$2.374 \cdot 10^3$
56	$2.654 \cdot 10^3$
57	$2.872 \cdot 10^3$
58	...

Value_y =

	0
0	-0.1
1	-0.098
2	-0.096
3	-0.094
4	-0.092
5	-0.09
6	-0.088
7	-0.086
8	-0.084
9	-0.082
10	-0.08
11	-0.078
12	-0.076
13	-0.074
14	-0.072
15	...

Value_p =

	0
0	$-3.51059 \cdot 10^3$
1	$-3.51059 \cdot 10^3$
2	$-3.51059 \cdot 10^3$
3	$-3.510589 \cdot 10^3$
4	$-3.510589 \cdot 10^3$
5	$-3.510588 \cdot 10^3$
6	$-3.510587 \cdot 10^3$
7	$-3.510586 \cdot 10^3$
8	$-3.510584 \cdot 10^3$
9	$-3.510581 \cdot 10^3$
10	$-3.510577 \cdot 10^3$
11	$-3.510572 \cdot 10^3$
12	$-3.510564 \cdot 10^3$
13	$-3.510554 \cdot 10^3$
14	$-3.51054 \cdot 10^3$
15	...



Layer 10:

- Elevation of the top: $\text{top} := 12.5 \quad \text{m}$
- Elevation of the bottom: $\text{bottom} := 13.5 \quad \text{m}$
- Elevation of the middle: $x := 0.5 \cdot (\text{top} + \text{bottom}) = 13 \quad \text{m}$
- Diameter of the pile: $D := 6 \quad \text{m}$

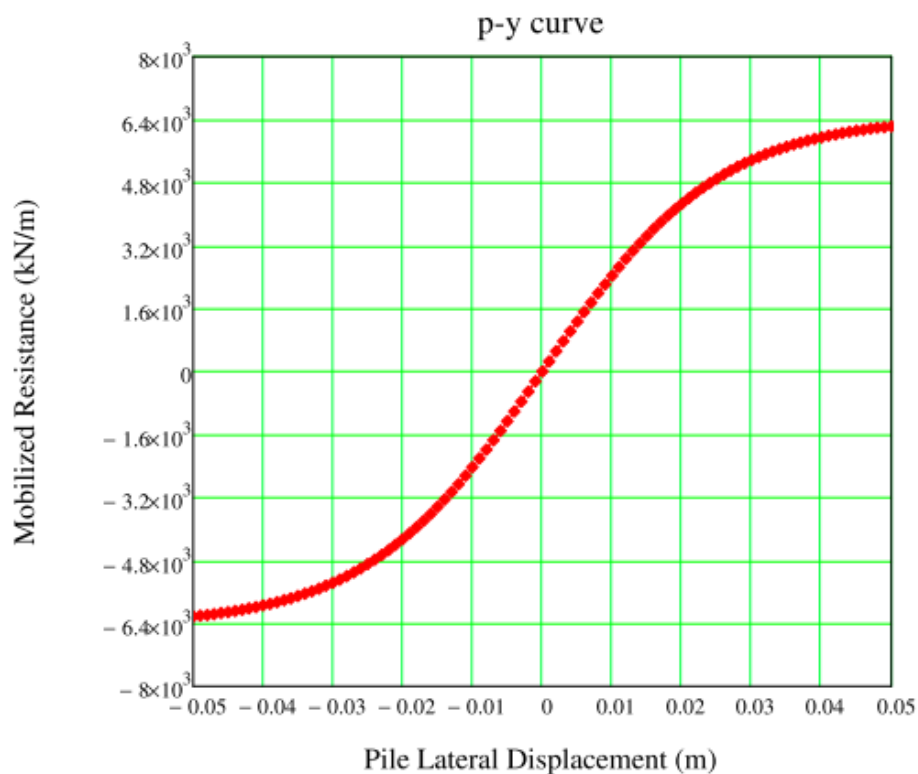
Calculation of p-y curve:

Value _y =	0
43	$-7 \cdot 10^{-3}$
44	$-6 \cdot 10^{-3}$
45	$-5 \cdot 10^{-3}$
46	$-4 \cdot 10^{-3}$
47	$-3 \cdot 10^{-3}$
48	$-2 \cdot 10^{-3}$
49	$-1 \cdot 10^{-3}$
50	0
51	$1 \cdot 10^{-3}$
52	$2 \cdot 10^{-3}$
53	$3 \cdot 10^{-3}$
54	$4 \cdot 10^{-3}$
55	$5 \cdot 10^{-3}$
56	$6 \cdot 10^{-3}$
57	$7 \cdot 10^{-3}$
58	...

Value _p =	0
43	$-1.749 \cdot 10^3$
44	$-1.509 \cdot 10^3$
45	$-1.264 \cdot 10^3$
46	$-1.016 \cdot 10^3$
47	-764.891
48	-511.254
49	-256.027
50	0
51	256.027
52	511.254
53	764.891
54	$1.016 \cdot 10^3$
55	$1.264 \cdot 10^3$
56	$1.509 \cdot 10^3$
57	$1.749 \cdot 10^3$
58	...

Value _y =	0
0	-0.05
1	-0.049
2	-0.048
3	-0.047
4	-0.046
5	-0.045
6	-0.044
7	-0.043
8	-0.042
9	-0.041
10	-0.04
11	-0.039
12	-0.038
13	-0.037
14	-0.036
15	...

Value _p =	0
0	$-6.229743 \cdot 10^3$
1	$-6.210156 \cdot 10^3$
2	$-6.189025 \cdot 10^3$
3	$-6.166232 \cdot 10^3$
4	$-6.141654 \cdot 10^3$
5	$-6.115158 \cdot 10^3$
6	$-6.086606 \cdot 10^3$
7	$-6.055847 \cdot 10^3$
8	$-6.022724 \cdot 10^3$
9	$-5.987069 \cdot 10^3$
10	$-5.948706 \cdot 10^3$
11	$-5.907448 \cdot 10^3$
12	$-5.8631 \cdot 10^3$
13	$-5.815455 \cdot 10^3$
14	$-5.764298 \cdot 10^3$
15	...

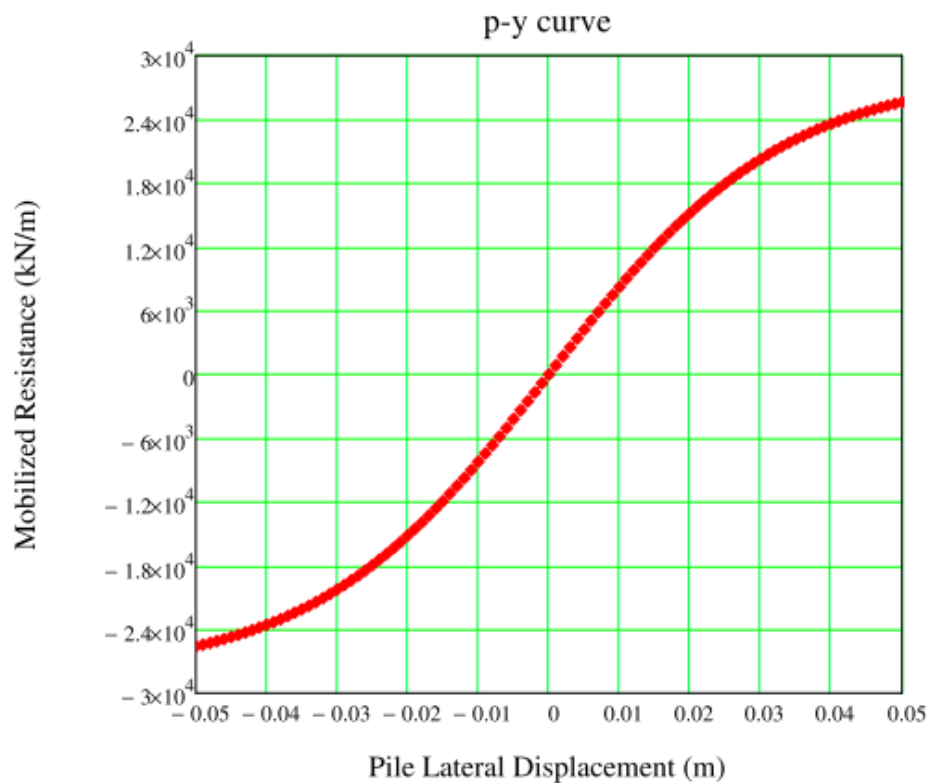


Layer 13 L26:

- Elevation of the top: $\text{top} := 25 \quad \text{m}$
- Elevation of the bottom: $\text{bottom} := 26 \quad \text{m}$
- Elevation of the middle: $x := 0.5 \cdot (\text{top} + \text{bottom}) = 25.5 \quad \text{m}$
- Diameter of the pile: $D := 6 \quad \text{m}$

Calculation of p-y curve:

Value _y =		Value _p =		Value _y =		Value _p =	
0		0		0		0	
43	$-7 \cdot 10^{-3}$	43	$-5.854 \cdot 10^3$	0	-0.05	0	$-2.561466 \cdot 10^4$
44	$-6 \cdot 10^{-3}$	44	$-5.037 \cdot 10^3$	1	-0.049	1	$-2.545682 \cdot 10^4$
45	$-5 \cdot 10^{-3}$	45	$-4.211 \cdot 10^3$	2	-0.048	2	$-2.529023 \cdot 10^4$
46	$-4 \cdot 10^{-3}$	46	$-3.378 \cdot 10^3$	3	-0.047	3	$-2.511447 \cdot 10^4$
47	$-3 \cdot 10^{-3}$	47	$-2.539 \cdot 10^3$	4	-0.046	4	$-2.492911 \cdot 10^4$
48	$-2 \cdot 10^{-3}$	48	$-1.695 \cdot 10^3$	5	-0.045	5	$-2.473369 \cdot 10^4$
49	$-1 \cdot 10^{-3}$	49	-848.335	6	-0.044	6	$-2.452776 \cdot 10^4$
50	0	50	0	7	-0.043	7	$-2.431086 \cdot 10^4$
51	$1 \cdot 10^{-3}$	51	848.335	8	-0.042	8	$-2.408248 \cdot 10^4$
52	$2 \cdot 10^{-3}$	52	$1.695 \cdot 10^3$	9	-0.041	9	$-2.384216 \cdot 10^4$
53	$3 \cdot 10^{-3}$	53	$2.539 \cdot 10^3$	10	-0.04	10	$-2.358939 \cdot 10^4$
54	$4 \cdot 10^{-3}$	54	$3.378 \cdot 10^3$	11	-0.039	11	$-2.332366 \cdot 10^4$
55	$5 \cdot 10^{-3}$	55	$4.211 \cdot 10^3$	12	-0.038	12	$-2.304448 \cdot 10^4$
56	$6 \cdot 10^{-3}$	56	$5.037 \cdot 10^3$	13	-0.037	13	$-2.275133 \cdot 10^4$
57	$7 \cdot 10^{-3}$	57	$5.854 \cdot 10^3$	14	-0.036	14	$-2.244371 \cdot 10^4$
58	...	58	...	15	...	15	...



Appendix 4. Sensitivity Analyses

These analyses are used to see the sensitivity of the initial subgrade reaction of the soil to the damping of the structure. In this calculation, the DNV initial subgrade modulus values are chosen using DNV standard (DNV-OS-J101, 2011). For each case, these initial subgrade modulus values will be changed with an amount of 10%. In APP. 2 the initial subgrade modulus values are varied from 50% to 150% of the DNV values. However, from the results of calculation, only the case of 60% and 140% are chosen to show because of their significant differences.

The equivalent viscous damping ratio is determined by modifying the free-vibration response equation (Ray W. Clough & Joseph Penzien, 2003):

$$A = A_0 e^{-\xi \omega t}$$

$$\rightarrow \ln(A) = \ln(A_0) - \xi \omega t$$

$$\rightarrow \frac{\partial \ln(A)}{\partial t} = -\xi \omega$$

$$\rightarrow \xi = -\frac{1}{\omega} \frac{\partial \ln(A)}{\partial t}$$

A_0 : Initial amplitude of the free-vibration response

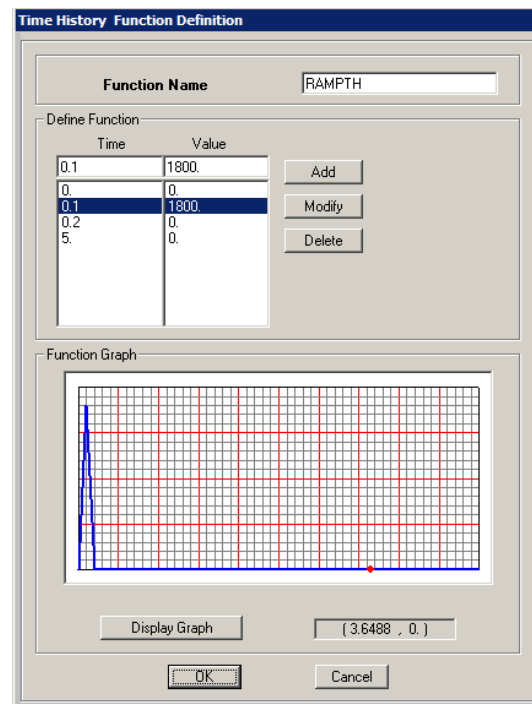
A : free-vibration response at the time t

ξ : the viscous damping ratio

ω : the circular frequency (considered as a constant values after each cycle)

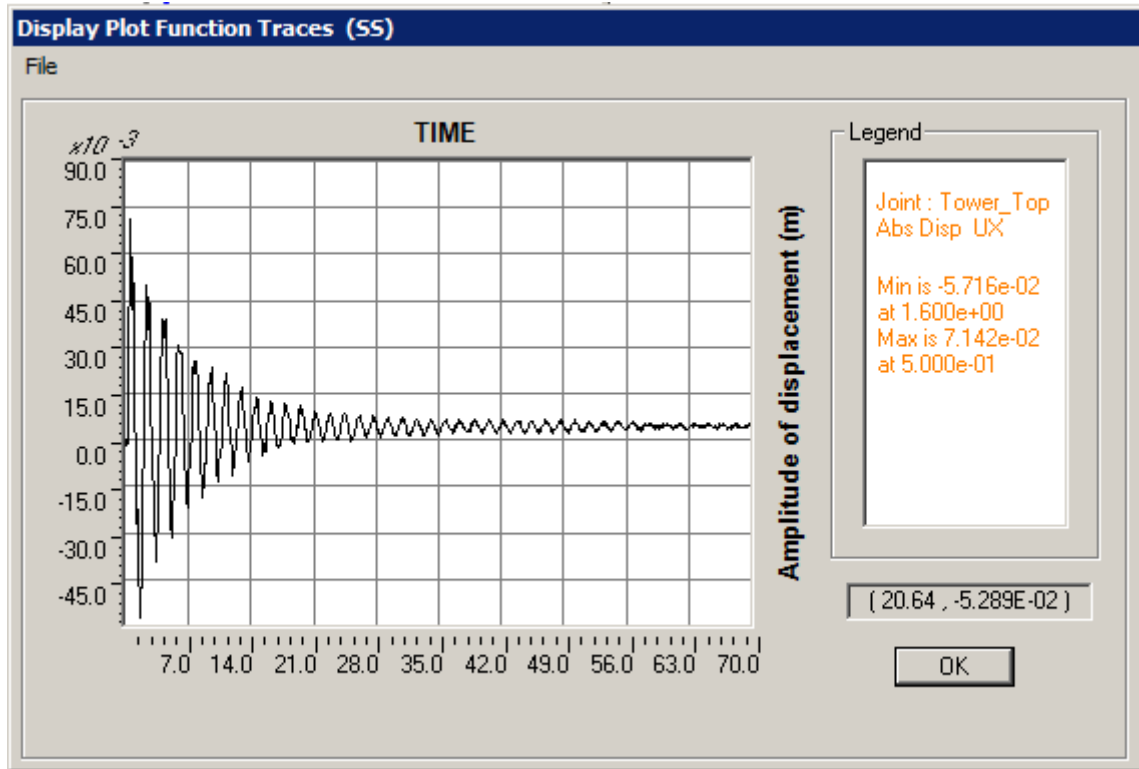
Layer	Initial subgrade modulus (kN/m2/m)		
	DNV	-40%	40%
1	42760	25660	59860
2	42760	25660	59860
3	42760	25660	59860
4	42760	25660	59860
5	42760	25660	59860
6	42760	25660	59860
7	42760	25660	59860
8	42760	25660	59860
9	30690	18410	42970
10	19700	11820	27580
11	27600	16560	38640
12	12830	7698	17960
13	33280	19970	45690

APP. 2: Initial subgrade modulus of layers



APP. 1: Excitation Load

a. Reduce 40% of the DNV initial subgrade modulus values



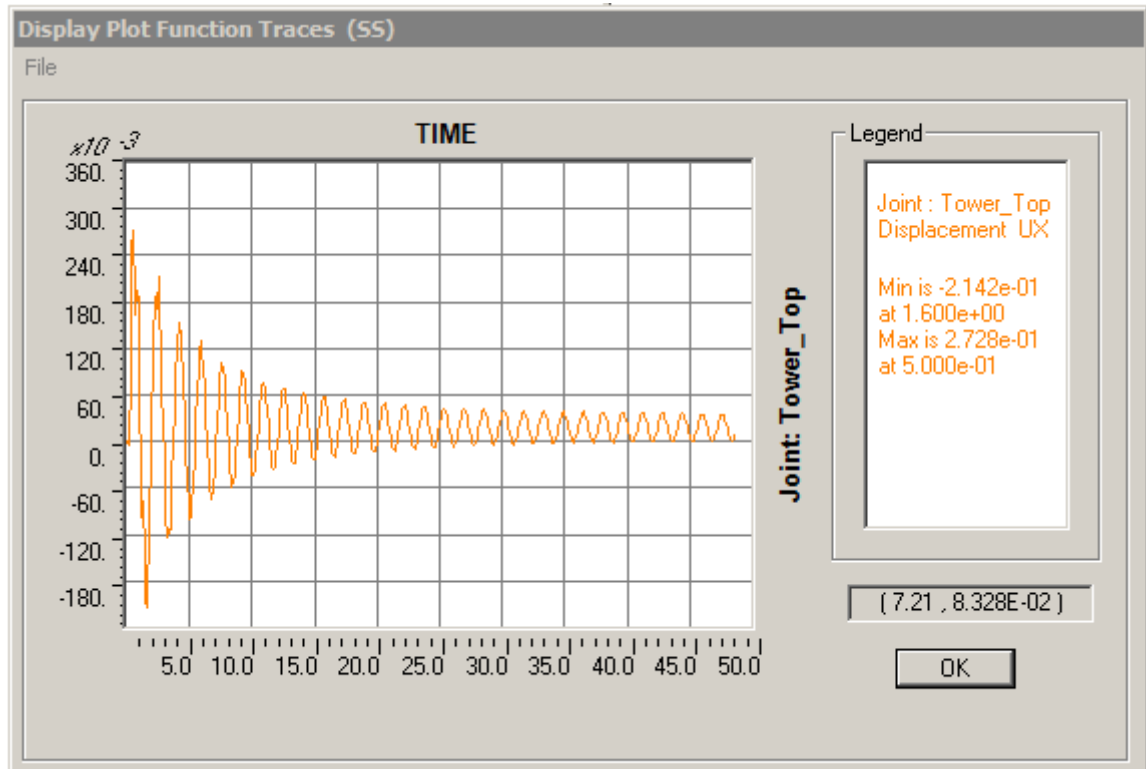
APP. 3: U_x of the tower top in the case 60% of the DNV values

APP. 4: Damping coefficient in the case 60% of the DNV values

Δt	t	A	$\ln(A)$	$\Delta \ln(A)$	ξ
(1)	(2)	(3)	(4)	(5)	(6)
1.9	0.50	0.3055	-1.1859	-0.5641	7.69%
1.9	2.40	0.1738	-1.7500	-0.2903	3.95%
1.7	4.30	0.1300	-2.0402	-0.2136	3.25%
1.6	6.00	0.1050	-2.2538	-0.1765	2.86%
1.7	7.60	0.0880	-2.4303	-0.1071	1.63%
1.7	9.30	0.0791	-2.5374	-0.1164	1.77%
1.6	11.00	0.0704	-2.6538	-0.1152	1.86%
1.6	12.60	0.0627	-2.7691	-0.0722	1.17%
1.6	14.20	0.0584	-2.8413	-0.0756	1.22%
1.6	15.80	0.0541	-2.9169	-0.0732	1.18%
1.6	17.40	0.0503	-2.9901	-0.0571	0.92%
1.6	19.00	0.0475	-3.0472	-0.0536	0.87%
1.6	20.60	0.0450	-3.1009	-0.0362	0.59%
1.6	22.20	0.0434	-3.1371	-0.0295	0.48%
1.6	23.80	0.0422	-3.1665	-0.0294	0.48%

Δt	t	A	$\ln(A)$	$\Delta \ln(A)$	ξ
(1)	(2)	(3)	(4)	(5)	(6)
1.6	25.40	0.0409	-3.1959	-0.0217	0.35%
1.6	27.00	0.0401	-3.2176	-0.0138	0.22%
1.6	28.60	0.0395	-3.2315	-0.0241	0.39%
1.6	30.20	0.0386	-3.2555	-0.0186	0.30%
1.6	31.80	0.0379	-3.2741	-0.0138	0.22%
1.6	33.40	0.0373	-3.2880	-0.0140	0.23%
1.5	35.00	0.0368	-3.3020	-0.0323	0.56%
1.6	36.50	0.0356	-3.3343	-0.0008	0.01%
1.6	38.10	0.0356	-3.3351	-0.0113	0.18%
1.6	39.70	0.0352	-3.3464	-0.0106	0.17%
1.6	41.30	0.0348	-3.3570	-0.0011	0.02%
1.6	42.90	0.0348	-3.3581	-0.0087	0.14%
1.6	44.50	0.0345	-3.3668	-0.0164	0.26%
1.6	46.10	0.0339	-3.3832	-0.0080	0.13%
1.6	47.70	0.0337	-3.3911	-0.0039	0.06%
	49.30	0.0335	-3.3950		

b. Increase 40% of the DNV initial subgrade modulus values



APP. 5: Ux of the tower top in case 140% of the DNV values

APP. 6: Damping coefficient in the case 60% of the DNV values

Δt	t	A	ln(A)	$\Delta \ln(A)$	ξ
(1)	(2)	(3)	(4)	(5)	(6)
2	0.50	0.2728	-1.2990	-0.2526	3.264%
1.6	2.50	0.2119	-1.5516	-0.3219	5.200%
1.8	4.10	0.1536	-1.8735	-0.1776	2.550%
1.7	5.90	0.1286	-2.0510	-0.2262	3.439%
1.6	7.60	0.1026	-2.2772	-0.1222	1.974%
1.7	9.20	0.0908	-2.3994	-0.1692	2.573%
1.6	10.90	0.0766	-2.5686	-0.1202	1.942%
1.7	12.50	0.0680	-2.6888	-0.1043	1.586%
1.6	14.20	0.0612	-2.7931	-0.0618	0.999%
1.6	15.80	0.0576	-2.8549	-0.0613	0.990%
1.6	17.40	0.0541	-2.9162	-0.0712	1.150%
1.6	19.00	0.0504	-2.9874	-0.0413	0.667%
1.6	20.60	0.0484	-3.0287	-0.0381	0.616%
1.6	22.20	0.0466	-3.0668	-0.0464	0.749%
1.6	23.80	0.0445	-3.1132	-0.0304	0.491%
1.6	25.40	0.0431	-3.1435	-0.0225	0.364%
1.6	27.00	0.0422	-3.1660	-0.0325	0.526%
1.6	28.60	0.0408	-3.1986	-0.0228	0.368%

Δt	t	A	ln(A)	$\Delta \ln(A)$	ξ
(1)	(2)	(3)	(4)	(5)	(6)
1.5	30.20	0.0399	-3.2214	-0.0020	0.035%
1.6	31.70	0.0398	-3.2234	-0.0154	0.249%
1.6	33.30	0.0392	-3.2388	-0.0219	0.354%
1.6	34.90	0.0384	-3.2607	-0.0068	0.110%
1.6	36.50	0.0381	-3.2675	-0.0191	0.308%
1.6	38.10	0.0374	-3.2866	-0.0159	0.257%
1.6	39.70	0.0368	-3.3025	-0.0145	0.234%
1.5	41.30	0.0363	-3.3170	-0.0089	0.153%
1.6	42.80	0.0359	-3.3259	-0.0047	0.077%
1.6	44.40	0.0358	-3.3306	-0.0135	0.218%
1.6	46.00	0.0353	-3.3442	-0.0120	0.193%
	47.60	0.0349	-3.3561	3.3561	